

**Intense Gigawatt Relativistic Electron Beam
generation Studies in Planar and Cylindrical
Diodes**

By

AMITAVA ROY

Bhabha Atomic Research Centre, Mumbai – 400 085 INDIA

A thesis submitted to the Board of Studies in Physical Sciences

In partial fulfillment of requirements

For the Degree of

DOCTOR OF PHILOSOPHY

of

HOMI BHABHA NATIONAL INSTITUTE, MUMBAI

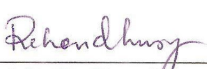


October, 2011

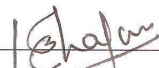
Homi Bhabha National Institute

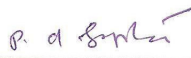
Recommendations of the Viva Voce Board

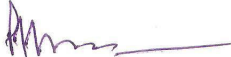
As members of the Viva Voce Board, we certify that we have read the dissertation prepared by Amitava Roy entitled "Intense Gigawatt Relativistic Electron Beam generation Studies in Planar and Cylindrical Diodes" and recommend that it may be accepted as fulfilling the dissertation requirement for the Degree of Doctor of Philosophy.


Chairman: Prof. R. K. Choudhury Date: April 24, 2012


Guide/ Convener: Prof. K. C. Mittal Date: April 24, 2012


Member 1: Prof. K. B. Thakur Date: April 24, 2012


Member 2: Prof. P. D. Gupta Date: April 24, 2012


External Examiner: Prof. P. I. John Date: April 24, 2012

Final approval and acceptance of this dissertation is contingent upon the candidate's submission of the final copies of the dissertation to HBNI. I hereby certify that I have read this dissertation prepared under my direction and recommend that it may be accepted as fulfilling the dissertation requirement.

Date: April 24, 2012

Place: Mumbai


Guide: Prof. K. C. Mittal

STATEMENT BY AUTHOR

This dissertation has been submitted in partial fulfillment of requirements for an advanced degree at Homi Bhabha National Institute (HBNI) and is deposited in the Library to be made available to borrowers under rules of the HBNI.

Brief quotations from this dissertation are allowable without special permission, provided that accurate acknowledgement of source is made. Requests for permission for extended quotation from or reproduction of this manuscript in whole or in part may be granted by the Competent Authority of HBNI when in his or her judgment the proposed use of the material is in the interests of scholarship. In all other instances, however, permission must be obtained from the author.

A handwritten signature in cursive script that reads "Amitava Roy". The signature is written in black ink and is positioned above the printed name.

Amitava Roy

DECLARATION

I, hereby declare that the investigation presented in the thesis has been carried out by me. The work is original and has not been submitted earlier as a whole or in part for a degree / diploma at this or any other Institution / University.

A handwritten signature in black ink that reads "Amitava Roy". The signature is written in a cursive style and is underlined with a single horizontal line.

Amitava Roy

Dedicated to

My Parents

Shri. Phanindra Nath Roy

Smt. Gita Roy

and

My Wife

Smt. Ballari Roy

ACKNOWLEDGEMENTS

I express my deep gratitude to the following persons who have helped me in various ways.

- To my guide Dr. K. C. Mittal, Project Manager, EBC, Kharghar, BARC, Dr. K. V. Nagesh, Head, Energetics & Pulse Power Systems Section, Accelerator and Pulse Power Division, BARC, Mumbai, and Dr. Archana Sharma for stimulating discussions, providing facilities, cheerful help, valuable guidance through the entire period and correction of manuscript.
- To my doctoral committee, HBNI, Dr. K. B. Thakur, Dr. P. D. Gupta and Dr. R. K. Choudhury for their valuable guidance during writing this thesis, putting me on the right track afterwards and also for meticulous suggestions & guidance to make this work complete and correction of manuscript.
- To D. P. Chakravarthy, Head, Accelerator and Pulse power Division, Bhabha Atomic Research centre, Mumbai for providing facilities, cheerful help, and valuable guidance.
- To Dr. A. K. Ray, Former Director, Beam Technology Development Group, and Raja Ramanna Fellow, BARC and Dr. L. M. Gantayet, Director, Beam Technology Development Group, for their support and encouragement.
- To my all younger colleagues at Accelerator and Pulse Power Division for useful discussions and participation in the experiments. In particular to Smt. Rakhee Menon, Sri. S. Mitra, Sri. D. D. P. Kumar, Sri. Senthil Kumar, Sri. Sandeep Singh and Sri. V. K. Sharma.
- To G. L. Patil, N. K. Lawangre and S. R. Raul for their help in assembly of experimental set up.
- To MTRDC, DRDO, Bangalore for participation in the HPM generation and measurement experiments and for valuable discussions/suggestions.
- Finally I express gratitude to my family for their heartfelt support without that I could not have done this work. In addition I express my gratitude to all persons who have not been listed here but helped to complete this work.

Amitava Roy

TABLE OF CONTENTS

SYNOPSIS	9
LIST OF FIGURES	20
LIST OF TABLES	30
CHAPTERS	
1. INTRODUCTION	32
2. LITERATURE SURVEY	38
2.1 SPACE-CHARGE LIMITED ELECTRON EMISSION FROM AN EXPANDING PLASMA CATHODE	39
2.2 MULTIDIMENSIONAL SPACE-CHARGE LIMITED FLOW	45
2.3 PLASMA-FILLED DIODE	54
2.4 EFFECT OF PREPULSE ON INTENSE RELATIVISTIC ELECTRON BEAM GENERATION	57
2.5 ELECTRON BEAM QUALITY AND UNIFORMITY	61
2.6 THE SHOT TO SHOT REPRODUCIBILITY OF THE ELECTRON BEAM DIODE	68
2.7 HPM GENERATION FROM VIRTUAL CATHODE OSCILLATOR USING IREB	70
2.8 CYLINDRICAL ELECTRON BEAM DIODE AND COAXIAL VIRTUAL CATHODE OSCILLATOR	74
3. EXPERIMENTAL SETUP AND PROCEDURE	80
3.1 KALI 5000 PULSE POWER SYSTEM	80
3.2 KALI 1000 PULSE POWER SYSTEM	82
3.3 ELECTRON BEAM DIODE	84
3.4 BEAM DIAGNOSTICS	86
3.4.1 Rogowski Coil	86
3.4.2 B-Dot Probe	88
3.4.3 Voltage Divider	90
3.5 VIRTUAL CATHODE OSCILLATOR FOR HIGH POWER MICROWAVE GENERATION	91
3.6 HPM DIAGNOSTICS	93
4. INTENSE RELATIVISTIC ELECTRON BEAM GENERATION STUDIES IN THE PRESENCE OF PREPULSE	95

4.1	INTENSE GIGAWATT RELATIVISTIC ELECTRON BEAM GENERATION IN THE PRESENCE OF PREPULSE	95
4.2	EFFECT OF CATHODE DIAMETER ON IREB GENERATION IN THE PRESENCE OF PREPULSE	103
4.3	IREB GENERATION IN HIGH POWER CYLINDRICAL DIODE IN THE PRESENCE OF PREPULSE	115
4.4	ELECTRON BEAM GENERATION WITH A BIPOLAR PULSE IN A HIGH POWER CYLINDRICAL DIODE	123
4.5	PREPULSE SUPPRESSION TECHNIQUES	129
4.5.1	Prepulse Suppression using a dielectric cathode holder	129
4.5.2	Prepulse Suppression by adding an Extra Inductance to the Charging Circuit of the Blumlein Line	135
4.6	CONCLUSIONS	136
5.	PLASMA CLOSURE VELOCITY MEASUREMENT IN HIGH POWER ELECTRON BEAM DIODE	140
5.1	SPACE CHARGE LIMITED ELECTRON FLOW IN A PLANAR DIODE	140
5.2	PLASMA EXPANSION VELOCITY MEASUREMENT IN A HIGH POWER PLANAR DIODE	142
5.3	PLASMA EXPANSION VELOCITY MEASUREMENT IN A HIGH POWER PLANAR DIODE WITH A DIELECTRIC CATHODE HOLDER	147
5.4	SPACE CHARGE LIMITED ELECTRON FLOW IN A CYLINDRICAL DIODE	151
5.5	PLASMA EXPANSION VELOCITY MEASUREMENT IN A HIGH POWER CYLINDRICAL DIODE	153
5.6	CONCLUSIONS	156
6.	HIGH POWER MICROWAVE GENERATION FROM VIRTUAL CATHODE OSCILLATOR (VIRCATOR)	158
6.1	HPM GENERATION FROM AXIAL VIRCATOR	158
6.2	HPM GENERATION FROM COAXIAL VIRCATOR	163
6.3	CONCLUSIONS	168
7.	SUMMARY AND CONCLUSIONS	169
	REFERENCES	174

LIST OF ABBREVIATIONS

HPM	–	High-power microwave
FXR	–	Flash X-ray
IREB	–	Intense relativistic electron beam
AK	–	Anode-cathode
KALI	–	Kilo Ampere Linear Injector
CsI	–	Cesium iodide
PFL	–	Pulse forming line
CL	–	Child-Langmuir
Viracator	–	Virtual cathode oscillator
SCL	–	Space-charge-limited
PIC	–	Particle-in-cell
PFD	–	Plasma filled diode
MHD	–	Magnetohydrodynamics
SS	–	Stainless steel
SEM	–	Scanning Electron Microscope
RF	–	Radio Frequency
UV	–	Ultra Violet
VC	–	Virtual cathode
FFT	–	Fast Fourier Transform

Intense Gigawatt Relativistic Electron Beam generation Studies in Planar and Cylindrical Diodes

SYNOPSIS

Intense gigawatt relativistic electron beams (IREB) with beam energies greater than 100 kilo electron volts, beam currents tens to hundreds of kiloamperes and duration few tens of nanosecond to few microsecond have found applications in the field of high-power microwave generation (HPM) [1], free electron lasers [2], flash X-ray (FXR) generation [3], and surface modification [4] etc. For all these applications, the intense electron beam is generated in REB diode by the explosive field emission process. When a high electric field (> 100 kV/cm) is applied on a cathode surface, electrons are emitted from the surface by field emission process. Due to resistive heating of the sharp points on the surface, an expanding plasma layer (called cathode plasma) is formed on the cathode surface in a few ns. When the intense electron beam hits the anode, anode plasma is produced. Space charge limited electron and ion emission occurs from these electrode plasmas. Movement of electrons, ions, electrode plasmas, plasma uniformity and associated self magnetic fields control various processes occurring in the high power vacuum diodes. Considerable experimental and theoretical work [5] has been done in the study of beam generation processes but the information available is far from complete. The numerous applications of these large devices, often insufficiently understood, create a need for establishing rules as precise as possible. An attempt has been made in this thesis to understand the beam generation process under various diode configurations and also production of HPM using these beams.

Chapter 1 of this thesis introduces the subject of intense relativistic electron beam generation in vacuum. Based on the review of available literature on the beam generation process, it is felt that plasma expansion velocities and presence of a high voltage pulse (known as pre pulse) before the main power pulse control the magnitude and duration of the beam produced. Consequently, the following problems were identified for investigation in this thesis.

- a) Intense Gigawatt Relativistic Electron Beam generation studies in the presence of prepulse in planar and cylindrical diodes.

- b) Prepulse suppression techniques.
- c) Measurement of electrode plasma expansion velocity from the perveance data during the main pulse using the bipolar space charge limited flow model.
- d) Generation and measurement of HPM power from axial and coaxial virtual cathode oscillator.

Chapter 2 of this thesis presents a review of the literature available on the various aspects of the intense gigawatt relativistic electron beam generation and its application on High Power Microwave generation.

A typical pulse power system consists of a primary charging device like Marx Generator (MG) or Tesla Transformer (TT), a pulse forming line, either Blumlein line or a simple two electrode coaxial line, spark gap switches, electron beam diodes as a load and peaker.

Fig. 1 shows the elements of the unified circuit for the production of nanosecond high-power pulses. An MG charges a primary energy store (capacitor or line) within about $1\mu\text{s}$. The pulsed charging of an energy store enables one to use nonconventional liquids for insulation of MG's, such as water, glycerin, castor oil, and not just transformer oil. Besides, it is possible to work with much stronger electric fields, allowing one to reduce the overall dimensions of the device and to use a nontriggered spark gap as the main switch. The primary energy store is discharged through the main switch into a pulse-forming line, which in turn is discharged through a peaker into a transmission line. The transmission line is connected to a load through another peaker. The load can be the diode of an accelerator of electrons or ions, a gas laser, the resonator of a high-power microwave generator, a z-pinch shell, the diode of a high-power x-ray generator, etc.

The circuit in Fig. 1 is a generalized one, since, depending on the parameters of the pulse and its purpose, some or other elements can be absent. In particular, the second peaker, as a rule, is used not only to shorten the pulse rise time, but also to reduce the amplitude of the prepulse. The latter, if an electron diode is used as a load, results in the occurrence of premature explosive electron emission and undesirable filling of the diode with plasma before the arrival of the main pulse. Therefore, in some circuits where the prepulse does not play a role, the second peaker may be absent. The transmission line can serve simultaneously as an impedance converter, for example, an exponential strip or coaxial line. In some generators, there is no

peaker at all, and the pulse, after pulse-forming line, arrives immediately at the load. For example KALI 5000 pulse power system does not have a peaker.

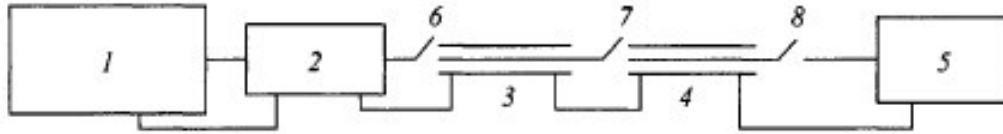


Figure 1. Elements of the unified circuit for the production of nanosecond high-power pulses: 1 - Marx generator, 2 - capacitive energy store, 3 - pulse-forming line, 4 - transmission line, 5 - load, 6 - main switch, 7 - first peaker, 8 - second peaker

In actual pulsed power systems, a voltage pulse of about 10%–30% of the main pulse voltage appears across the vacuum diode at about 300–800 ns before the arrival of the main pulse. This pulse is known as a prepulse and appears in the charging cycle of the Blumlein pulse forming line. This prepulse is produced due to the charging inductor connected between the central and outer electrodes of the Blumlein. The prepulse voltage becomes more pronounced due to the imbalance of the charging lines of the Blumlein. Presence of prepulse in the pulse power systems [6, 7] poses some problem in the beam generation process. The onset of the prepulse prior to the arrival of the main pulse in the IREB diode leads to the evaporation of cathode whiskers and subsequent launching of significant amount of plasma and neutral vapors into the vacuum diode region. The plasma thus created affects the performance of the IREB generation significantly [7]. In the past, beam generation studies were carried out in IREB diode in the presence of a prefilled plasma of different densities [8]. The beam generation mechanism in the presence of a prepulse is not exactly the same as that of the earlier works on plasma filled diodes.

For shorter pulse duration < 100 ns and at the comparatively low current density ~ 10 A/cm² electron flow remains unipolar [9]. However at the higher current density greater than few hundreds of A/cm² electron flow becomes bipolar [10]. The charge neutralizations of the electrons by the ions allows approximately 1.86 times the current to flow as compared to single species Child–Langmuir, with the limiting electron current independent of the ion mass [6].

The anode and cathode plasma, can cross the diode gap, resulting in collapse of the diode impedance during the high voltage pulse. This behavior adversely affects the diode performance, limits the duration of the electron beam pulse and results in poor efficiency of

coupling between the electron beam diode and the pulse power system. From the plasma luminosity measurement it was seen that a cathode plasma appears on the cathode surface immediately after the rise of the beam current at about $t=20$ ns [11]. An anode plasma on the anode surface has been seen to be formed at $t=30$ ns [11]. The cathode plasma expands at 1.8-4.2 cm/ μ s and the anode plasma expands at 2.6-9.4 cm/ μ s for various AK gaps [11].

To delay the impedance collapse of the diode, it has been suggested to use cesium iodide (CsI) coated carbon fiber cathode and heat the anode [12] at 800–1200 K. Heating the anode may reduce the amount of gas that is desorbed and thereby reduce the amount of plasma exploding in to the diode region [12]. CsI coating produces slower and/or more uniform cathode plasma through easier emission at lower electric field [12].

IREB's have been used extensively to generate HPM using Virtual Cathode Oscillator (VIRCATOR) device. In a VIRCATOR device IREB's are injected into drift tube in excess of the space charge limited current. In this case, a virtual cathode forms and reflects electrons back toward the accelerator. This is an inherently unstable situation, and it leads to quite efficient production of electromagnetic radiation. The self space charge of the electrons forms a deep electrostatic well, which results in the virtual cathode. Power levels between 10 MW and several gigawatts at frequencies in the range of 2-13 GHz, with electron beam power conversion efficiencies between 1.5 and 14 % have been reported.

Chapter 3 of this thesis describes the experimental setup and procedure. KALI 1000 (Kilo Ampere Linear Injector) (300 kV, 20 kA, 100 ns) and KALI 5000 (1MV, 60 kA, 100 ns) pulse power system has been used to investigate the various aspects of IREB generation. KALI 5000 pulse power system has been operated without a prepulse switch (or peaker) to study the effect of prepulse on IREB generation. The typical electron beam parameters studied in this thesis were 200-450 keV, 10-40 kA, 100 ns with few hundreds of A/cm² current density. A copper sulfate resistive voltage divider has been developed to measure the diode voltage. A self integrating Rogowski coil and a B-Dot probe has been designed and developed to measure the fast rise time diode current. In order to generate HPM using the IREB, axial and coaxial vircators have been designed and developed.

Chapter 4 of this thesis presents the IREB generation studies in the presence of prepulse. To understand the prepulse effect on the relativistic electron beam diode, beam generation experiments have been carried out with various AK gaps and voltages. Electron beam

generation mechanism in the presence of the prepulse has been analyzed by the expansion of the prepulse generated plasma and plasma filled diode. Increasing the AK gap reduces the prepulse electric field and eventually drops it below the explosive emission threshold and eliminates its creation. As this threshold is approached, the plasma that is turned on may be non-uniform as explosive sites become few and far between. This will make the cathode plasma very dependent on surface preparation and the resulting plasma will be wispy, spotty, and very nonreproducible. For perveance more than $200 \mu\text{Perv}$ we can consider the diode as short. The diode can be considered short if the Marx voltage/ $(\text{Anode Cathode Gap})^2$ is more than 56 kV/cm^2 . Below 56 kV/cm^2 the effect of the prepulse will be negligible.

In order to study the effect of prepulse on cathode diameter, an intense relativistic electron beam has been generated from planar and annular graphite cathodes at a fixed 25 mm AK gap in the presence of prepulse. A bipolar prepulse voltage has been recorded at the diode. It was found that the positive prepulse voltage has no significant effect on the diode perveance and impedance. Annular graphite cathodes of 40 and 70 mm diameters and 98 mm diameter planar graphite cathodes are not very suitable for reliable operation in the presence of prepulse.

High Power Cylindrical diodes have been employed for intense relativistic electron beam generation in coaxial virtual cathode oscillator [13] and in high resolution radiography sources [3]. Intense relativistic electron beam has been generated in a high power cylindrical diode in the presence of prepulse. A bipolar prepulse voltage has been recorded at the diode. The amplitude and the time duration of the prepulse voltage vary with the Marx generator voltage. It was found for the AK gap $\leq 1.65 \text{ cm}$ that there is shot to shot variation in the cylindrical diode voltage and current for the same Marx generator voltage. It was shown that the positive prepulse voltage has no significant effect on the diode perveance. For the cylindrical diode the prepulse generated plasma decreases the impedance of the diode and, respectively, increases the diode perveance. However, one can conclude that the plasma does not completely fill the diode gap, resulting in $\geq 170 \text{ kV}$ diode voltage.

Studies have been carried out to generate intense electron beam in the cylindrical electron beam diode when subjected to a high voltage bipolar pulse. In the positive voltage pulse, a copper mesh acts as a source of electrons. The diode perveance in the positive voltage pulse linearly increases with time due to the increase in the emission area. The electrode plasma closure is a small effect on the positive voltage pulse. During the negative voltage pulse, the

diode impedance decreases with time due to the plasma expansion. Thus, even though there is a plasma formation on the anode during the positive voltage pulse, the electron beam can be generated from the graphite cathode in the negative voltage pulse with a modest perveance ($\sim 1.1 \times 10^{-4} \text{ A/V}^{3/2}$).

So the effect of prepulse is more pronounced in the planar cathode of higher diameter due to a decrease in the uniformity of the prepulse generated plasma with the corresponding increase in the cathode diameter. The effect of the prepulse is less pronounced in the cylindrical diode as compared to planar diode that allows one to operate the cylindrical diode with the AK gap $\leq 1.85 \text{ cm}$. Annular cathodes are not very suitable for reliable operation in the presence of prepulse.

In order to reduce prepulse voltage to an acceptable level ($\leq 5\%$), prepulse switches are used after the pulse forming line [7]. It is also possible to reduce prepulse by introducing a surface flashover switch into the conductor feeding the diode in vacuum. IREB generation studies were carried out with a Perspex cathode holder. The dielectric cathode holder acts as a surface flashover switch. It was found that corrugated Perspex of length $\geq 35 \text{ mm}$ can eliminate the prepulse voltage but affects the rise time of the diode voltage. The prepulse voltage reduces significantly ($\leq 10\%$) when an inductance is added to the charging circuit of the Blumlein line. But with an added inductance the slower rise time ($\sim 2 \mu\text{s}$) of the Marx charging voltage can increase the jitter in the output switch and increase the voltage stress in the Blumlein line. With an added inductor at the charging circuit of the Blumlein line the KALI 5000 system can be operated up to $\sim 400 \text{ kV}$ with an acceptable level of prepulse voltage. In order to operate the diode up to 1 MV a low capacitance gas prepulse switch has to be installed after the pulse forming line

Chapter 5 of this thesis presents the electrode plasma expansion velocity measurements for various diode configurations and diode voltages. We have measured the electrode plasma expansion velocity from the perveance data for various diode configurations. The time varying electron beam diode impedance and perveance were measured in a planar diode for 18, 25 and 31 mm AK gaps. For 31 mm AK gap the anode and cathode plasmas expand at $9.5 \text{ cm}/\mu\text{s}$ toward each other. The peak current density in this case was $J = 401 \text{ A/cm}^2$. Such a high plasma expansion velocity has also been observed with carbon nanotube cathode [14] with a high current density $J = 309 \text{ A/cm}^2$, the plasma velocity reported $v = 9.1 \text{ cm}/\mu\text{s}$. It was found

that the plasma expansion velocity decreases for lower AK gap. It may be possible that the higher electric field at lower AK gap is slowing down one of the two plasmas. It was also found that for the same AK gap the plasma expansion velocity increases with the increase of the diode voltage due to an increase in the corresponding current density.

The plasma expansion velocity has also been measured for cylindrical diode for three different AK gaps using a time dependent Langmuir-Blodgett space charge limited flow model. Electron beam diode perveance was measured for 1.85, 1.65, and 1.2 cm AK gaps. It was found that for 1.85 cm radial AK gap the anode and cathode plasmas expand at $5 \text{ cm}/\mu\text{s}$ toward each other. Plasma expansion velocity decreases for 1.2 cm AK gap.

Using interferometry, observed velocities of upto $30 \text{ cm}/\mu\text{s}$ has been reported in axial plumes of anode plasma in a pinch-reflex diode operating at 1.5 MA and 1.5 MV. In an applied B-ion diode (1.7 MV, 1.7 MA) an expansion velocity of 5 to $10 \text{ cm}/\mu\text{s}$ throughout the voltage pulse was required for surface-flashover anode plasma in order to explain the temporal impedance decrease [15]. In higher power diodes the higher plasma-pressure gradient may result in a fast plasma expansion [15]. Expansion velocities of $5 \text{ cm}/\mu\text{s}$ correspond to the ion thermal velocity of 25-eV protons.

Chapter 6 of this thesis presents HPM generation and measurement from axial and coaxial virtual cathode oscillator. HPM generation studies have been carried out using the pulsed power generator KALI 1000. The typical electron beam parameter was 200 kV, 14 kA, 100 ns. High power microwave has been detected by neon lamp discharge by HPM illumination when placed a few meter distances from the vircator window. Microwave power has been optimized by changing the AK gap. It was found that the peak power occurs around 6 mm AK gap. HPM measurements were done using zero bias Schottky diode detectors along with a horn antenna and sufficient attenuation so as to reduce the power level below the power rating of the diode detector. Various components used in the diagnostics were calibrated using standard modulated RF source. The estimated microwave peak power is $\sim 1 \text{ kW}$ (within the effective aperture area of the receiving antenna) at 7 m distance from the vircator window.

HPM generation studies were carried out with a coaxial vircator using cylindrical electron beam diode in the presence of significant prepulse voltages. For 1.2 cm diode gap HPM has got more peak power as the diode detector was getting saturated even when the antenna has been placed at around 4.5 meter distance from the vircator output window. At this place the

measured HPM peak power was more than 20 dBm (within the effective aperture area of the receiving antenna). The estimated peak power of the Coaxial Vircator was more than 1 MW.

Chapter 7 presents summary and conclusions. Based on the above studies following conclusions were made.

- a) It was shown that intense gigawatt relativistic electron beams can be generated in the presence of significant prepulse voltages in planar, annular and cylindrical diodes with a larger gap than that estimated by the space charge limited law.
- b) It was found that for lesser AK gap there is shot to shot variation in the diode voltage and current for the same Marx generator voltage due to the nonreproducibility of the prepulse generated plasma.
- c) Inserting a dielectric at the cathode holder could be a very effective method to reduce prepulse voltage at the electron beam diode, but it increases the rise time of the diode voltage and reduces the effective electron beam pulse width.
- d) In the case of the added inductance to the Blumlein circuit, the slower rise time reduces the prepulse voltage from 32% to $\leq 10\%$. A gas prepulse switch is required to increase the diode voltage up to 1 MV.
- e) It was found that during the main pulse the diode impedance collapses due to plasma expansion from the cathode and anode surfaces. Electrode plasma expansion velocities are measured from the perveance data for planar and cylindrical graphite cathodes. It was found the plasma expansion velocities vary from 3.4 to 9.5 cm/ μ s for various diode configurations and diode voltages.
- f) HPM has been generated from axial and coaxial virtual cathode oscillator using the IREB and the HPM power has been measured using a diode detector and receiving horn antenna set up.

Finally some suggested future work is being outlined.

- a) Beam generation studies should be carried out with a gas prepulse switch.
- b) Cathode and anode plasma expansion velocities should be measured more accurately with a streak camera.
- c) Plasma expansion velocities should be measured for other cathode materials like velvet and carbon fiber and CsI coated cathodes.

- d) HPM generation and measurements should be carried out with more accurate diagnostics.

Present work has contributed to a better understanding of intense gigawatt relativistic electron beam generation process and its usefulness towards HPM generation. The results of the study are useful in the design of a reliable and efficient large electron beam system and HPM devices.

REFERENCE

- [1] Steven H. Gold, Gregory S. Nusinovich, "Review of high-power microwave source research," *Rev. Sci. Instrum.* Vol. 68, pp. 3945-3974, 1997.
- [2] H. P. Freund, T. M. Antonsen, *Principles of free-electron lasers* Published by Springer, 1996.
- [3] Maenchen, J.; Cooperstein, G.; Oapos; Malley, J.; Smith, I., "Advances in pulsed power-driven radiography systems," *Proceedings of the IEEE*, Vol. 92, pp. 1021-1042, 2004.
- [4] L. X. Schneider, K. W. Reed, and R. J. Kaye, in *Applications of Accelerators in Research and Industry*, edited by J. L. Duggan and I. L. Morgan (AIP, New York, 1997), p. 1085.
- [5] John A. Nation, Levi Scha Chater, Frederick M. Mako, L. K. Len, William Peter, Cha-Mei Tang, and Triveni Srinivasan-Rao, "Advances in Cold Cathode Physics and Technology," *Proceedings of the IEEE*, Vol. 87, No. 5, May 1999.
- [6] R. B. Miller, *An Introduction to the Physics of Intense Charge Particle Beams*, (Plenum. New York. 1982, ch. 2).
- [7] Ian D. Smith, "Induction voltage adders and the induction accelerator family," *Phys. Rev. ST Accel. Beams* Vol. 7, pp. 064801, 2004.
- [8] B. V. Weber, D. D. Hinshelwood, D. P. Murphy, S. J. Stephanakis, and V. Harper-Slaboszewicz, "Plasma-Filled Diode for High Dose-Rate Bremsstrahlung," *IEEE Trans. Plasma Sci.* Vol. 32, 1998-2003, 2004.
- [9] Yuri M. Saveliev, Wilson Sibbett and David M. Parkes, "On anode effects in explosive emission diodes," *J. Appl. Phys.* Vol. 94, pp. 5776-5781, 2003.
- [10] Donald A. Shiffler, John W. Luginsland, Ryan J. Umstattd, M. LaCour, K. Golby, Michael D. Haworth, M. Ruebush, D. Zagar, A. Gibbs, and Thomas A. Spencer, "Effects of

anode materials on the performance of explosive field emission diodes,” *IEEE Trans. Plasma Sci.* Vol. 30, pp. 1232-1237, 2002.

[11] Mitsuyasu Yatsuzuka, Masakazu Nakayama, Mitsuru Tanigawa, Sadao Nobuhara, Douglas Young, and Osamu Ishihara, “Plasma Effects on Electron Beam Focusing and Microwave Emission in a Virtual Cathode Oscillator,” *IEEE Trans. Plasma Sci.* Vol. 26, pp. 1314-1321, 1998.

[12] N. R. Pereira and A. Fisher, “Slower impedance collapse with hot anode and enhanced emission cathode,” *IEEE Trans. Plasma Sci.* Vol. 27, pp. 1169-1174, 1999.

[13] Wook Jeon, Jeong Eun Lim, Min Wug Moon, Kyu Bong Jung, Won Bae Park, Hee Myung Shin, Yoonho Seo, and Eun Ha Choi, “Output Characteristics of the High-Power Microwave Generated From a Coaxial Vircator With a Bar Reflector in a Drift Region,” *IEEE Trans. Plasma Sci.* Vol. 34, pp. 937-944, 2006.

[14] Qingliang Liao, Yue Zhang, Yunhua Huang, Junjie Qi, and Zhanjun Gao, “Explosive field emission and plasma expansion of carbon nanotube cathodes,” *Appl. Phys. Lett.* Vol. 91, pp. 151504, 2007.

[15] Y. Maron, E. Sarid, O. Zahavi, L. Perelmuter, and M. Sarfaty, “Particle-velocity distribution and expansion of a surface-flashover plasma in the presence of magnetic fields,” *Phys. Rev. A* Vol. 39, pp. 5842-5855, 1989.

List of Publication during Ph.D. work

1. **Amitava Roy**, J. Mondal, R. Menon, S. Mitra, D.D.P.Kumar, Archana Sharma, K.C.Mittal, K.V.Nagesh, D.P.Chakravarthy, “Intense Gigawatt Relativistic Electron Beam Generation in the Presence of Prepulse. Part II,” *J. Appl. Phys.***102**, 064902 (2007).
2. **Amitava Roy** , R. Menon, S. Mitra, D. D. P. Kumar, Senthil Kumar, Archana Sharma, K. C. Mittal, K.V. Nagesh, D. P. Chakravarthy, “Intense Relativistic Electron Beam Generation and Prepulse effect in High Power Cylindrical Diode,” *J. Appl. Phys.***103**, 014905 (2008).

This article has been selected for publication on February 2008 issue of **VIRTUAL JOURNAL OF ULTRAFAST SCIENCE**.

3. **Amitava Roy** , R. Menon, S. Mitra, D. D. P. Kumar, Senthil Kumar, Archana Sharma, K. C. Mittal, K.V. Nagesh, D. P. Chakravarthy, "Intense Electron Beam Generation in a High Power Cylindrical Diode with a Bipolar Pulse," *J. Appl. Phys.* **103**, 096104 (2008).
4. **Amitava Roy** , R. Menon, S. Mitra, D. D. P. Kumar, Senthil Kumar, Archana Sharma, K. C. Mittal, K.V. Nagesh, D. P. Chakravarthy, "Impedance collapse and beam generation in a high power planar diode," *J. Appl. Phys.* **104**, 014904 (2008).
5. **Amitava Roy**, R. Menon, S. Mitra, D. D. P. Kumar, Senthil Kumar, V. K. Sharma, Ankur Patel, Archana Sharma, K. C. Mittal, K.V. Nagesh, and D. P. Chakravarthy, "Effect of cathode diameter on intense relativistic electron beam generation in the presence of prepulse," *J. Appl. Phys.* **104**, 014905 (2008).
6. **Amitava Roy**, S. Mitra, R. Menon, D. D. P. Kumar, Senthil Kumar, Archana Sharma, K. C. Mittal, K.V. Nagesh, D. P. Chakravarthy, "Prepulse Suppression on a High Power Electron Beam Accelerator using a Dielectric Cathode Holder," *IEEE Trans. Plasma Sci.* Vol. **37**, pp. 67-75 (2009).
7. **Amitava Roy**, S. K. Singh, R. Menon, D. Senthil Kumar, R Venkateswaran, M. R. Kulkarni, P. C. Saroj, K. V. Nagesh, K. C. Mittal, D. P. Chakravarthy, "Measurement of high-power microwave pulse under intense electromagnetic noise," *Pramana – Journal of Physics*, **74**, pp. 123-133 (2010).

LIST OF FIGURES

FIG. 2.1 High Power Electron beam Diode. Schematic geometries of typical sites of field enhanced electron emission.

FIG. 2.2 luminosity of anode and cathode plasmas for the AK gap length of 5 mm using an annular cathode of outer radius 1.5 cm, 1mm thickness and an aluminum (Al) foil anode of 15 μm in thickness (300 kV, 35 kA, 50 ns) [11].

FIG. 2.3 Expanding plasma boundaries in the diode region as a function of time. Expanding plasmas are observed by their luminosity as shown in the previous figure [11].

FIG. 2.4 Side-view images of plasma movement within the diode for the bare carbon fibre cathode. The anode appears on the right and the cathode on the left. Images (a), (b) and (c) were, respectively, captured at ~ 100 ns, ~ 200 ns and ~ 300 ns after the beginning of the HV pulse. The initial AK gap was 50mm and the anode was a stainless steel disc [39].

FIG. 2.5 Light emission from the diode with the CsI-coated carbon fibre cathode. Images (a), (b) and (c) were captured at ~ 100 ns, ~ 200 ns and ~ 300 ns after the beginning of the HV pulse, respectively. The anode appears on the right and the cathode on the left. The AK gap was 50 mm. Note that the light intensity increased only slightly as the voltage increased [39].

FIG. 2.6 Plasma expansion velocity calculated from diode perveance. A best fit was obtained when the plasma velocity was set equal to 2.8 cm/ μs [40].

FIG. 2.7 Variation of the diode perveance P normalized to Child–Langmuir values P_{CL} with the dimensionless geometrical parameter d_{ak}/R_k . Data obtained with 20 (open

circles), 60 (full circles), and 100 mm (triangles) diameter velvet explosive emission cathodes are shown. The fitting curve (solid line 1) is calculated in accordance with Eq. (2) in Ref. 36. The dashed line 2 is a result of a PIC modeling of the finite width, infinite length diode (See Ref. 32). The dotted curve 3 is calculated from Eq. (2.7).

FIG. 2.8 Geometry and relevant parameters for the baseline 2D emission simulation [33].

FIG. 2.9 Simulated normalized current density emitted at cathode versus position (normalized to gap distance) for a variety of emission strip widths (W) and gap distances (D) in cm; each trace is labeled with its corresponding (W, D) value [33].

FIG. 2.10 Reduction of total emitted current due to the reduction of an allowed emission area on a 4-cm-wide cathode strip. The current is normalized to the simulation result for emission from 100% of the cathode area. The cathode is divided into 40 individual sections which are gradually turned off (discrete patches), or a sole nonemitting hole is allowed to expand from the cathode center (central hole) [33].

FIG. 2.11 Optical images showing the electron beam uniformity for each cathode: (a) the velvet cathode, (b) the tufted carbon fiber cesium iodide cathode, and (c) the carbon slat cathode. Note that the slatted cathode has very nonuniform emission, although the current wave form for it is nearly identical to the two cases of more uniform emission.

FIG. 2.12 Current and voltage traces from the experiment: (a) applied diode voltage, (b) current traces for the three cathodes. A is the velvet cathode, B is the tufted carbon fiber cesium iodide cathode, and C is the carbon slat cathode. Note the similarity in the current wave forms for the same applied voltage.

FIG. 2.13 (a) Diode current and (b) diode voltage drop obtained from Particle in Cell simulation for case with spatially uniform plasma density $n = 10^{13} \text{ cm}^{-3}$ hydrogen plasma fill and SCL electron emission from cathode surface [24].

FIG. 2.14 PFD configurations tested on Gamble II. Dashed lines indicate current flow direction [25].

FIG. 2.15 Data from the highest dose-rate PFD shot on Gamble II (solid lines), compared with data from a shot with no plasma (dashed lines). (a) Generator current waveforms. (b) Diode voltage waveforms. (c) Diode impedance waveforms. (d) X-ray (dose rate) signals. The vertical line indicates the time of maximum X-ray signal for the PFD shot [25].

FIG. 2.16 Modelled (a) Marx-Blumlein charging voltage and (b) raw prepulse voltage on the Blumlein inner conductor, for a peak operating voltage of 1.7MV on PIM machine [54].

FIG. 2.17 (a) Needle-shaped annular carbon fiber cathode. (b) Photo of nylon target bombarded once by beam emitted by a stainless steel cathode. (c) Photo of nylon target bombarded once by beam emitted by a needle-shaped annular carbon fiber cathode [2].

FIG. 2.18 (a) Macroscopic photograph and (b) SEM image of the CsI carbon fiber cathode. The cathode consists of carbon fibers that have been attached to a carbon surface. These fibers are then coated with a CsI salt. The SEM is at 50-times magnification with the fibers of $6\text{-}\mu\text{m}$ diameters [59].

FIG. 2.19 AFRL relativistic magnetron normalized average (rms) RF power waveforms for the cases of POCO graphite, CsI-coated carbon velvet on a graphite substrate

(conventional processing), and uncoated low-hydrogen carbon velvet on a graphite substrate (high-temperature processing) cathodes [59].

FIG. 2.20 Uniformity data from an uncoated (a) and a CsI coated (b) carbon-on-epoxy cathode. Regions of intense are red and regions of low emission are blue. The uncoated cathode shows flaring, or nonuniform emission [58].

FIG. 2.21 False-color images of the cathode plasma generated by explosive emission processes in a vircator high-power microwave source (300 kV, 5-8 kA, 60 ns). Three different cathode materials are shown. The camera intensifier gate width was 200 ns. Each cathode was attached to a brass plate which is located at the top of each image. The anode structure is seen at the bottom of each image. The spacing between the anode and cathode was 10 mm. The images show the plasma formation to be fairly uniform across the surface of all three cathode types. The light emission from the brass attachment plate in the milled aluminum cathode case indicates that differences in either the delay time or peak voltage required for emission for this particular cathode design allowed points on the brass to explosively emit [75].

FIG. 2.22 Images of the anode scintillator: (a) with magnetic field; (b) without magnetic field. Line profiles shown were taken along horizontal diameters [76].

FIG. 2.23 Histogram showing the variation in current for a carbon velvet, cesium-iodide-coated cathode. Other cathode produces similar results with variation in standard deviation and skewness [31].

FIG. 2.24 Axial virtual cathode oscillator.

FIG. 2.25 An axial vircator with HPM diagnostics [81].

FIG. 2.26 (a) Vircator microwave power and (b) frequency versus various initial AK gap distances d [81].

FIG. 2.27 Microwave signal and time-varying effective AK gap distance d_{eff} along with the diode voltage V_d and diode current I_d under initial AK gaps d are (a) 2 mm and (b) 5 mm, respectively [81].

FIG. 2.28 Coaxial virtual cathode oscillator.

FIG. 2.29 A coaxial Vircator with HPM diagnostics [88].

FIG. 2.30 Typical oscilloscope traces of the diode voltage, current, and microwave [37].

FIG. 2.31 Field magnitude of FFT at the output port [37].

FIG. 2.32 Plot of (a) microwave frequency and (b) power according to the variation of AK gap distance in the coaxial vircator without a reflector [37].

FIG. 2.33 Plot of (a) microwave frequency and (b) power according to the variation of the reflector position [37].

FIG. 3.1 The schematic of the KALI-5000 system.

FIG. 3.2 A Photograph of the KALI 5000 system.

FIG. 3.3 A photograph of the KALI 1000 system.

FIG. 3.4 Schematic of the KALI 1000 system.

FIG. 3.5 Schematic of the planar electron beam diode with the beam diagnostics.

FIG. 3.6 A planar graphite cathode.

FIG. 3.7 Schematic of the cylindrical electron beam diode and coaxial vircator.

FIG. 3.8 Annular graphite cathodes of various diameters.

FIG.3.9 Schematic of the rogowski coil.

FIG. 3.10 Calibration curve of the KALI 5000 rogowski coil.

FIG. 3.11 B-Dot Probe.

FIG. 3.12 Coaxial vircator graphite annular cathode.

FIG. 3.13 Coaxial vircator copper anode mesh.

FIG. 3.14 HPM diagnostics setup.

FIG. 4.1 Waveform of the electron beam voltage and current for 11.3 mm Gap, 70 mm dia cathode.

FIG. 4.2 Marx generator output voltage with impedance mismatch.

FIG. 4.3 Waveform of the electron beam voltage and current for 21 mm Gap 70 mm dia cathode.

FIG. 4.4 Marx generator output voltage with matched impedance.

FIG. 4.5 Waveform of the electron beam voltage and current for 31 mm Gap 70 mm diameter cathode.

FIG. 4.6 Diode impedance and beam perveance with time.

FIG. 4.7 Diode impedance for various Marx Voltage / (Anode Cathode Gap)² at the diode.

FIG 4.8 Diode perveance for various Marx Voltage / (Anode Cathode Gap)² at the diode.

FIG. 4.9 Marx generator output and Prepulse waveform along with the main voltage pulse for 280 kV diode voltage in Phase I experiment with 67 mm diameter planar cathode.

FIG. 4.10 (a) The temporal behavior of the diode impedance in Phase I experiment with 67 mm diameter planar cathode. (b) Experimental perveance for Phase I experiment.

FIG. 4.11 The diode voltage and current waveform in Phase I experiment with 98 mm diameter planar cathode for (a) $\phi_M = 334$ kV, (b) $\phi_M = 306$ kV.

FIG. 4.12 (a) The temporal behavior of the diode impedance in Phase I experiment with 98 mm diameter planar cathode for two different Marx generator voltages. (b) Experimental perveance for Phase I experiment for two different Marx generator voltages.

FIG. 4.13 The diode voltage and current waveform in Phase II experiment with 40 mm diameter annular cathode for (a) $\phi_M = 278$ kV, (b) $\phi_M = 320$ kV.

FIG. 4.14 The temporal behavior of the diode impedance in Phase II experiment with 40 mm diameter annular cathode for two different Marx generator voltages.

FIG. 4.15 The diode voltage and current waveform in Phase II experiment with 70 mm diameter annular cathode for (a) $\phi_M = 320$ kV, (b) $\phi_M = 348$ kV.

FIG. 4.16 The temporal behavior of the diode impedance in Phase II experiment with 70 mm diameter annular cathode for two different Marx generator voltages.

FIG. 4.17 (a) Voltage waveform in the Phase I experiment. (b) Current waveform in the Phase I experiment.

FIG. 4.18 (a) The temporal behavior of the diode impedance in Phase II experiment. (b) Experimental and theoretical perveance for Phase II experiment. Solid triangle represent perveance for 310 kV Marx voltage and open circles represent 240 kV Marx voltage. Continuous line represents theoretical perveance.

FIG. 4.19 (a) The temporal behavior of the diode impedance in Phase III experiment. (b) Experimental and theoretical perveance for Phase III experiment. Solid circles represent perveance for 250 kV Marx voltage and open circles represent 320 kV Marx voltage. Continuous line represents theoretical perveance.

FIG. 4.20 Prepulse waveform along with the main voltage pulse for 240 kV Marx voltage in Phase II experiment.

FIG. 4.21 Prepulse waveform along with the main voltage pulse for 250 kV Marx voltage in Phase III experiment.

FIG. 4.22 Prepulse waveform along with the main voltage and current waveform for 320 kV Marx voltage in Phase III experiment.

FIG. 4.23 (a) The diode voltage waveform. (b) The diode positive and the second negative voltage waveform with the corresponding current wave form.

FIG. 4.24 The temporal behavior of the diode perveance for positive voltage pulse. The dashed line is the perveance calculated from Langmuir-Blodgett law.

FIG. 4.25 The temporal behavior of the diode perveance for negative voltage pulse. The dashed line is the perveance calculated from Langmuir-Blodgett law.

FIG. 4.26 (a) The temporal behavior of the diode impedance for positive voltage pulse. (b) The temporal behavior of the diode impedance for negative voltage pulse.

FIG. 4.27 Schematic of the experimental setup showing Perspex cathode holder and the electron beam diode.

FIG. 4.28 Diode voltage and current waveform for 18 mm AK gap and 35 mm Perspex insulator.

FIG. 4.29 Diode voltage and current waveform for 18 mm AK gap and 35 mm Perspex insulator with a higher Marx generator voltage.

FIG. 4.30 Diode voltage and current waveform for 25 mm AK gap and 40 mm Perspex insulator.

FIG. 4.31 Diode voltage and current waveform for 25 mm AK gap and 40 mm Perspex insulator with a higher Marx generator voltage.

FIG. 4.32 Marx output and Prepulse waveform along with the main voltage pulse with an inductance added to the charging circuit of the Blumlein line.

FIG. 5.1 (a) Diode voltage and current waveform for 18 mm AK gap. (b) The temporal behavior of the diode impedance and perveance for 18 mm AK gap. Continuous line represents theoretical perveance.

FIG. 5.2 (a) Diode voltage and current waveform for 25 mm AK gap. (b) The temporal behavior of the diode impedance and perveance for 25 mm AK gap. Continuous line represents theoretical perveance.

FIG. 5.3 (a) Diode voltage and current waveform for 31 mm AK gap. (b) The temporal behavior of the diode impedance and perveance for 31 mm AK gap. Continuous line represents theoretical perveance.

FIG. 5.4 The temporal behavior of the diode impedance and perveance for 18 mm AK gap and 35 mm Perspex insulator. Continuous line represents theoretical perveance.

FIG. 5.5 The temporal behavior of the diode impedance and perveance for 18 mm AK gap and 35 mm Perspex insulator with a higher Marx generator voltage. Continuous line represents theoretical perveance.

FIG. 5.6 The temporal behavior of the diode impedance and perveance for 25 mm AK gap and 40 mm Perspex insulator. Continuous line represents theoretical perveance.

FIG. 5.7 The temporal behavior of the diode impedance and perveance for 25 mm AK gap and 40 mm Perspex insulator. Continuous line represents theoretical perveance.

FIG. 5.8 The temporal behavior of the diode impedance and perveance for Phase I experiment.

Continuous line represents theoretical perveance.

FIG. 5.9 (a) The temporal behavior of the diode gap in Phase I and Phase III experiment. (b)

The temporal behavior of the diode gap in Phase II experiment.

FIG. 6.1 Diode voltage and current waveform for 6 mm AK gap 70 mm diameter graphite cathode.

FIG. 6.2 The temporal behavior of the diode perveance and impedance for 6 mm AK gap.

FIG. 6.3 HPM signal recorded from axial vircator.

FIG. 6.4 Coaxial vircator diode voltage (Top 100 kV/Div) and diode current (Bottom 10kA/Div) (Time 200 ns/Div).

FIG. 6.5 Marx output voltage (Bottom 80 kV/Div) and diode current (Top 10 kA /Div) (Time 200 ns/Div).

FIG. 6.6 HPM signal from coaxial vircator detected by diode detector and horn antenna setup.

LIST OF TABLES

CHAPTER 2.4

TABLE I. Voltage levels at onset of prepulse plasmas for various cathodes.

CHAPTER 2.6

TABLE II. Statistical data for the shot to shot variation in the diode current.

CHAPTER 4.2

TABLE I. Results of the phase I experiment with 67 mm diameter cathode showing prepulse voltages and time durations for three different shots.

TABLE II. Results of the phase I experiment with 98 mm diameter cathode showing prepulse voltages and time durations for two different shots.

TABLE III. Results of the phase II experiment with 40 mm diameter cathode showing prepulse voltages and time durations for two different shots.

TABLE IV. Results of the phase II experiment with 70 mm diameter cathode showing prepulse voltages and time durations for two different shots.

CHAPTER 4.3

TABLE I. Results of the phase II experiment showing prepulse voltages and time durations for two different Marx generator output voltages.

TABLE II. Results of the phase III experiment showing prepulse voltages and time durations for two different Marx generator output voltages.

CHAPTER 4.5

TABLE I. Results of the experiment with 66 mm diameter cathode showing diode voltage and current for various AK gaps and Perspex insulator length.

CHAPTER 5.2

TABLE I. Results of the experiment with 67 mm diameter cathode showing diode voltage and current for various AK gaps.

CHAPTER 6.2

TABLE I. Coaxial diode impedance for various anode cathode radiuses.

TABLE II. The calculated coaxial vircator frequency for various anode cathode radiuses and diode voltages.

CHAPTER 1

INTRODUCTION

Intense gigawatt relativistic electron beams has received considerable attention during last 40 years due to its use in such diverse applications as high-power microwave generation (HPM) [1, 2], free electron lasers [3], flash X-ray (FXR) generation [4], and surface modification [5] etc. The intense relativistic electron beam (IREB) is generated from the cold cathode by explosive electron emission process, and the electron emission occurs from the plasma which is formed on the cathode surface when the strong electric field $E \geq 10^7$ V/cm is applied to the anode-cathode (AK) gap [6]. Intense pulsed relativistic electron beams were first developed to provide sources for flash X-radiography to simulate nuclear weapon effects in the laboratory. J. C. Martin [7] and his colleagues at Atomic Weapon Research Establishment (AWRE), Aldermaston, UK did pioneering work in this area in early 1960's. The first experimental investigation of IREB's was reported by Graybill and Nablo [8] in 1966 and similar experiments were carried out in many laboratories. Since that time lot of developments has taken place in pulsed power technology during last 40 years, IREB's with beam currents upto 10 MA, powers of 10^{13} Watt and energies of 10^6 Joule are presently available for experiments. The numerous applications of these large devices, often insufficiently understood, create a need for establishing rules as precise as possible.

KALI 1000 and KALI 5000 (Kilo Ampere Linear Injector) pulse power system has been used to investigate the various aspects of IREB generation in planar and cylindrical diodes. KALI-5000 consists of a 1.5 MV, 25 kJ Marx generator [9], [10] 1 MV, 5 kJ Blumlein type transmission line, and 60 kA electron beam diode with voltage and current diagnostics. KALI-1000 (Maximum output voltage 300 kV, output impedance 15Ω , and pulse duration 100

ns).consists of a radial tesla transformer, a water transmission line and electron beam diode with voltage and current diagnostics.

When the intense electron beam hits the anode, an anode plasma is produced. These anode and cathode plasma, however, can cross the diode gap, resulting in collapse of the diode impedance during the high voltage pulse. The diode closure occurs later in the pulse duration due to the expansion of these plasmas. This behavior adversely affects the diode performance, limits the duration of the electron-beam pulse and results in poor efficiency of coupling between the electron beam diode and the pulse power system. From the plasma luminosity measurement it was seen that a cathode plasma appears on the cathode surface immediately after the rise of the beam current at about $t = 20$ ns [11]. An anode plasma on the anode surface has been seen to be formed at $t = 30$ ns [11]. Expansion velocity for cathode plasma may be different than for the anode plasma. The plasma expansion velocity has been calculated from the temporal behavior of the AK gap.

Impedance collapse due to expansion of the electrode plasmas in the AK gap is a well-known phenomenon and has been studied by various authors, both theoretically [12] and experimentally [13]. For shorter pulse duration < 100 ns, and at the comparatively low current density ~ 10 A/cm² electron flow remains unipolar [14]. But at the higher current density $>$ few hundreds of A/cm² electron flow becomes bipolar [15]. In this thesis the operation of a diode has been investigated in the bipolar regime to understand the effect of plasma expansion on the impedance of the diode. To delay the impedance collapse of the diode, it has been suggested to use cesium iodide (CsI) coated carbon fiber cathode and heat the anode [13] at 800-1200 K. Heating the anode may reduce the amount of gas that is desorbed, and thereby reduce the amount of plasma exploding in to the diode region [13]. CsI coating produces

slower and/or more uniform cathode plasma through easier emission at lower electric field [13].

Presence of prepulse in the pulse power systems [6, 16] poses some problem in the beam generation process. In order to achieve full voltage at the diode, impedance of the diode should match with the impedance of the pulse forming line. But the presence of prepulse could reduce the diode impedance significantly. In actual pulsed power systems, a voltage pulse of about 10%–30% of the main pulse voltage appears across the vacuum diode at about 300–800 ns before the arrival of the main pulse. This pulse is known as a prepulse and appears in the charging cycle of the Blumlein pulse forming line (PFL). This prepulse is produced due to the charging inductor connected between the central and outer electrodes of the Blumlein PFL. The prepulse voltage becomes more pronounced due to the imbalance of the charging lines of the Blumlein PFL. A bipolar prepulse voltage of $\sim \pm 90$ kV peak voltages has been recorded at the diode [17].

The onset of the prepulse prior to the arrival of the main pulse in the IREB diode leads to the evaporation of cathode whiskers and subsequent launching of significant amount of plasma and neutral vapors into the vacuum diode region. The plasma thus created affects the performance of the IREB generation significantly [16]. Due to the presence of the prepulse, a plasma with a density of 10^{13} cm⁻³ is produced in the diode gap [18]. This plasma is in addition to the plasma produced at the surface of the cathode ($\geq 10^{18}$ cm⁻³) when the main pulse appears across the gap [19, 20]. Accordingly the beam generation process is governed by the presence and movement of prepulse created plasma and the main plasma created at the cathode surface. In the past, beam generation studies were carried out in IREB diode in the presence of a prefilled plasma of different densities [21]-[25]. The beam generation mechanism in the

presence of a prepulse is not exactly the same as that of the earlier works on plasma filled diodes. Unlike the plasma filled diode, the prepulse initiated plasma is not homogeneously distributed within the AK gap of the IREB diode. In order to avoid effect of prepulse on IREB generation it has been suggested to use a prepulse switch [26] or increase the anode cathode gap [17] or reduce the prepulse voltage to a consistent level of less than 5% [27].

To understand the prepulse effect on the relativistic electron beam diode, beam generation experiment were carried out with various AK gaps and voltage. Beam generation and flow mechanisms in the diode are affected by the presence of the prepulse generated plasma in the AK gap. Experiments were carried out with same AK gap but with various cathode diameters and diode voltages. Experiments were also carried out with planar and annular graphite cathodes. Annular cathodes are used in self-magnetically pinched diodes to produce smaller diameter electron beams at the anode [28]. The shot to shot reproducibility of the diode voltage and current versus the prepulse generated plasma has been investigated for planar diode configuration.

It was also shown that there is a statistical correlation between emission uniformity and the shot-to-shot variation in diode current [31]. The perveance expression for the electron flow in the planar diode can be defined based on the Child-Langmuir (CL) “3/2” law [6]. The CL law is correct for nonrelativistic voltages and cathode dimensions much larger than AK gap. If the cathode radius is comparable with the diode gap, however, the diode perveance may be significantly larger [32] than that determined from the classical CL law. It was shown both theoretically [33] and experimentally [34] that a large percentage of the cathode can fail to take part in the emission process and yet the voltage and current can appear identical from the case in which the entire cathode contributes electrons to the emission process. Merely

measuring the current and voltage waveform may not be sufficient to estimate the emission uniformity [34]. But the current waveforms can provide some assessment of cathode emission uniformity if the data is of a statistical nature taken over large number of shots rather than examining single shot waveform shapes [31]. It was shown that the standard deviation and skewness of the current histograms increase as the cathode emission becomes less uniform [31]. Several factors may affect the perveance of the diode with explosive emission cathodes. The most important of these are the cathode plasma expansion, vacuum electric field [35], ion flow from the anode and electron backscattering [36].

IREB's from a planar diode has been used to generate HPM in an axial vircator [1] configuration using KALI 1000 pulse power system. HPM pulse has been successfully detected using wide band double-ridge horn antenna, RF cable and diode detector setup. The estimated HPM peak power was ~ 59.8 dBm [~ 1 kW] (within the effective aperture area of the receiving antenna) at 7 m distance from the vircator window. The corresponding diode peak voltage and current was 256 kV and 9 kA respectively.

High Power Cylindrical diodes have been employed for intense relativistic electron beam generation in coaxial virtual cathode oscillator (Vircators) [37] and in high resolution radiography sources [4]. In order to enhance the conversion efficiency of High Power Microwaves the Coaxial Vircators have been proposed [37]. In fact, the coaxial vircator presents a cylindrical diode which consists of an annular cathode and grounded mesh anode. To understand the prepulse effect and plasma expansion characteristics on the cylindrical electron diode experiments were carried out with various AK gaps and voltages. The shot to shot reproducibility of the diode voltage and current versus the prepulse generated plasma has

been investigated. The intense electron beam generation studies have been carried out in the cylindrical electron beam diode when subjected to a high voltage bipolar pulse.

Finally IREB's from a cylindrical electron beam diode has been used to generate HPM in a coaxial vircator [37] configuration using KALI 5000 pulse power system in the presence of significant prepulse voltage. The HPM radiation was received by a double-ridge horn antenna located a distance 4 meter away from the output window and after suitable attenuation given to a diode detector. For 1.2 cm diode gap HPM has got more peak power as the diode detector was getting saturated even when the antenna has been placed at around 4.5 meter distance from the vircator output window. At this place the measured HPM peak power was more than 20 dBm (within the effective aperture area of the receiving antenna).

CHAPTER 2

LITERATURE SURVEY

INTRODUCTION

This chapter presents a review of the literature available on the various aspects of the intense gigawatt relativistic electron beam generation and its application on High Power Microwave generation. The intense electron beam is generated using the metal, metal-dielectric cathode, from explosive emission plasma which is formed when the strong electric field $E \geq 10^7$ V/cm is applied to the AK gap. Velvet or carbon fiber cathodes are characterized by surface flashover plasma. Space charge limited electron emission occurs from the high density cathode plasma. When the intense electron beam hits the anode, an anode plasma is produced. These cathode and anode plasmas expand toward each other which causes the decrease in the diode impedance. The diode closure occurs later in the pulse duration due to the expansion of these plasmas. The plasma uniformity, space charge limited electron and ion emission from these cathode and anode plasmas and the associated self magnetic fields controls various process occurring in the high power vacuum diode. Section 2.1 describes space-charge limited electron emission from an expanding plasma cathode. The electrode plasma expansion and the impedance characteristic of the diode have also been included in this section. Section 2.2 describes multidimensional space-charge limited flow. Plasma-filled diode has been described in section 2.3. Section 2.4 describes effect of prepulse on intense relativistic electron beam generation. Electron beam quality and uniformity has been discussed in section 2.5. The shot to shot reproducibility of the electron beam diode and its effect on electron beam quality has been described in section 2.6.

Axial virtual cathode oscillator employed for high power microwave generation using the intense relativistic electron beams is presented in section 2.7. Various aspects of cylindrical electron beam diode and the coaxial virtual cathode oscillator have been described in section 2.8.

2.1 SPACE-CHARGE LIMITED ELECTRON EMISSION FROM AN EXPANDING PLASMA CATHODE

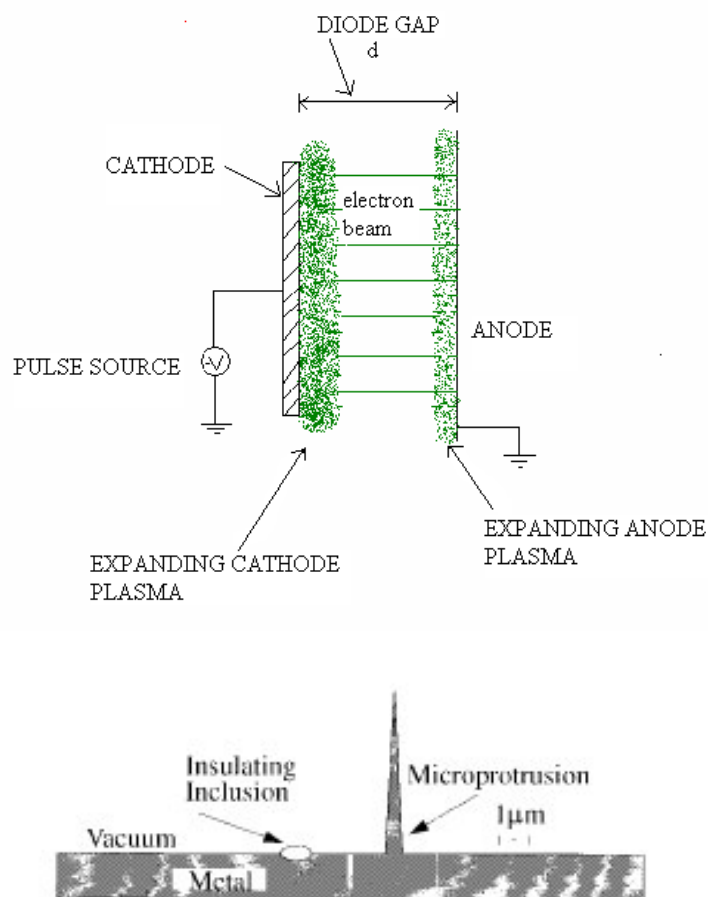


FIG. 2.1 High Power Electron beam Diode. Schematic geometries of typical sites of field enhanced electron emission.

The Relativistic Electron Beam Diode system consists of a planar, cylindrical or annular cathode and anode with a suitable gap enclosed in a vacuum chamber and connected to the pulse forming line. Fig. 2.1 shows the expanding cathode and anode plasmas in a planar high power electron beam diode. The anode is kept grounded. When a negative high voltage, short duration pulse is applied to the diode, a high electric field ($\sim 10^7$ - 10^8 V/cm) is produced at the cathode due to micro projections on the cathode surface. Electrons are pulled out of the surface by field emission. The micro projections blow up due to high local current density leading to rapid resistive heating and vaporization of cathode material. The vapour is easily ionized resulting in the formation of high density plasma near the cathode called ‘cathode plasma’. This cathode plasma spread over the cathode surface and acts as a rich source of electrons. This is known as Explosive Field Emission.

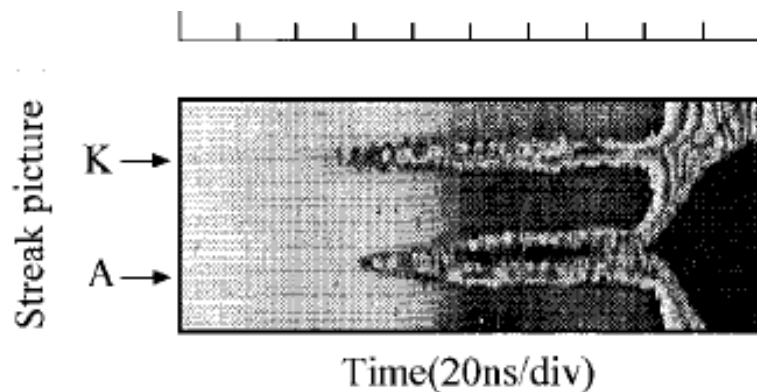


FIG. 2.2 luminosity of anode and cathode plasmas for the AK gap length of 5 mm using an annular cathode of outer radius 1.5 cm, 1mm thickness and an aluminum (Al) foil anode of 15 μ m in thickness (300 kV, 35 kA, 50 ns) [11].

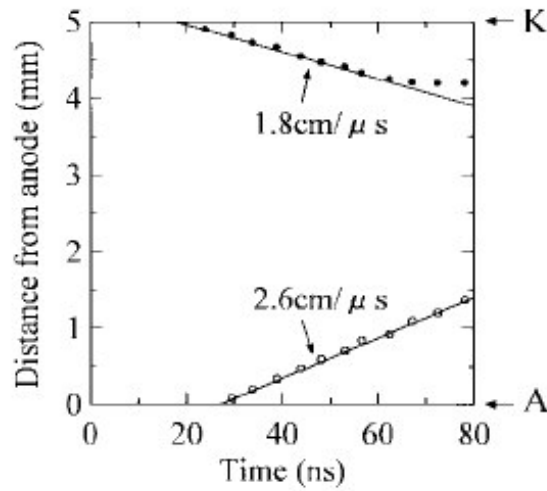


FIG. 2.3 Expanding plasma boundaries in the diode region as a function of time. Expanding plasmas are observed by their luminosity as shown in the previous figure [11].

The electron beam heats the anode material and causes desorption from the anode surface. The desorbed gases are rapidly ionized by the electron beam and by avalanching of the secondary electrons. Thus creating plasma near the anode surface called “anode plasma”. In general, around 0.2 kJ/g of the energy density deposited to the anode is enough to generate anode plasma. The plasmas expand radially and axially (typical expansion velocity of the plasma ~ 2-4 cm/ μ s which is ion acoustic velocity [38]) filling the gap with enough plasma to ‘short’ the diode. No beam current can be drawn after shorting. Figure 2.2 and 2.3 shows the expanding plasma boundaries in the diode region as a function of time [11]. The side-view images of plasma movement within the diode for the bare carbon fiber cathode are shown in Fig. 2.4. Fig. 2.5 shows the light emission from the diode with the CsI-coated carbon fiber cathode [39].

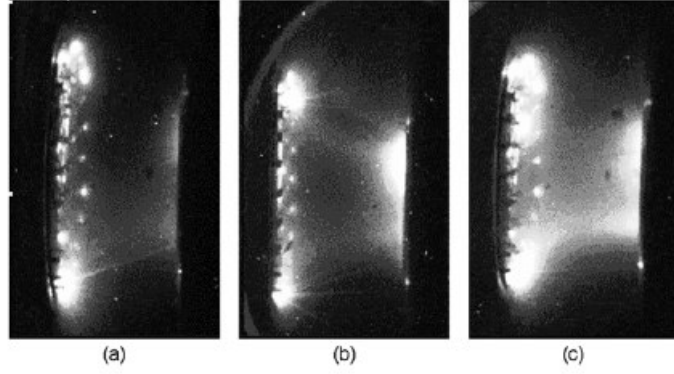


FIG. 2.4 Side-view images of plasma movement within the diode for the bare carbon fiber cathode. The anode appears on the right and the cathode on the left. Images (a), (b) and (c) were, respectively, captured at ~ 100 ns, ~ 200 ns and ~ 300 ns after the beginning of the HV pulse. The initial AK gap was 50mm and the anode was a stainless steel disc [39].

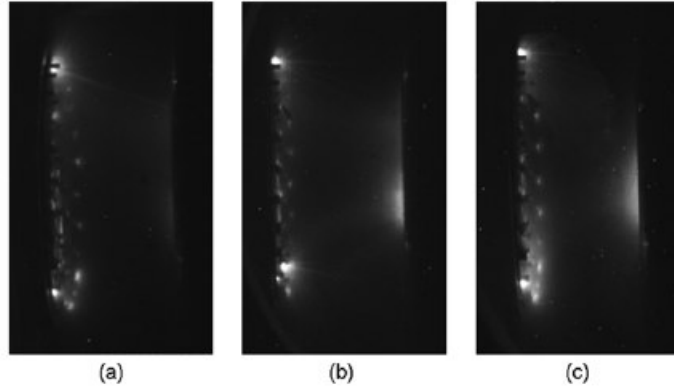


FIG. 2.5 Light emission from the diode with the CsI-coated carbon fiber cathode. Images (a), (b) and (c) were captured at ~ 100 ns, ~ 200 ns and ~ 300 ns after the beginning of the HV pulse, respectively. The anode appears on the right and the cathode on the left. The AK gap was 50 mm. Note that the light intensity increased only slightly as the voltage increased [39].

The diode current density j_e at time t during the pulse and total current I_e are given by the Child-Langmuir law [6, 47, and 48]. For a plane parallel diode consisting of a cylindrical cathode of radius ' r ' and a anode-cathode gap ' d ' the j_e and I_e are given by,

$$j_e = \frac{4\epsilon_0}{9} \left(\frac{2e}{m_e} \right)^{1/2} \frac{V^{3/2}}{(d-vt)^2} = 2.33 \times 10^{-6} \frac{V^{3/2}}{(d-vt)^2}, \quad (2.1)$$

and

$$I_e = j_e \pi r^2 = 2.33 \times 10^{-6} \frac{\pi r^2 V^{3/2}}{(d-vt)^2}, \quad (2.2)$$

where V is applied voltage, v is the plasma expansion velocity, t is the time during pulse at which j_e and I_e are measured; e and m_e are electron charge and mass. However, in Eq. (2.2) the radius of the emitting area of the cathode plasma assumes constant which is in not correct in major cases. In that case the radius r in Eq. (2.2) modifies as $r = r_0 + vt$, where r_0 is the initial emission radius.

The diode impedance Z_d is given by,

$$Z_d = \frac{V}{I_e} = \frac{136}{V^{1/2}} \frac{(d-vt)^2}{r^2} \quad (V \text{ in } MV) , \quad (2.3)$$

The perveance expression for the electron flow in the planner region of the diode can be defined by

$$P = \frac{I_e}{V^{3/2}} = 2.33 \times 10^{-6} \frac{\pi r^2}{(d-vt)^2} . \quad (2.4)$$

So the perveance is related to the effective diode geometry. If the electron flow remains unneutralized, the cathode emission area, the effective diode separation and the beam envelope are the only parameters which can affect the perveance. These interpretations are strictly valid only in the nonrelativistic limit. But the error associated will be small if the electron kinetic energy is less than 500 KeV [40].

The plasma expansion largely determined by the thermal and electrical properties of the cathode material (which determine the specific energy required to cause cathode flare formation) as indicated in Eq. (2.5), which has been found to give good agreement with experiment [41] if the resistivity is taken to be in the range 30–100 times its room temperature value.

$$v = \sqrt{\left[\frac{4\lambda_A}{\lambda_A - 1} \right]} E, \text{ where } E = \frac{j^2 t_d \kappa}{\pi^2 \rho} \quad (2.5)$$

λ_A	adiabatic parameter, 1.24 [42] for a plasma (1.67 for atomic gas);
κ	resistivity;
E	thermal energy (per unit mass) heating the solid whisker;
j	emission current density;
t_d	transition time to explosion;
ρ	density of the cathode material.

Information about the velocity, creation time, and closure rate of the diode plasmas emerging from the electrode surfaces has been measured by streak cameras [11] and by detail analysis of the diode perveance and impedance variations with time [40]. Fig. 2.6 illustrates plasma expansion velocity calculated from the temporal behavior of the diode perveance [40]. Double-exposure interference holography has been used to measure the temporal and spatial dependence of plasma densities and velocities in IREB diodes [43]. The exposure variation of the fringe pattern and motion of plasmas between pictures taken at different times during the pulse have indicated plasma velocities vs spatial position that varies from 10^6 to 10^7 cm/sec [43]. In the near-UV range the plasma expansion speed in vacuum IREB diode has also been measured by the Doppler-shift and by the time-of-flight methods [38]. The maximum observed speed of 2.4×10^7 cm/sec for the C^{+3} ions lead to the estimation of the electric field probably in the range of 1-6 kV/cm.

Maenchen et. al. [44] using interferometry, observed velocities of upto 30 cm/ μ s in axial plumes of anode plasma in a pinch-reflex diode operating at 1.5 MA and 1.5 MV. In an applied B-ion diode (1.7 MV, 1.7 MA) Johnson et al. [45] have reported that an expansion velocity of 5 to 10 cm/ μ s throughout the voltage pulse was required for their surface-flashover anode plasma in order to explain the temporal impedance decrease. In higher power diodes the

higher plasma-pressure gradient may result in a fast plasma expansion [46]. Expansion velocities of 5 cm/ μ s correspond to the ion thermal velocity of 25-eV protons.

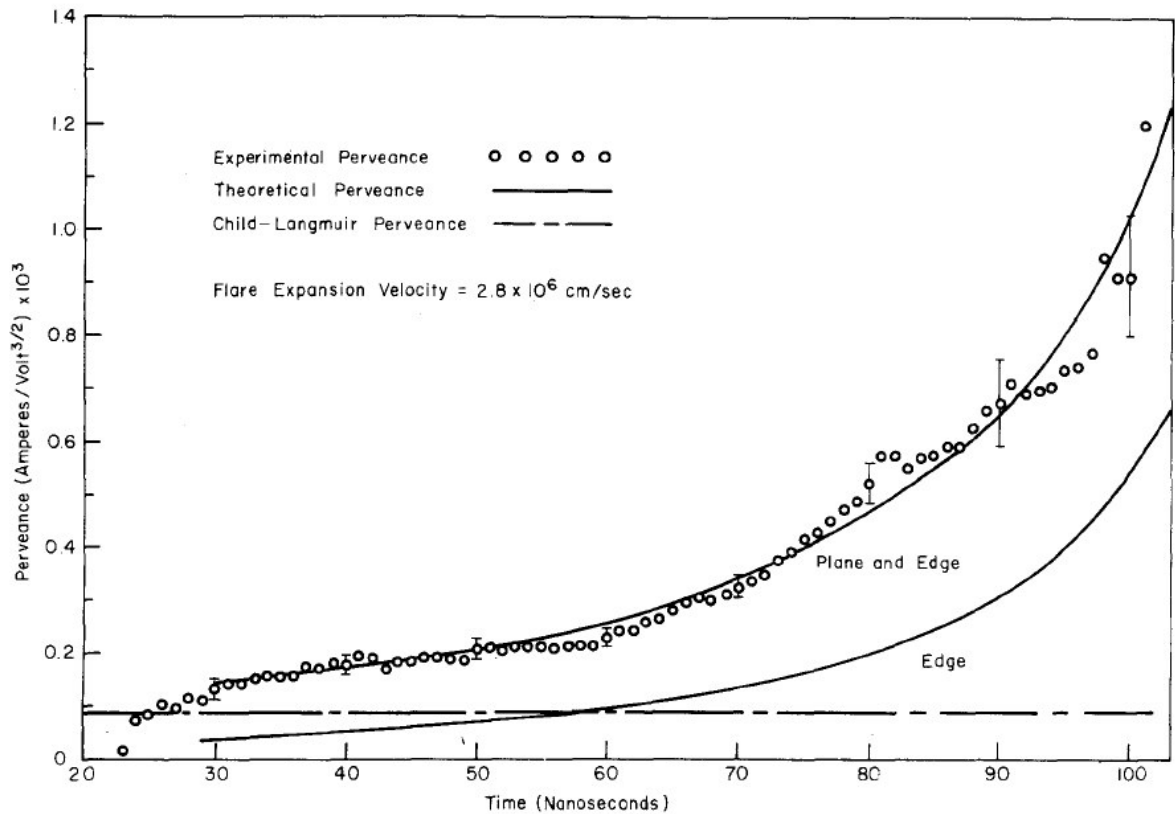


FIG. 2.6 Plasma expansion velocity calculated from diode perveance. A best fit was obtained when the plasma velocity was set equal to 2.8 cm/ μ s [40].

2.2 MULTIDIMENSIONAL SPACE-CHARGE LIMITED FLOW

Space-charge-limited (SCL) flows in diodes have been an area of active research since the pioneering work of Child and Langmuir [47, 48] in the early part of the last century. Indeed, the scaling of current density with the voltage to the 3/2's power is one of the best-known limits in the fields of nonneutral plasma physics, accelerator physics, sheath physics, vacuum electronics, and high power microwaves. The physics of SCL flows and emission appear throughout the literature of plasma physics. These theories, however, focus typically on SCL

flows in one-dimension only. Recently lot of studies has been carried out to extend the classical Child-Langmuir law to finite dimension [49].

Recent particle-in-cell (PIC) Calculations [50] have shown that for a spatially constant current density strip the true limiting current can exceed the one dimensional limiting current by a significant degree. These calculations used an emission method called ‘‘overinjection.’’ A current density, that is constant over the entire strip w , is emitted into the diode. This current density J is progressively increased until a virtual cathode is observed. In other words, the calculations are repeated until the greatest current is found that allows the beam to propagate without reflected particles. This current is then interpreted as the limiting current as it satisfies the original expectations of Child and Langmuir, namely the largest current with laminar, steady-state flow. This case have relevance to various physical emission mechanisms, such as thermionic and photoemission, where the maximum emitted current density is specified by conditions other than the applied voltage (i.e., when not running completely space charge limited).

The enhancement in constant current density that can be injected over a finite strip on the cathode without virtual cathode formation can be synthesized from the PIC data in the following empirical scaling law: [50]

$$\frac{J_{CL}(2-D)}{J_{CL}(1-D)} = 1 + \frac{0.3145}{w/d} + \frac{0.0004}{(w/d)^2}, \quad (2.6)$$

for w/d as small as 0.1. Equation (2.6) clearly recovers the Child–Langmuir result in the one-dimensional limit as w/d goes to infinity. Lau recently derived a similar result from first principles for the case of w/d on the order of one or greater where the last term in Eq. (2.6) is negligible [51]. For a planar strip, he found $J_{CL}(2-D)/J_{CL}(1-D) = 1 + (d/w\pi)$. The agreement

with Eq. (2.6) is excellent. Furthermore, he extended the theory to describe other geometries, the most important being a circular patch of radius R . In this case, the scaling becomes $J_{CL(2-D)}/J_{CL(1-D)} = 1 + (d/4R)$. PIC calculations similar to Ref. 50 verified this scaling for R/d on the order of one and greater. Equation (2.6) and the analytic results presented herein given valuable rules of thumb for the onset of virtual cathode formation in two-dimensional flows.

PIC calculations are carried out to find out the current and the current density of a finite-width, space-charge-limited electron beam in two-dimensional, parallel-plate geometry [32]. The results obtained show that the total current follows a universal function of the dimensionless parameter w/d that can be described empirically as

$$I = 1 + \frac{0.23033}{w/d} - \frac{0.00665}{(w/d)^2}, \quad (2.7)$$

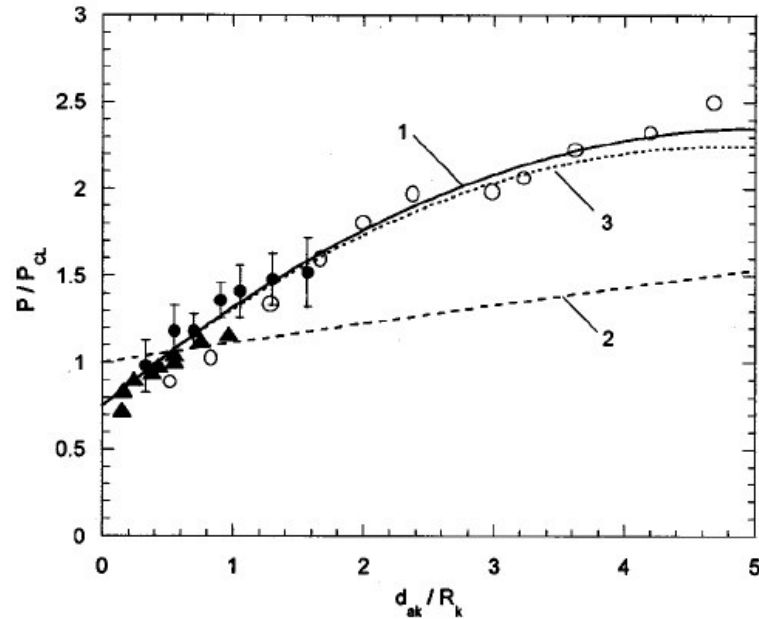


FIG. 2.7 Variation of the diode perveance P normalized to Child–Langmuir values P_{CL} with the dimensionless geometrical parameter d_{ak}/R_k . Data obtained with 20 (open circles), 60 (full circles), and 100 mm (triangles) diameter velvet explosive emission cathodes are shown. The fitting curve (solid line 1) is calculated in accordance with Eq. (2) in Ref. 36. The dashed line 2 is a result of a PIC modeling of the finite width, infinite length diode (See Ref. 32). The dotted curve 3 is calculated from Eq. (2.7).

At present, there is no analytical theory for the most commonly used planar diodes with circular cathodes that would allow determination of perveance P at arbitrary AK gap d_{ak} and cathode radius R_k . An experimental investigation of the explosive emission planar diodes with R_k comparable to d_{ak} therefore becomes important for the analysis of experimental data and for validation of theoretical models. The dependence of P/P_{CL} on d_{ak}/R_k that combines all of the experimental data obtained with 20, 60, and 100 mm-diameter velvet cathodes is shown in Fig. 2.7. A good matching of the simulation curve Eq. 2.7 with experimental data could be obtained in the relation [36]

$$\frac{P}{P_{CL}} = a_0 \left[a_1 + b_1 k \left(\frac{d_{ak}}{R_k} \right) + c_1 k^2 \left(\frac{d_{ak}}{R_k} \right)^2 \right], \quad (2.8)$$

where $a = 0.75$ as above, and $k = 7.2$ (see curve 3 in Fig. 2.7) While the coefficient a_0 takes account of the initial nonuniformity of the cathode emission, the coefficient k allows the 2D simulation results to be applied to the 3D diode configurations.

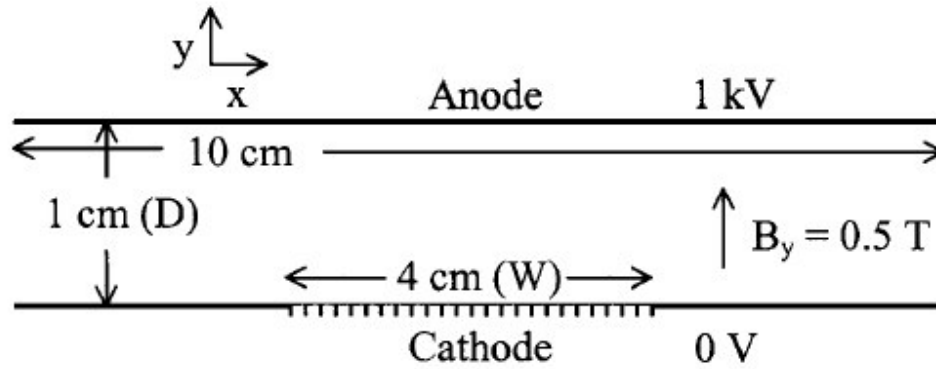


FIG. 2.8 Geometry and relevant parameters for the baseline 2D emission simulation [33].

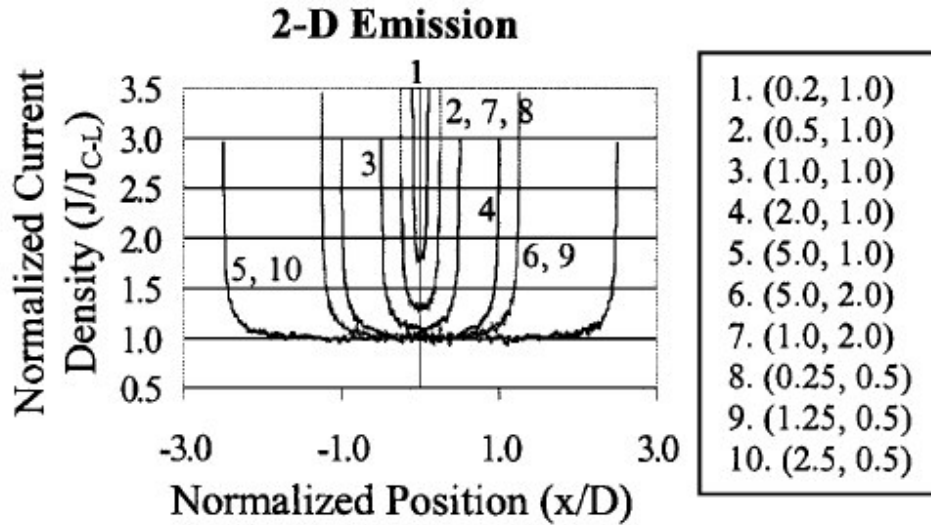


FIG. 2.9 Simulated normalized current density emitted at cathode versus position (normalized to gap distance) for a variety of emission strip widths (W) and gap distances (D) in cm; each trace is labeled with its corresponding (W, D) value [33].

Figure 2.9 shows the current density emitted at the cathode surface (normalized to the analytic 1D Child-Langmuir value) as a function of position along the cathode (normalized to AK gap distance) for a sampling of emission strip widths (W) and gap distances (D) [33]. FIG. 2.8 displays the geometry and relevant parameters for the baseline 2D emission simulation [33]. At the beam edge of a flat cathode, there exists no space charge just outside the beam in order to help drive the normal electric field at the last emission point to zero; thus, one can posit that extra space charge is emitted (above the 1D Child-Langmuir limit) in order to help drive this local field down. From the scans it is apparent that these high current density “wings” at the beam edge scale with the emission strip width divided by gap distance, W/D (i.e., scans with the same W/D value overlay on the graph). In addition, as the emission strip narrows ($W/D \leq 1$), even the current density at the center of the beam begins to rise above the analytic 1D predicted value. (Such W/D scaling was previously seen by Luginsland *et al.* [50] when simulating *uniform* current density transported in a comparable 2D geometry. Emitted current

density wing structure is independent of applied magnetic field, B_y , for tested values of 0, 0.05, 0.1, 0.5, and 0.8 T.

To examine how these increased current density wings might affect total current, emission from some portion of the cathode has been suppressed in two different fashions and changes in the total current has been monitored. In the first method, the baseline 4-cm-wide emission region has been divided into 40 separate, equal-width subregions. As the portion of each subregion that is allowed to emit systematically decreased, little effect is seen on the total current emitted until nearly all of the cathode emission area has been turned off. This behavior is shown in the upper trace of Fig. 2.10.

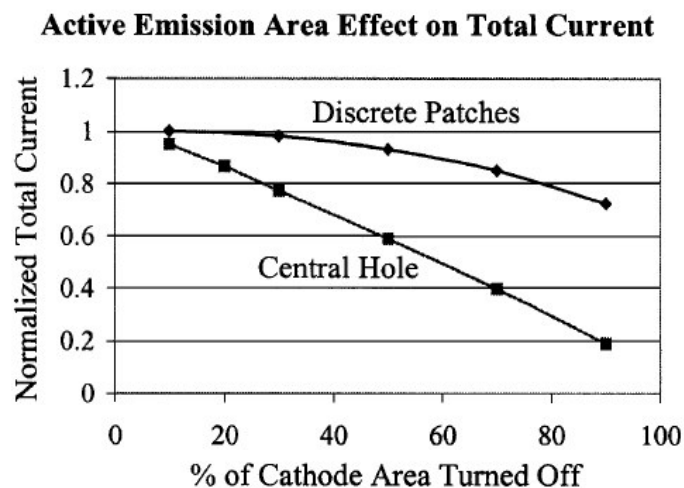


FIG. 2.10 Reduction of total emitted current due to the reduction of an allowed emission area on a 4-cm-wide cathode strip. The current is normalized to the simulation result for emission from 100% of the cathode area. The cathode is divided into 40 individual sections which are gradually turned off (discrete patches), or a sole nonemitting hole is allowed to expand from the cathode center (central hole) [33].

Almost 80% of the full emission area current can be supplied by a mere 20% of emitting cathode area due to the ability of the enhanced current density wings to compensate for the paucity of emission area. In the second method, this effect was further examined by suppressing emission from only a central portion of the cathode. The nonemitting portion was

gradually increased in size as the total current was monitored (also shown in Fig. 2.10). From the figure it is clear that the 2 sets of wings present at the two edges of the nonemitting portion cannot compensate for the nonemitting area nearly as well as the 40 sets of wings available in the discrete patches case. Such an effect has direct relevance to understanding space-charge-limited emission from explosive emission cathodes, plasma cathodes, ferroelectric cathodes, photocathodes, and even thermionic cathodes (if operating well above the temperature limited regime). Ferroelectric emission is electron emission from the plasma formed at the surface of ferroelectric as a result of non-complete surface discharges [33a]. *Many small portions of the emission surface may be completely inactive before a significant change is detected in the observed total current.* In a plasma-based cathode (including explosive or ferroelectric emission) such an effect may be masked due to plasma filling in the gaps between emission sites. Nevertheless, as these cathodes are driven into regimes where the plasma is cooler and less dense, the total current emitted is not expected to change even if the plasma no longer completely fills the gaps between emission sites. This effect must be taken into account when developing an understanding of a plausible death mechanism for such cathodes. If a sole region ceases to emit and then continues to enlarge in area, one would expect to see a nearly linear reduction in the total current. If the emission is instead being provided by numerous microsites, many such sites could be turning off and on multiple times during the life of a given cathode with little or no effect on the observed total current.

It was found experimentally that a large percentage of the cathode can fail to take part in the emission process and yet the voltage and current can appear identical from the case in which the entire cathode contributes electrons to the emission process [34]. Three cathodes are reported, each cathode has a corona bushing surrounding the emitting surface. The inner

diameter of the bushing is 14.9 cm, and the width of the bushing annulus is 2.8 cm and the axial thickness of the bushing is 2.54 cm. The bushing has a full radius in the axial dimension. The bushings for these short pulse lengths are aluminum which has been painted with Glyptol paint.

Therefore, the electron emission in high-current diode almost always occurs from the plasma boundary according to the space charge law. The currents which are obtained "above" space-charge law is simple due to edge effect, i.e., non validity of ID approximation and, respectively, larger current of electrons is required to screen enhanced electric field.

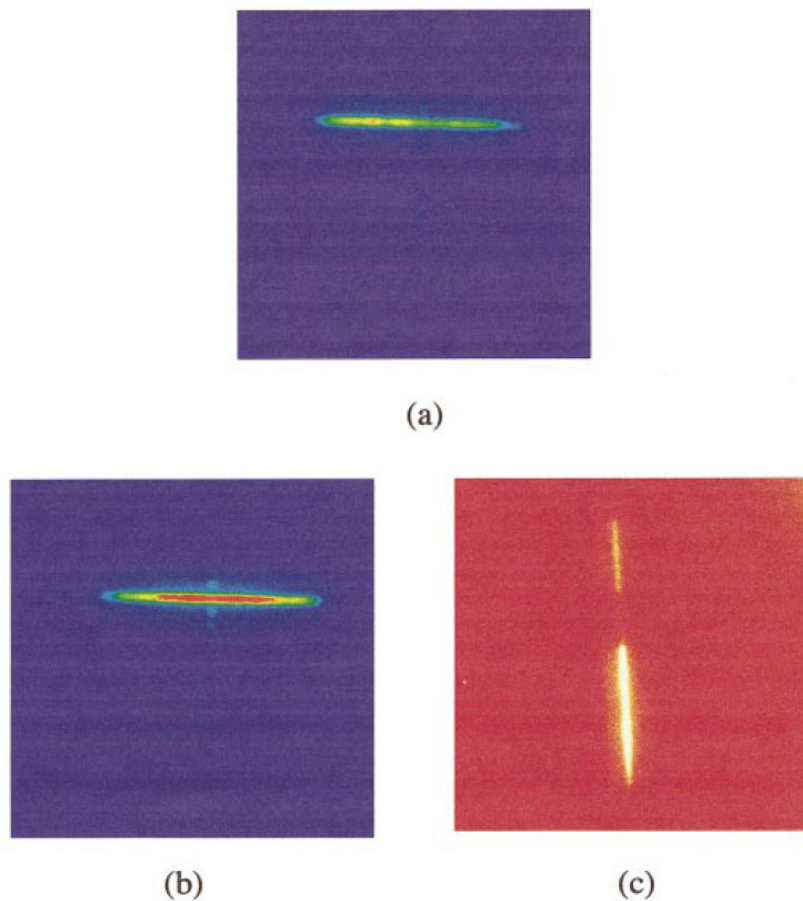


FIG. 2.11 Optical images showing the electron beam uniformity for each cathode: (a) the velvet cathode, (b) the tufted carbon fiber cesium iodide cathode, and (c) the carbon slat cathode. Note that the slatted cathode has very nonuniform emission, although the current wave form for it is nearly identical to the two cases of more uniform emission.

The significant feature of these results is that while the emission area can vary considerably between three cathodes, the current amplitude can be the same and nearly indistinguishable merely by measuring the total current (Shown in Figs. 2.11 and 2.12). This result is consistent with theoretical results described above, which indicate that edge effects play a significant role in the emission process [33]. In particular, the field enhancement at the edges where there is no emission offsets the lack of emission in other regions of the cathode. Therefore, it is not necessary to conjecture extensive plasma formation on the cathode surface to achieve space charge limited flow. Further, it is notable that merely measuring the current wave form may not be sufficient to estimate emission uniformity.

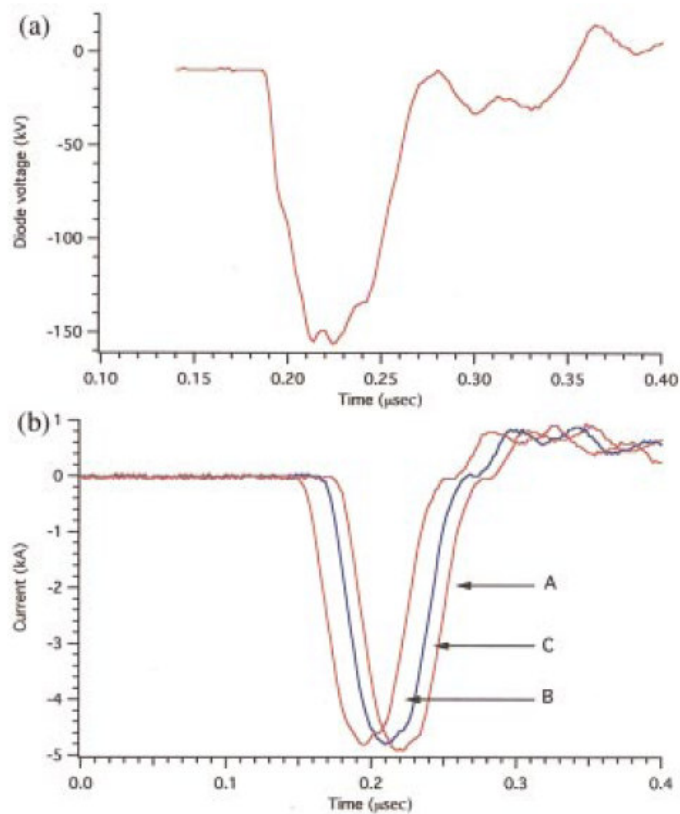


FIG. 2.12 Current and voltage traces from the experiment: (a) applied diode voltage, (b) current traces for the three cathodes. A is the velvet cathode, B is the tufted carbon fiber cesium iodide cathode, and C is the carbon slat cathode. Note the similarity in the current wave forms for the same applied voltage.

2.3 PLASMA-FILLED DIODE

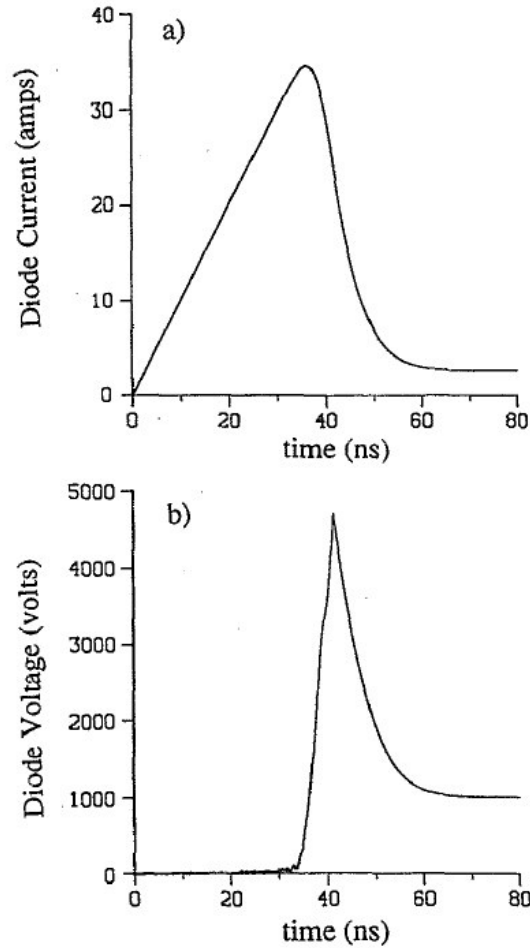


FIG. 2.13 (a) Diode current and (b) diode voltage drop obtained from Particle in Cell simulation for case with spatially uniform plasma density $n = 10^{13} \text{ cm}^{-3}$ hydrogen plasma fill and SCL electron emission from cathode surface [24].

In plasma filled diode (PFD) the injected plasma initially causes the vacuum diode to behave like a short circuit. As the diode current increases, some combination of magnetohydrodynamics (MHD) effects, plasma thinning, and plasma erosion cause the diode impedance to increase [24]. If the initial plasma density is low, the diode can increase to its vacuum impedance. If the initial plasma density is high, a small effective AK gap can form that allows the diode to operate at much lower impedance than possible with the initial vacuum

gap. A typical diode current and diode voltage drop obtained from Particle in Cell simulation for case with spatially uniform plasma density $n = 10^{13} \text{ cm}^{-3}$ hydrogen plasma fill and SCL electron emission from cathode surface is shown in Fig. 2.13 [24].

The high voltage opening phase of a PFD with an emitting cathode can be described by the following arguments. When a high voltage is applied at the anode cathode gap containing low density plasma a collisionless sheath form over the cathode [24, 21]. At low currents flow is one dimensional and the behavior can be explained by a one dimensional model. Electron emission occurs from the high density cathode plasma via field emission and whisker-explosion mechanisms as discussed in the previous section.

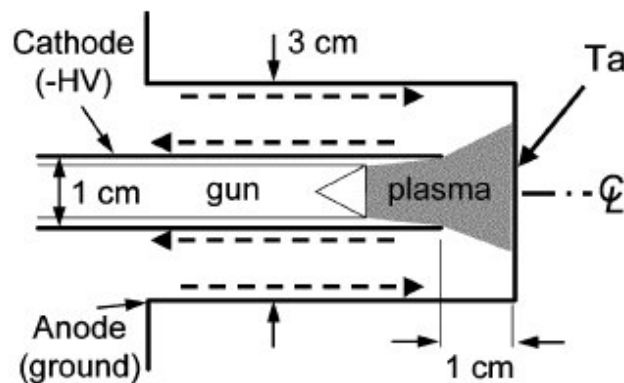


FIG. 2.14 PFD configuration tested on Gamble II. Dashed lines indicate current flow direction [25].

The electrons in the plasma are initially repelled by the large negative potential of the cathode to some well defined distance, producing a transient sheath [52]. This occurs before the ions have time to respond to the applied potential. The bare ions, exposed in the transient sheath, are accelerated by the potential and rapidly absorbed at the cathode. The ion current then quickly becomes space charge limited. If the pulse duration is short enough compared to the reciprocal of the ion plasma frequency then a steady-state sheath will not form. Let us assume that our pulse duration is short and a sheath of thickness x exists between the cathode plasma

at voltage $-V$ and the field free bulk plasma. Across this sheath flow space charge limited ion and electron currents given by [21]

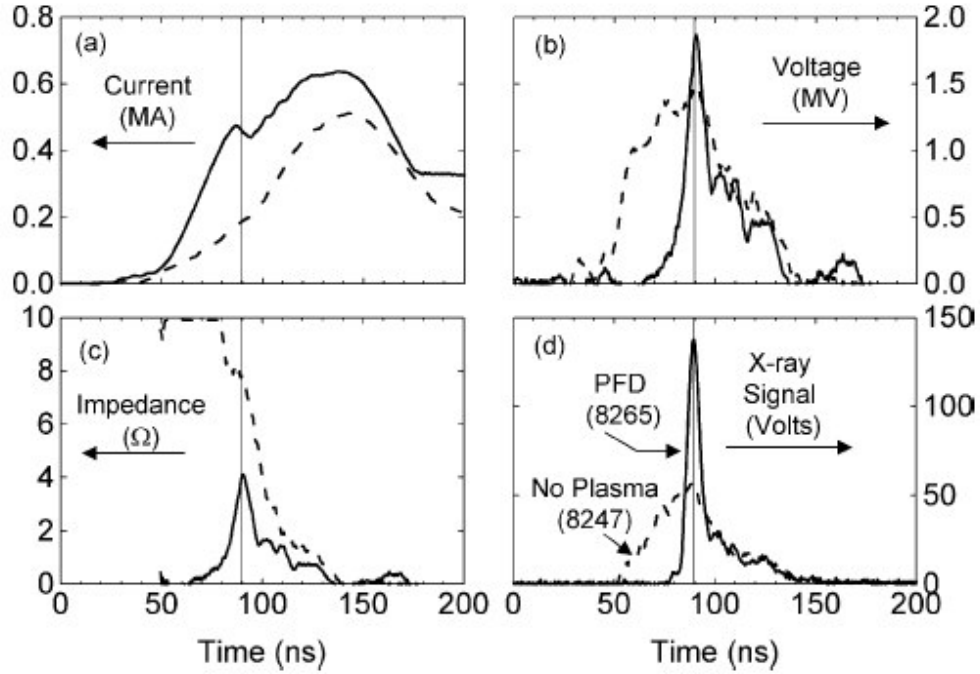


FIG. 2.15 Data from the highest dose-rate PFD shot on Gamble II (solid lines), compared with data from a shot with no plasma (dashed lines). (a) Generator current waveforms. (b) Diode voltage waveforms. (c) Diode impedance waveforms. (d) X-ray (dose rate) signals. The vertical line indicates the time of maximum X-ray signal for the PFD shot [25].

$$j_i = 1.86 \left(\frac{4\epsilon_0}{9} \right) \left(\frac{2e}{m_i} \right)^{1/2} \frac{V^{3/2}}{x^2}, \quad (2.9)$$

$$j_e = \left(\frac{m_i}{m_e} \right)^{1/2} j_i, \quad (2.10)$$

where m_i and m_e are the ion and electron masses, e is the electron charge, ϵ_0 is the vacuum permittivity.

If the ion current is much greater than the saturation current

$$j_{is} \sim ne \left(\frac{kT_e}{m_i} \right)^{1/2},$$

where n is the plasma density.

Then the sheath boundary must move into the plasma to provide ion flux given by

$$j_i = ne \frac{dx}{dt}. \quad (2.11)$$

But the short circuit phase of the PFD cannot be explained by the above argument [24]. Plasma-filled diodes have been employed for producing high dose-rate bremsstrahlung over small areas [25]. Fig. 2.14 shows PFD configuration tested on Gamble II pulse power generator. Fig. 2.15 displays the data from the highest dose-rate PFD shot on Gamble II (solid lines), compared with data from a shot with no plasma (dashed lines) [25]. Prepulse generated plasma can completely fill the diode gap if the anode cathode gap is small and the diode behaves as a PFD. PFD operation is very similar to plasma opening switch which was extensively investigated in many laboratories [25a].

2.4 EFFECT OF PREPULSE ON INTENSE RELATIVISTIC ELECTRON BEAM GENERATION

Beam generation studies were carried out in Sandia National Laboratories, U.S.A, with HERMES I (MV, kA, 100 ns) pulse power system in the presence of prepulse [53]. Figure 2.16 shows modelled Marx-Blumlein charging voltage and raw prepulse voltage on the Blumlein inner conductor, for a peak operating voltage of 1.7MV on PIM machine at AWE, UK[54].The erratic tube behavior was characterized by low impedance and unrepeatable spatial distribution of the electron stream. It was hypothesized that the prepulse voltage causes plasmas to form inside the tube. These plasmas then act as electron sources during the main pulse. Thus, the apparent geometrical shape of the cathode was not the electron emitting shape during the main pulse.

An experiment was conducted to determine the approximate voltage level at which the plasma formation occurs by simulating the prepulse voltage across a tube structure. A Marx generator

capable of generating 500 kV, 300 ns pulse was assembled and operated across the HERMES I X-ray tube. During the experiment the time coincidence between the voltage trace and the plasma glow was verified by a streak camera. A typical AK gap of approximately three inches was used for these experiments. A summary of data is given in Table. I

TABLE I. Voltage levels at onset of prepulse plasmas for various cathodes.

Cathode Type	AK Gap (in.)	Tube Pressure (Torr) x 10 ⁴	Average Breakdown (B.D) Voltage (kV)	<i>t_{eff}</i> (ns)
Single Sharp				
Needle	2-3/4	3.5	180	300
Multipoint				
Sharp Needles	3	3.6	180	300
Blunted				
Single Needle	3	4	250	300
Round Lucite				
Insert	3	2.3-2.5	170	400
Long Lucite				
Cathode	2-3/4	10	No B.D at 455 kV	> 2 μ s
Hemisphere End	2-3/4	2.8	No B.D at 460 kV	> 2 μ s

The conclusions from these tests were:

1. Considerable ionization can occur in the AK gap which distorts the apparent electron emitting shape of the cathode.

2. There exists at least a factor of three in the breakdown voltage between sharp pointed and smooth blunt cathodes.
3. Short blunt Lucite cathodes ionize at levels similar to sharp pointed metal rods.
4. Only a negative prepulse was used on these experiments. The prepulse actually alternates polarity and lower breakdown voltages probably occur during actual machine operation.

In subsequent experiments, a simple Hemispherical tipped or blunt cathode has been utilized to minimize plasma formations.

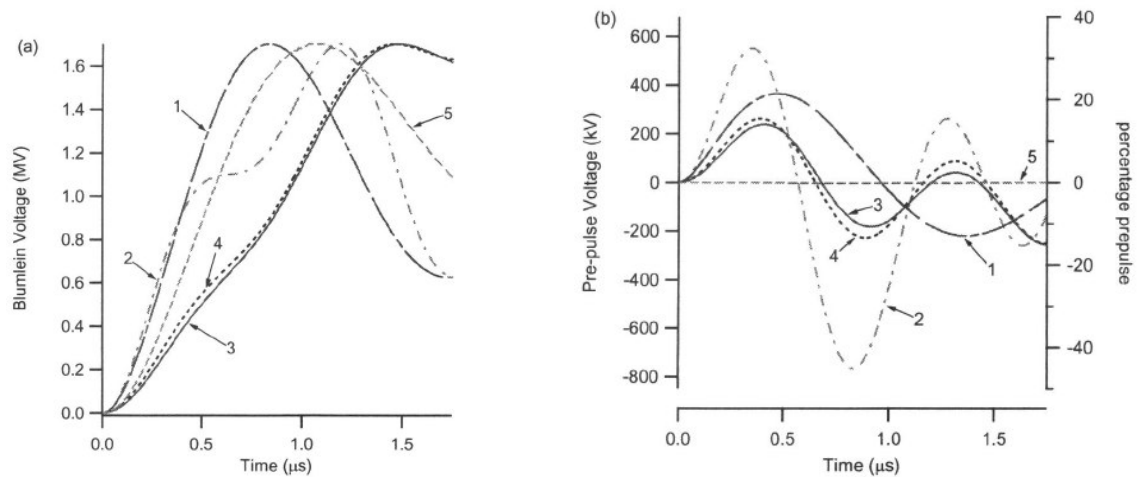


FIG. 2.16 Modelled (a) Marx-Blumlein charging voltage and (b) raw prepulse voltage on the Blumlein inner conductor, for a peak operating voltage of 1.7MV on PIM machine [54].

Another experiment has been carried out by D. A. Phelps et. al. [55] at Maxwell Laboratories, San Diego, California, U.S.A, to control impedance of the relativistic electron diodes with externally applied prepulse. In this paper, a technique for externally introducing a typically 100 kV, low power conditioning pulse prior to the main pulse of a low impedance relativistic electron diode is described. The typical electron beam parameter was 1 MV, 1 MA, 50 ns. For various cathode geometries, the breakdown field, closure velocity, and time-dependent

impedance established by this external prepulse is measured and compared with an empirical model of space charge limited emission from a hydro-dynamically expanding plasma. The best results were obtained with one and four ring razor blade cathodes which produced very symmetric emission for over 100 kV/cm stresses. The prepulse impedance collapses with a roughly 2.3 cm/ μ s closure velocity, producing a 15 Ω -25 kV diode just prior to the main pulse. After about 25 ns of the main pulse, Child's Law scaling predicts an 2 Ω impedance which is consistent with the data. Noticeably, the main pulse impedance collapses a little faster (about 4 cm/ μ s, probably due to the creation of anode plasma by the high current density).

Experimental evidence is presented that the high current accelerator impedance is effectively controlled by the relative time delay between the start of the prepulse and the main pulse. The reason for this impedance control lies in the fundamental emission efficiency, plasma closure velocity and approach to space charge limited emission of a given diode geometry in the presence of sufficient prepulse electric field. In addition to determining the proper pre-shot timing, this external prepulse is useful for checking the diode gap setting (since the closure velocity is repeatable to within 5 % if the emission efficiency is good); for checking the diode pressure near the cathode (i.e., the presence of local outgassing, that could ruin a shot, usually shows up as premature flashover of the prepulse insulator); and finally, for removing surface contaminants from the primary cathode-anode regions (the first few prepulse firings normally exhibit earlier gap closure than the quite repeatable subsequent shots-evidently due to the removal of volatile impurities).

Effect of prepulse has also been observed on ASTERIX [56] high voltage (6 to 7 MV), \sim 60 Ω , 50 ns pulse generator at Centre d'Etudes de Gramat (CEG) in Gramat, France. With 4 MV on the diode, a positive prepulse of 365 kV peak voltage $>$ 100 ns duration was predicted. The

peak occurred about 250 ns before the main pulse and generated an electric field on the cathode four times greater than the 100 kV/cm normally required to initiate plasma formation on the cathode surface. When operated without a prepulse switch the current oscillated between +500 to -1000 A starting about 500 ns before the main pulse. The diode impedance was near zero at the start of the main pulse and only increased to a peak of about 20 Ω during the pulse. This behavior was consistent with a plasma filled diode [24], the result of the prepulse current. The prepulse in the ASTERIX Rod-Pinch Diode Experiments has been minimized by a vacuum prepulse switch [56].

So there are some reports available on effect of prepulse on electron beam diode but those are done either by simulating the prepulse voltage across a diode structure [53] or by externally applied prepulse voltage [55]. Also many literatures are available on prepulse suppression by various techniques [16]. There are no reports available on systematic study of intense electron beam generation in the presence of prepulse.

2.5 ELECTRON BEAM QUALITY AND UNIFORMITY



(a)



(b)



(c)

FIG. 2.17 (a) Needle-shaped annular carbon fiber cathode. (b) Photo of nylon target bombarded once by beam emitted by a stainless steel cathode. (c) Photo of nylon target bombarded once by beam emitted by a needle-shaped annular carbon fiber cathode [2].

Quality and uniformity of the electron beam is an important factor in context to its usefulness in high power microwave generation [2, 29]. Experimental results show that the carbon fiber cathode can improve the electron beam quality and dramatically enhance the beam-to-microwave efficiency of the reflex triode vircator [2]. It was found that the beam-to-microwave efficiency increased from about 4%–6% in the case of the stainless steel cathode to over 10% in the case of the carbon fiber cathode. Experimental results indicate that the plasma forming on the carbon fiber cathode is more uniform as a result of the surface flashover discharge along the whole surface of the carbon fiber. But, the electron emission of the metal cathode is confined to the tips of the emitters on the cathode, which obviously differs from the electron emission mechanism of the carbon fiber cathode. In addition, the slower plasma expansion velocity was achieved with the cathode made with carbon fibers, and the electron beam extracted from the carbon fiber cathode has a higher quality than the case of the stainless steel cathode [2]. Fig. 2.17 (a) shows needle-shaped annular carbon fiber cathode. Fig. 2.17 (b) displays the photo of nylon target bombarded once by beam emitted by a stainless steel

cathode and the Fig. 2.17 (c) shows the photo of nylon target bombarded once by beam emitted by a needle-shaped annular carbon fiber cathode [2].

Several key factors must be present to achieve a low-emittance electron beam, not the least of which is a uniform electric field across the emitting surface of the cathode [57]. Cathodes that emit nonuniformly have large nonuniformities in the electron space charge, independent of the emission mechanism. Hence, the radial-electric field across the cathode surface is also nonuniform, as required by the boundary conditions between regions of high and low space charge. Cathodes with poor uniformity develop large radial-electric fields at the emission surface. These electric fields impart transverse momentum to the electrons as they accelerate toward the anode, increasing the emittance. It was shown that, the cathodes with the lowest turn-on field for emission exhibited the best uniformity and the lowest emittance [29]. The cesium iodide (CsI) coated carbon fiber cathode is compared to polymer velvet, metal-dielectric, and carbon-slat cathodes. However, most of the cathodes typically suffers from large amounts of outgassing, nonuniform emission, and very high emittance.

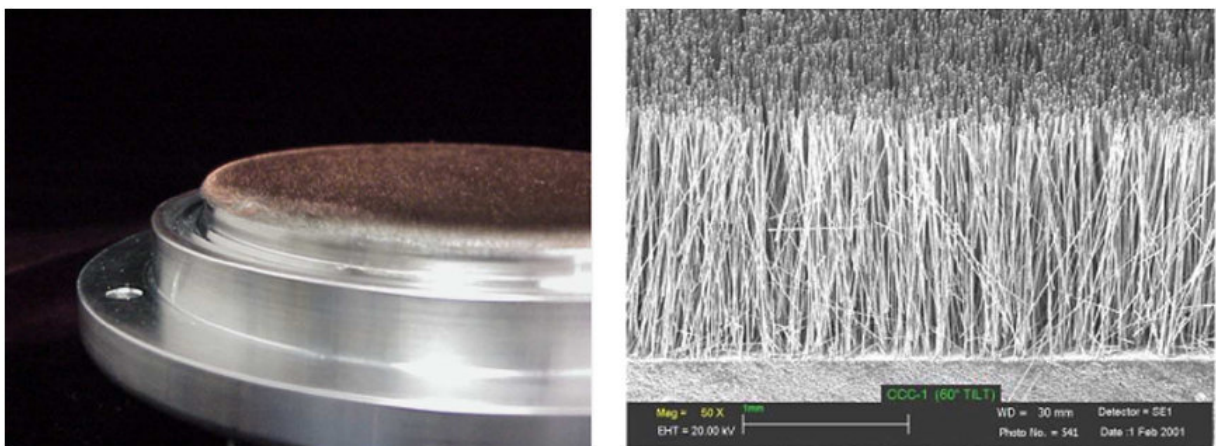


FIG. 2.18 (a) Macroscopic photograph and (b) SEM image of the CsI carbon fiber cathode. The cathode consists of carbon fibers that have been attached to a carbon surface. These fibers are then coated with a CsI salt. The SEM is at 50-times magnification with the fibers of $6\text{-}\mu\text{m}$ diameters [59].

The CsI-coated carbon fiber consistently shows the best emission uniformity of all four cathode types [29]. It was shown that, the uniformity and emittance are related for all of these cathodes. In general, the more uniform the electron emission, the lower the emittance of the cathode. The CsI coating makes a significant improvement over the uncoated cathodes. Cesium iodide serves to eliminate impedance collapse, as well as to reduce the turn-on field and greatly reduce the neutral outgassing. Furthermore, the CsI coating eliminates flaring on the cathode surface, thus improving the uniformity of the emission. The reduction of nonuniformities acts to reduce the normalized emittance for the cathodes [58]. Figure 2.18 shows macroscopic photograph and SEM image of the CsI carbon fiber cathode. The cathode consists of carbon fibers that have been attached to a carbon surface. These fibers are then coated with a CsI salt. The SEM is at 50-times magnification with the fibers of 6- μm diameters [59].

The main advantages of the carbon-fiber cathode are its nanosecond timescale turn-on, relatively good vacuum compatibility, long lifetime, and the unnecessary of an additional power supply for its ignition. However, in spite of the intensive experimental research carried out by different groups, the nature of the electron emission (either field emission or plasma emission) has still remained unclear [59a, 59b, 59c]. The same concern is related to the influence of CsI coating on the carbon-fiber cathode operation. For instance, in the recent review by Shiffler *et al.*, [59] both emission phenomena are used to characterize the operation of the CsI coated carbon-fiber cathode.

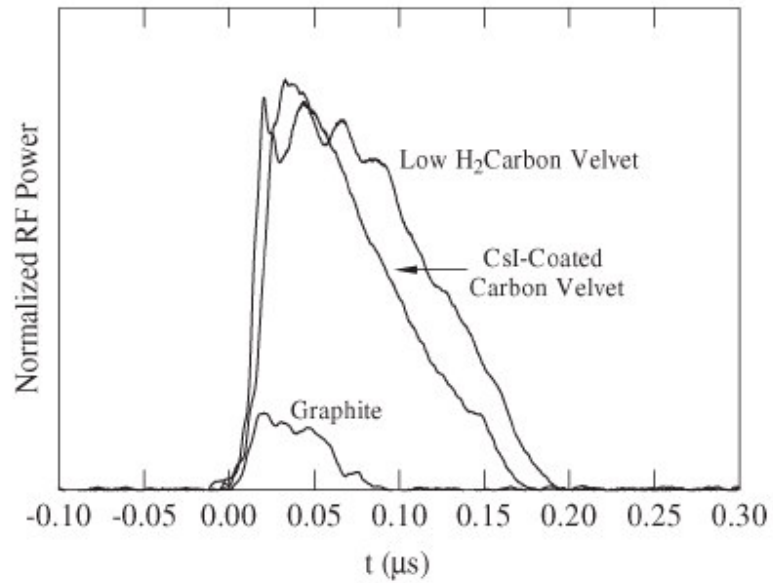


FIG. 2.19 AFRL relativistic magnetron normalized average (rms) RF power waveforms for the cases of POCO graphite, CsI-coated carbon velvet on a graphite substrate (conventional processing), and uncoated low-hydrogen carbon velvet on a graphite substrate (high-temperature processing) cathodes [59].

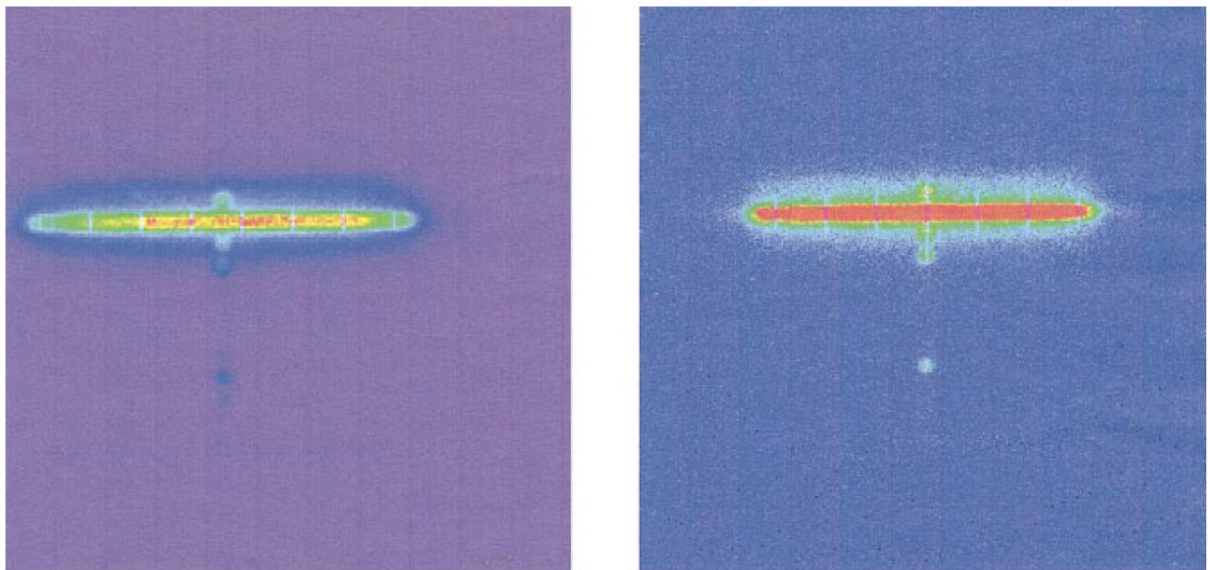


FIG. 2.20 Uniformity data from an uncoated (a) and a CsI coated (b) carbon-on-epoxy cathode. Regions of intense are red and regions of low emission are blue. The uncoated cathode shows flaring, or nonuniform emission [58].

Figure 2.19 shows AFRL relativistic magnetron normalized average (rms) RF power waveforms for the cases of POCO graphite, CsI-coated carbon velvet on a graphite substrate (conventional processing), and uncoated low-hydrogen carbon velvet on a graphite substrate (high-temperature processing) cathodes [59].

Several, research have been performed on carbon fiber cathodes [60]-[63]. These cathodes have consisted of either bare carbon fiber or carbon fiber with a coating of cesium iodide (CsI) [64]-[66]. CsI not only is well known as an emitter of ultraviolet (UV) radiation when stimulated properly, but also has the advantage that the cesium has a very low first ionization potential of 3.89 eV [67]-[70]. Carbon fiber has the advantage of low outgasing, which keeps the gas evolution and thus plasma formation in the diode to a minimum [39, 71]-[73]. The addition of the CsI and its subsequent UV emission and low ionization potential contributes to the photoemission and field emission of electrons early in the diode voltage pulse. These emitted electrons allow the diode to turn on quickly and uniformly, presumably limiting the effects of explosive emission and plasma formation in the diode. Thus, CsI-coated carbon fiber cathodes would appear to have many good characteristics as electron emitters for long pulse cathodes [66, 74]. Figure 2.20 displays uniformity data from an uncoated and a CsI coated carbon-on-epoxy cathode. Regions of intense are red and regions of low emission are blue. The uncoated cathode shows flaring, or nonuniform emission [58]. However it is still doubtful that UV emission influences on plasma formation and electron emission [59a]. Coating by CsI simply allows one to achieve more uniform flashover surface plasma formation and heavy Cs and I ions make this plasma expansion slower [59a].

Figure 2.21 displays false-color images of the cathode plasma generated by explosive emission processes in a vircator high-power microwave source (300 kV, 5-8 kA, 60 ns). Three different

cathode materials are shown [75]. The images show the plasma formation to be fairly uniform across the surface of all three cathode types.

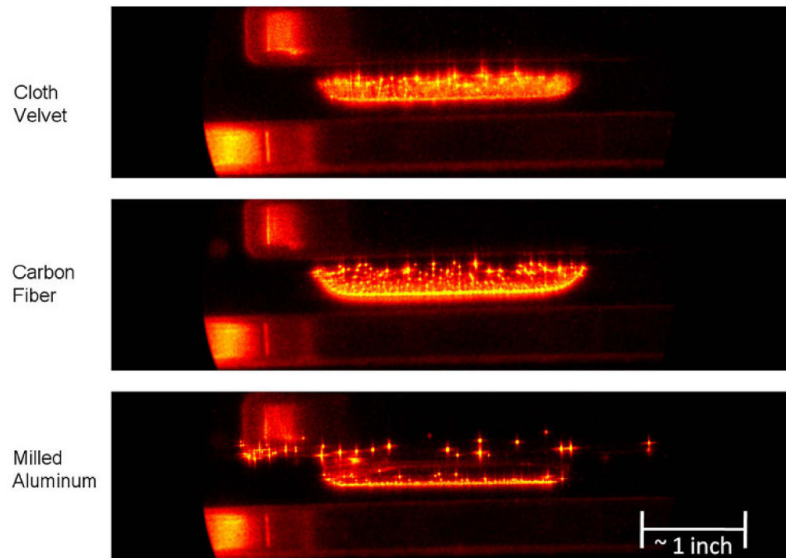


FIG. 2.21 False-color images of the cathode plasma generated by explosive emission processes in a vircator high-power microwave source (300 kV, 5-8 kA, 60 ns). Three different cathode materials are shown. The camera intensifier gate width was 200 ns. Each cathode was attached to a brass plate which is located at the top of each image. The anode structure is seen at the bottom of each image. The spacing between the anode and cathode was 10 mm. The images show the plasma formation to be fairly uniform across the surface of all three cathode types. The light emission from the brass attachment plate in the milled aluminum cathode case indicates that differences in either the delay time or peak voltage required for emission for this particular cathode design allowed points on the brass to explosively emit [75].

Spatial uniformity of electron emission from velvet cathodes has been measured by observing the distribution of electrons hitting the anode in a planar high-voltage diode [76]. It is shown that unless all electrons move parallel to the diode axis, the electron distribution measured at the anode does not represent the cathode emission pattern. Here, parallel trajectories were achieved by applying a strong, uniform axial magnetic field. A 5 ns gated ICCD camera recorded light from a fast anode scintillator. The emission from two brands of velvet was found to be mostly concentrated in small spots with density of about $55/\text{cm}^2$. The pixel-to-pixel standard deviation of the emission amounted to at least 16%. Figure 2.22 shows images of the anode scintillator with magnetic field and without magnetic field.

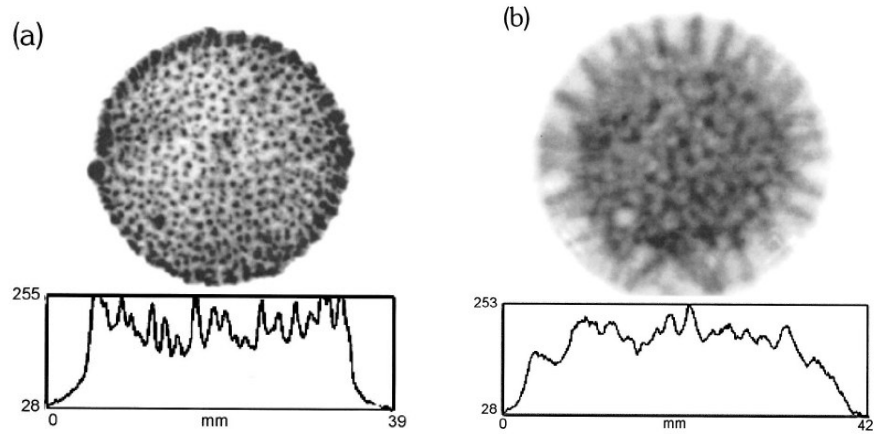


FIG. 2.22 Images of the anode scintillator: (a) with magnetic field; (b) without magnetic field. Line profiles shown were taken along horizontal diameters [76].

2.6 THE SHOT TO SHOT REPRODUCIBILITY OF THE ELECTRON BEAM DIODE

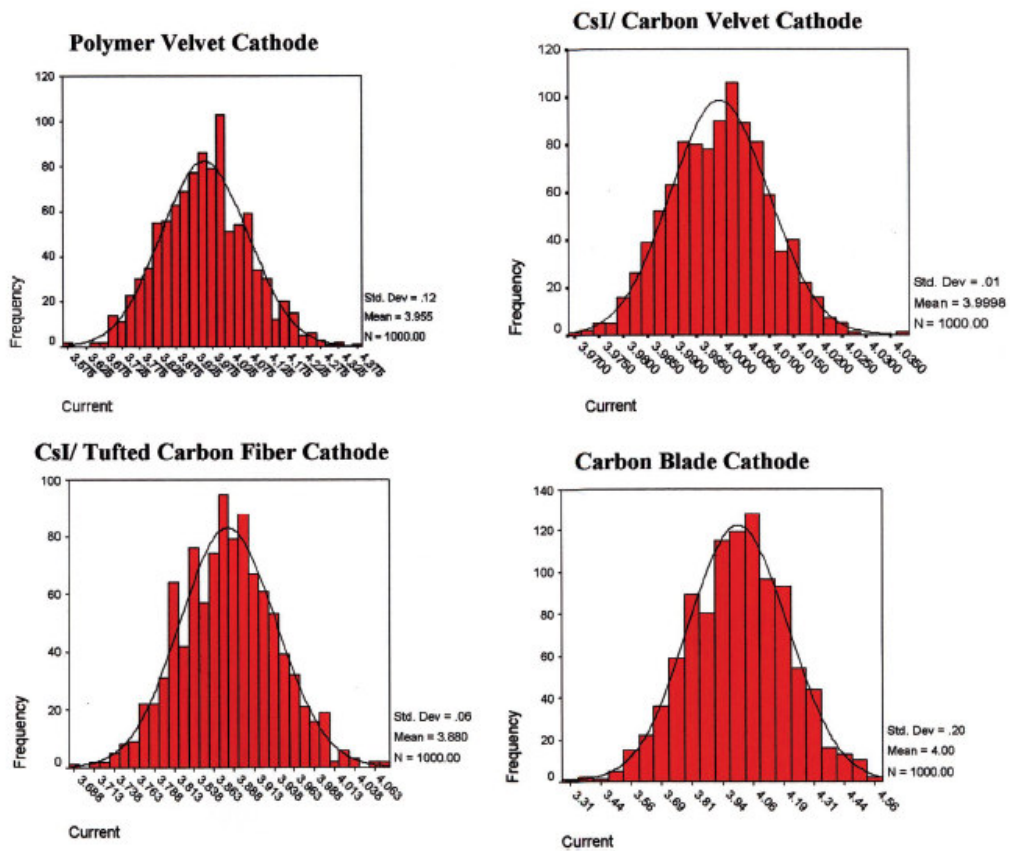


FIG. 2.23 Histogram showing the variation in current for a carbon velvet, cesium-iodide-coated cathode. Other cathode produces similar results with variation in standard deviation and skewness [31].

The shot to shot reproducibility of the intense electron beam diode is an important property both for single shot or repetitive operation [60]. Good shot-to-shot reproducibility is a requirement for many environments. In fact, there is a statistical correlation between emission uniformity and the shot-to-shot variation in diode current [31]. The current waveforms can provide some assessment of cathode emission uniformity if the data is of a statistical nature taken over thousands of shots rather than examining single shot waveform shapes. Comparing to the data in [34], one finds that the standard deviation and skewness of the current histograms increase as the cathode emission becomes less uniform. As the emission uniformity decreases, the variability of the current increases significantly. Perhaps this appears obvious; however, the demonstration in a controlled simulation environment strengthens the conjecture that shot-to-shot variability can provide a viable surrogate for emission uniformity. The shot to shot variation in current is because of the fact that the nonemission areas vary randomly on a shot-to-shot basis [31]. As these areas vary randomly, cathode emission comes from a combination of small patches and larger, relatively uniform segments, resulting in significant variability in the measured current.

TABLE II Statistical data for the shot to shot variation in the diode current.

<u>Cathode Type</u>	<u>Standard Deviation</u>	<u>Skewness</u>
Carbon Slat	200	-0.72
Polymer Velvet	120	0.137
Tufted Cesium Iodide Coated Carbon Fiber	60	0.06
Cesium Iodide Coated Carbon Velvet	12	0.015

The shot to shot variation of cathodes consist of a carbon slat cathode, polymer velvet cathode, a tufted carbon fiber cathode with the individual fibers bundles coated with cesium iodide (CsI) salt have been studied. The histogram showing the variation in current closely resembles a Gaussian, with a slight skewness to the curve as shown in Fig. 2.23. Statistical data shows that the slat cathode being the least uniform and the cesium-iodide-coated carbon velvet being the most uniform [31]. Statistical data for four different types of cathodes are summarized in Table II. But the shot to shot variation in the diode perveance has not been studied so far. The shot to shot variation in the diode voltage and current due to the prepulse generated plasma has also not been studied so far.

2.7 HPM GENERATION FROM VIRTUAL CATHODE OSCILLATOR USING IREB

It was known that, in planar gaps with self-consistent account for space charge under certain conditions, a so-called virtual cathode (VC) forms [6]. Figure 2.24 shows axial virtual cathode oscillator. For a long time this phenomenon was not applied in practice. During the 1970s the situation changed when high-current relativistic electron beam technology reached the level which provided 10^4 - 10^6 A beams at 0.1-10 MeV acceleration energy quite easily. Then, certain proposals emerged for employing VC-based devices in various technical applications (for example, ultra-short-pulse current generation with VC discharges [77] and ion collective acceleration with a moving VC [78]).

However, the most important VC-based device application is the generation of super-powerful microwave pulses. This idea was first published by Kapetanacos *et. al.*, who suggested one version of such a device-the reflex triode [79]; later, Sullivan proposed another microwave device based on the VC-the Vircator [80].

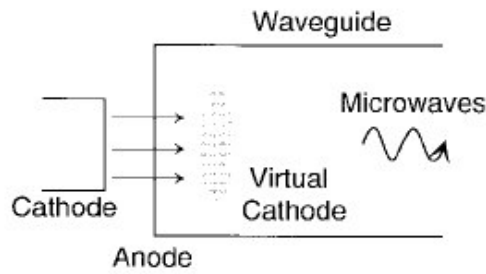


Fig. 2.24 Axial virtual cathode oscillator.

The merits of VC-based microwave devices include simple design and device control with an external microwave signal. Moreover, VC-based microwave devices are one of the high power devices which can operate without external magnetic fields, making them competitive with other classes of microwave devices, especially for repetitive pulse radiation sources. Figure 2.25 shows an axial vircator with HPM diagnostics [81].

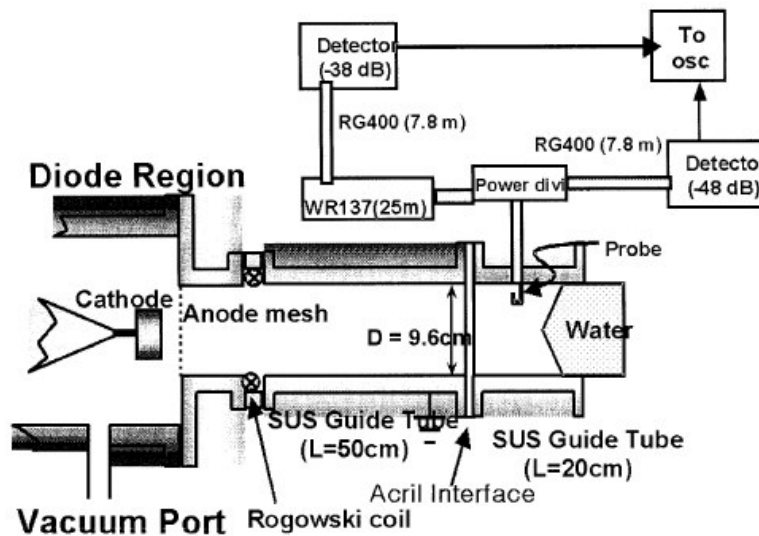


FIG. 2.25 An axial vircator with HPM diagnostics [81].

In a virtual cathode device, there are two possible sources of microwave radiation; one from electrons oscillating between the real cathode and virtual cathode and the other from the oscillating electron cloud or virtual cathode [82].

The electron reflection frequency f is given by $f = 1/4T$, where T is the transit time of electrons to move back and forth between the cathode and anode. The transit time is given by $T = \int_0^v (dz/v)$, where v is electron velocity, and d is the distance between the anode and cathode. The oscillation frequency, f_v , for the virtual cathode ranges from $\omega_p/2\pi$ to $5\omega_p/4\pi$, where ω_p is the electron beam plasma frequency [77] defined by $\omega_p = \sqrt{ne^2/\gamma m \epsilon_0}$. Here, n is electron density, e is electronic charge, m is electron mass, ϵ_0 is vacuum permittivity, and γ is relativistic energy factor.

The vircator's have been studied extensively by various authors both theoretically [83] and experimentally [84, 81, 85]. Much of the research in recent years has been focused on increasing the efficiency of microwave generation [2]. Many experimental studies have been carried out on the vircator in order to improve its beam-wave energy conversion efficiency. Despite these efforts, the highest efficiency is still limited to several percent. To improve the vircator efficiency various cathode materials have been investigated [2, 86]. It was found that the beam-to-microwave efficiency increased from about 4%–6% in the case of the stainless steel cathode to over 10% in the case of the carbon fiber cathode [2]. Figure 2.26 shows Vircator microwave power and frequency versus various initial AK gap distances d [81]. Double gap vircator also has superior parameters as compared with commonly used vircators [81a]. Figure 2.27 shows microwave signal and time-varying effective AK gap distance d_{eff} along with the diode voltage V_d and diode current I_d under initial AK gaps 2 mm and 5 mm, respectively [81].

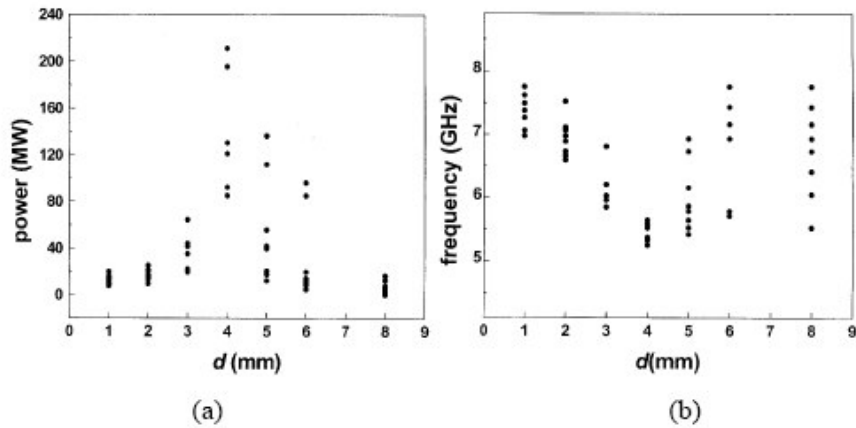


FIG. 2.26 (a) Vircator microwave power and (b) frequency versus various initial AK gap distances d [81].

One method used to increase microwave output involves tuning the cavity in which the vircator is housed [86]. Reflecting strips are placed downstream of the microwave output which reflects a portion of the microwaves back toward the virtual cathode. The oscillations of the vircator are then improved by the upstream traveling waves. This method has been used successfully in the past on the reflex triode and cylindrical vircators [37]. Several different cathodes and anodes have been tested with different diagnostics. It has been shown that the metal and carbon fiber cathodes have uniform current emission in both time and space. The carbon fiber and the aluminum etched cathode both recorded higher peak microwave power than the velvet with no signs of degradation over the lifetime test. A Tantalum anode constructed with a honeycomb hole pattern has been tested to provide similar results with the original stainless steel weave meshes at a greater lifetime potential. It has also been shown the anode transparency has a significant effect on peak microwave power. Reflector tests have also shown some success in amplifying the peak microwave power [86].

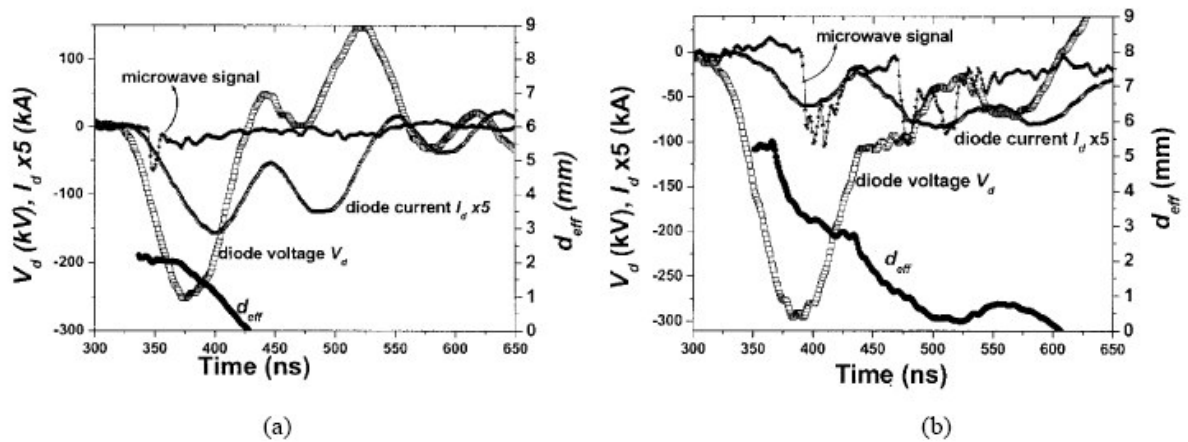


FIG. 2.27 Microwave signal and time-varying effective AK gap distance d_{eff} along with the diode voltage V_d and diode current I_d under initial AK gaps d are (a) 2 mm and (b) 5 mm, respectively [81].

2.8 CYLINDRICAL ELECTRON BEAM DIODE AND COAXIAL VIRTUAL CATHODE OSCILLATOR

High Power Cylindrical diodes have been employed for intense relativistic electron beam generation in coaxial virtual cathode oscillator [Fig. 2.28] (Vircators) [37] and in high resolution radiography sources [4]. In fact, the coaxial vircator presents a cylindrical diode which consists of an annular cathode and grounded mesh anode [87]. Figure 2.29 shows a coaxial Vircator with HPM diagnostics [88].

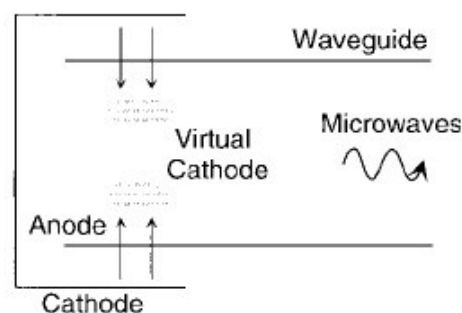


Fig. 2.28 Coaxial virtual cathode oscillator.

In the vircator device an electron beam is accelerated in the diode gap where pulsed high voltage is applied between the anode and the cathode. The beam passes through the anode,

which is usually a thin foil or a mesh, and is injected into the area on the other side of the anode. When the beam current is higher than the space-charge-limited current of this area, a virtual cathode is formed at a certain position that reflects a certain part of the electron beam. The position of the virtual cathode and the ratio of beam reflection depend very much on the electron energy.

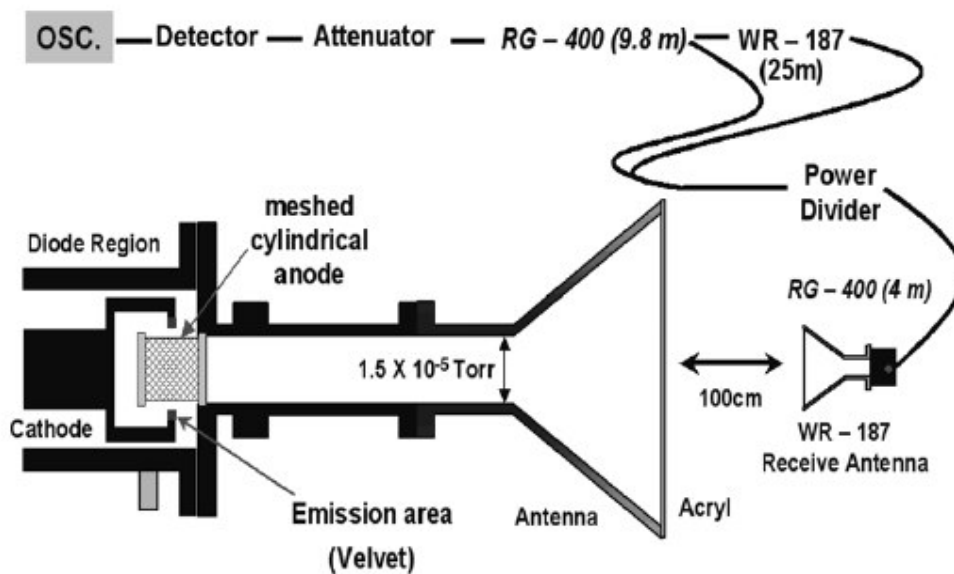


FIG. 2.29 A coaxial Vircator with HPM diagnostics [88].

Therefore, if the electron energy is modulated at a given frequency, both the virtual cathode position and reflected beam current will oscillate at the same frequency. The electron energy can be modulated by an electromagnetic field and the same field may interact with the modulated reflection current because they have the same frequency. In this interaction, if the phase relation is such that the electromagnetic field obtains energy from the modulated current, the result will be field amplification by the virtual cathode oscillation [89]. It is obvious that the amplitude of the beam current modulation and the strength of the electromagnetic field are very important to the beam-field interaction. The interaction is between the electron beam

current and the radial electric field of the waveguide mode. Compared with the axial vircator, the coaxial vircator is expected to have the following advantages.

1) Due to the absence of the end wall of the waveguide, the electromagnetic field may also exist in the diode area and give rise to stronger beam modulation than that which only exists in the waveguide. In other words, the interaction area is extended from the waveguide to include the diode area.

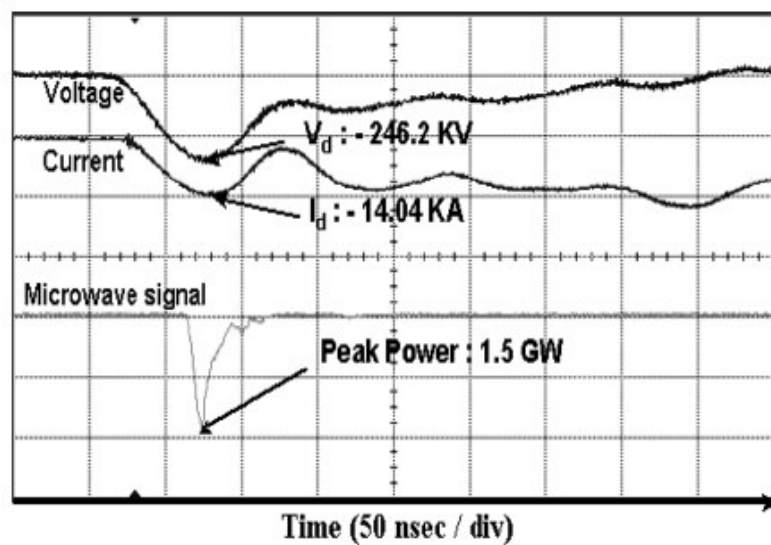


FIG. 2.30 Typical oscilloscope traces of the diode voltage, current, and microwave [37].

2) The electron movement is only in the radial direction which eliminates the loss carried by the transmitted electron beam (through the virtual cathode) in the axial vircator. In addition, any modification of the waveguide configuration close to the vircator would not affect the electron beam behavior, in contrast with inevitable variation of the space-charge limited current in the axial vircator. The modification of the waveguide configuration can be planned in order to increase the feedback of the electromagnetic wave to the vircator.

3) Due to the large area of the diode gap, the current density is significantly reduced compared with the axial vircator. As a result, the damage on both the cathode and the anode is decreased,

allowing longer lifetime of the electron beam diode, which is especially important for repetitive operation.

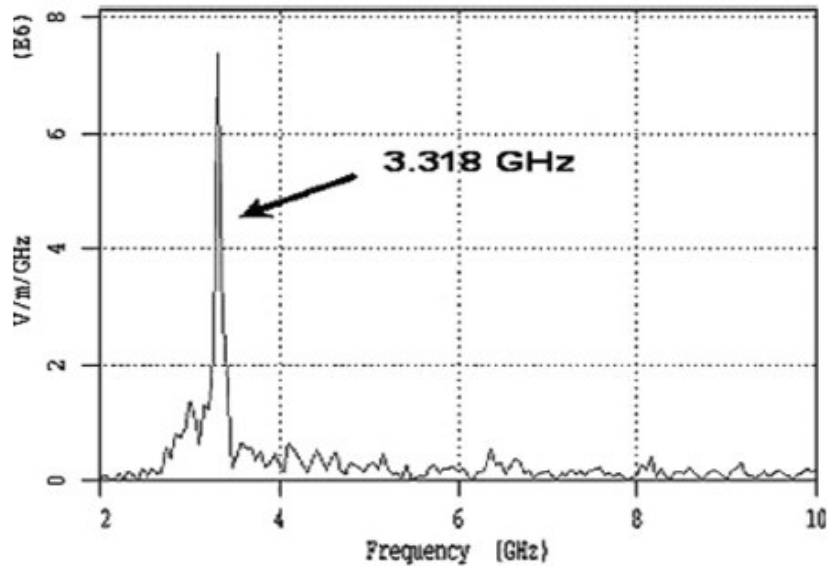


FIG. 2.31 Field magnitude of FFT at the output port [37].

For these advantages coaxial vircator has been studied extensively by various authors both theoretically [90, 91] and experimentally [37, 92-93, 88]. The measured microwave frequency and peak power in a coaxial vircator have been investigated to be about 3.34 GHz and 1.57 GW, respectively. Using the bar reflector, the power conversion efficiency from the electron beam to the microwave is enhanced from 28.9% up to 45.4% [37]. Figure 2.30 shows a typical oscilloscope traces of the diode voltage, current, and microwave in a coaxial vircator [37]. Figure 2.31 shows the field magnitude of FFT at the output port used for frequency measurement [37]. Figure 2.32 shows plot of microwave frequency and power according to the variation of AK gap distance in the coaxial vircator without a reflector [37]. Figure 2.33 illustrates the power conversion efficiency (from the electron beam to the microwave) enhancement using the bar reflector at the wave guide [37].

At the heart of the coaxial vircator technology is the cylindrical electron-beam diode where electrons are accelerated by strong electric fields. For design of the pulsed power systems that power the diode, it is useful to be able to predict the diode current for a given voltage and geometry. The space charge limited current in a cylindrical diode in one dimension can be described by the Langmuir-Blodgett law [94]. The Langmuir-Blodgett law has been extended to two dimensions by performing 2D particle in cell simulations [95]. But the results are limited to low voltage and low current regime (few kilovolts and few Amps).

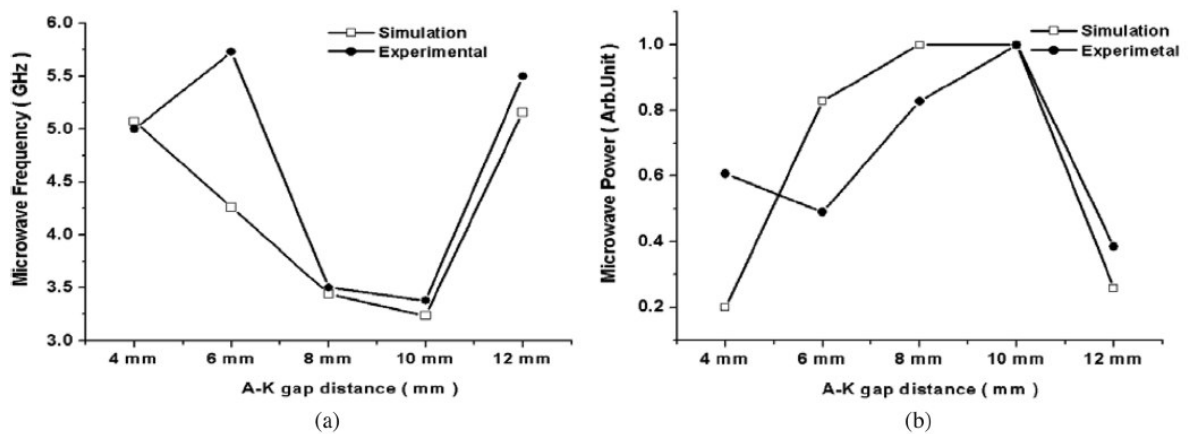


FIG. 2.32 Plot of (a) microwave frequency and (b) power according to the variation of AK gap distance in the coaxial vircator without a reflector [37].

Approximate analytical solutions for the space charge limited current in 1D and 2D cylindrical diodes are also calculated by various authors [96, 97]. When the self magnetic field of the electron beam is large enough for the electron Larmor radius to be comparable to the anode cathode gap spacing, space charge theory breaks down and the diode current becomes Magnetically Limited [98]. At the low currents, the self magnetic fields can be ignored and the charged-particle flow in the diode is space charge limited [98]. Particle in cell simulations of charged particle flows of cylindrical pinch beam diodes can be found in Ref.28, 99 and also in Ref.98.

Although several works has been carried out in connection with the intense relativistic electron beam generation in cylindrical electron beam diodes, the electrode plasma expansion and the effect of prepulse are not studied in detail. Another important issues concerning vacuum

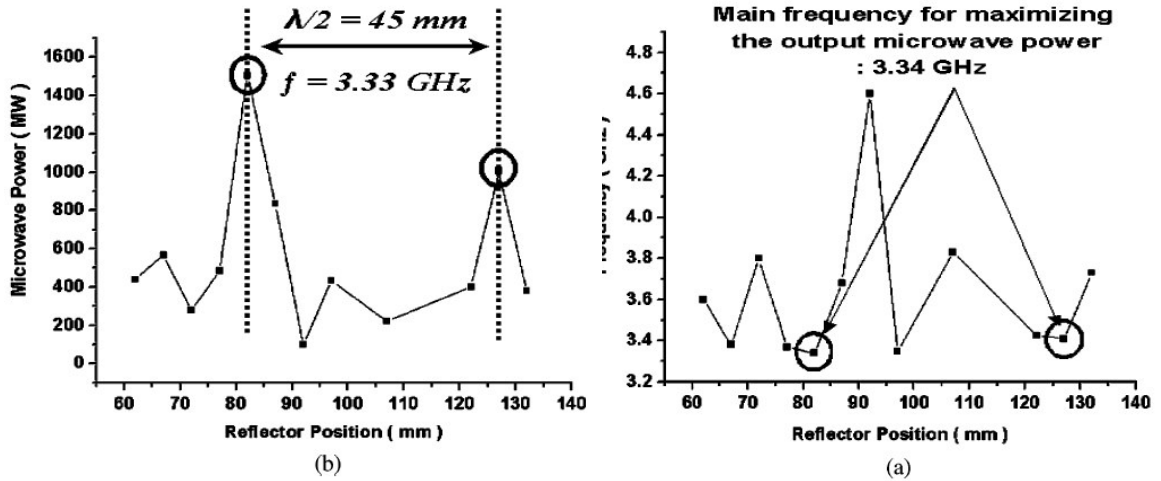


FIG. 2.33 Plot of (a) microwave frequency and (b) power according to the variation of the reflector position [37].

diodes is the increase of the perveance of the electron beam, which effects various applications, including high power microwave generation, transport of high current electron beams, and production of intense bremsstrahlung. The temporal behavior of perveance of the cylindrical electron beam diode is also not studied in detail.

CHAPTER 3

EXPERIMENTAL SETUP AND PROCEDURE

INTRODUCTION

Intense relativistic electron beam generation studies were carried out using KALI-5000 and KALI 1000 pulse power source. The experimental set up used for IREB generation studies composed of a field emission vacuum diode and beam diagnostics. HPM generation studies were carried out with axial and coaxial virtual cathode oscillator. The salient features of these sub systems are described in the following sections. Section 3.1 describes the KALI 5000 pulse power system. Section 3.2 describes the KALI 1000 pulse power system. Section 3.3 describes the details of planar and cylindrical electron beam diode. Section 3.4 describes the various diagnostics developed and employed for IREB generation studies. Section 3.5 describes the axial and coaxial vircator. HPM diagnostics is described in section 3.6.

3.1 KALI 5000 PULSE POWER SYSTEM

Since 1970, BARC has indigenously developed many pulsed power systems such as KALI-75, KALI-200, KALI-1000, and KALI-5000 to generate intense relativistic electron beams, high power microwaves, flash X-rays and neutron beams etc.. KALI is the short form abbreviation for kilo ampere linear injector. The KALI-5000 system is capable of generating an IREB of 1 MeV, 60 kA, and 100 ns when connected to an impedance matched electron beam diode [100]. The schematic diagram of the KALI-5000 system is shown in Fig. 3.1. The KALI 5000 pulse power system has two main stages, namely a high voltage generator (Marx Generator) and pulse forming (Blumlein Line) line. A bipolar Marx generator with 30 stages generates at its output ~ 1.5MV voltage pulse. Each stage is charged to a maximum voltage of 50 kV. The

Marx generator has 15 spark gaps filled with Nitrogen gas. Variable output voltage from the Marx generator is obtained by changing the Nitrogen pressure in the Spark Gap. The Blumlein line has three coaxial lines, with the grounded outer line. The Marx generator output is connected to the intermediate line of Blumlein pulse forming line. A pulse initiating spark gap with SF₆ gas is connected between intermediate and inner lines. The inner line is grounded using a 8 μH Blumlein spiral inductor. The voltage across the inductor during the charging of the Blumlein line appears as a prepulse voltage across the diode terminals. The amplitude of this prepulse voltage depends on the ratio between the Marx generator and the inductor inductances. The inductance of the Marx generator is 15μH. A prepulse of 30 % of the magnitude of the Marx generator output voltage is expected across the diode electrodes. The duration of the prepulse voltage is equal to the charging time of the Blumlein line, which in turn depends on Marx generator capacitance, inductance and the Blumlein line capacitance. Depending on the pressure in the Blumlein line spark gap variation in the charging time are expected. The simulation of the prepulse circuit for KALI-5000 pulse power system has been described in Ref. 17. A photograph of the KALI 5000 system is shown in Fig. 3.2.

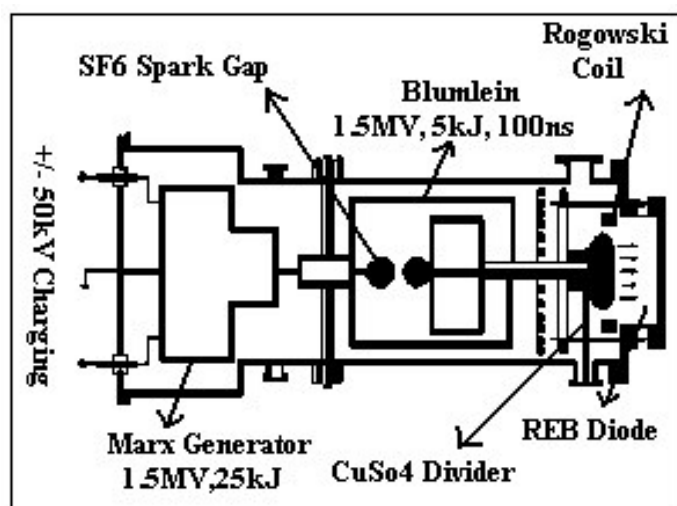


FIG. 3.1 The schematic of the KALI-5000 system

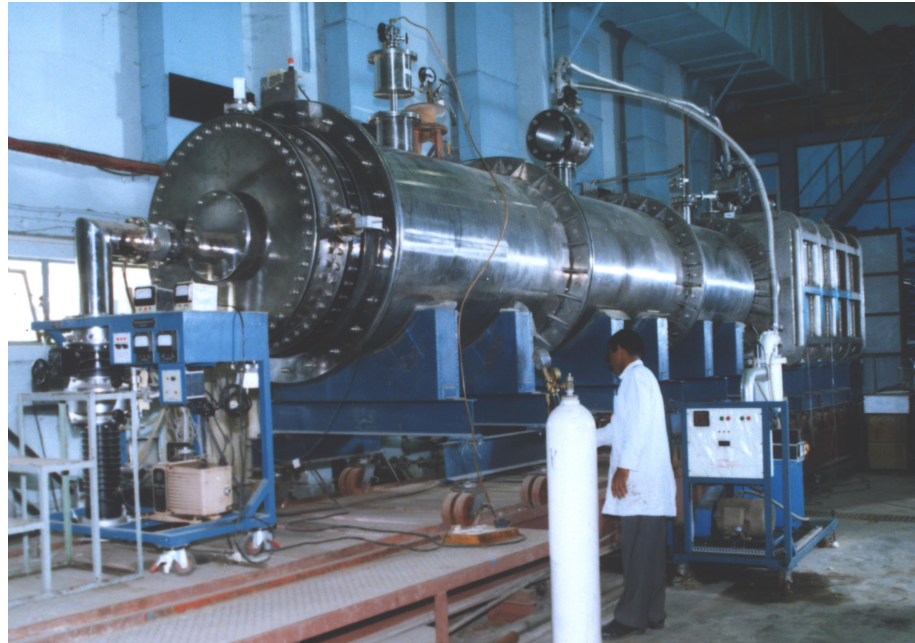


FIG. 3.2 A Photograph of the KALI 5000 system.

3.2 KALI 1000 PULSE POWER SYSTEM



FIG. 3.3 A photograph of the KALI 1000 system.

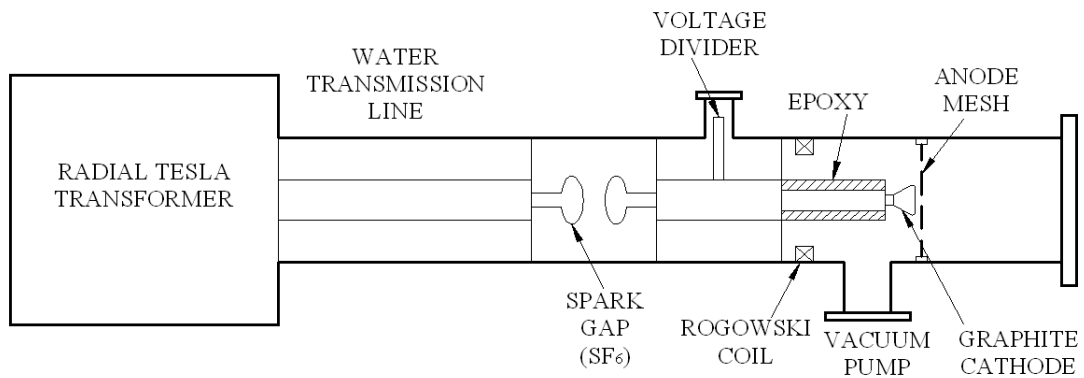


FIG. 3.4 Schematic of the KALI 1000 system.

The KALI-1000 Pulse Power System is an indigenously developed system at APPD, BARC [101]. A photograph of the KALI 1000 system is shown in Fig. 3.3. Fig. 3.4 shows a schematic of KALI 1000 pulse power system. It has a Radial Tesla Transformer, a water Transmission Line and a gas spark gap to generate the high voltage pulse. The Radial Tesla transformer has a single turn primary and 60 turn secondary windings. The water Transmission Line is 1.3m long and uses demineralised water as dielectric and the capacitance is 4nF. The spark gap contains two electrodes of Rogowski profile separated by 2 cm and uses SF₆ gas at pressure of 2.0 kg/cm² in a cylindrical chamber of diameter 25 cm and length 30 cm. A vacuum Field Emission Diode was used to generate Intense Electron Beam. The high voltage pulse generated from the pulse power system is applied to the field emission diode. The diode consists of a planar graphite cathode (70 mm diameter) and copper anode mesh (240 mm diameter) at various anode-cathode (AK) gaps and various voltage levels. A resistive CuSO₄ Voltage Divider and a self integrating Rogowski Coil were used to measure the diode voltage and current pulses respectively.

3.3 ELECTRON BEAM DIODE

The schematic of the planar electron beam diode is shown in Fig. 3.5. The planar electron beam diode consists of a planar graphite cathode and SS or copper mesh anode. Electron beam currents were measured using a Rogowski coil and a B-dot probe. The diode voltage was measured by a copper sulphate resistive divider at a location close to the cathode. The diode chamber was evacuated using a diffusion pump backed by a rotary pump. The vacuum in the diode chamber was $\leq 1 \times 10^{-4}$ mbar. The vacuum vessel is a stainless steel cylinder. Fig. 3.6 displays a planar graphite cathode.

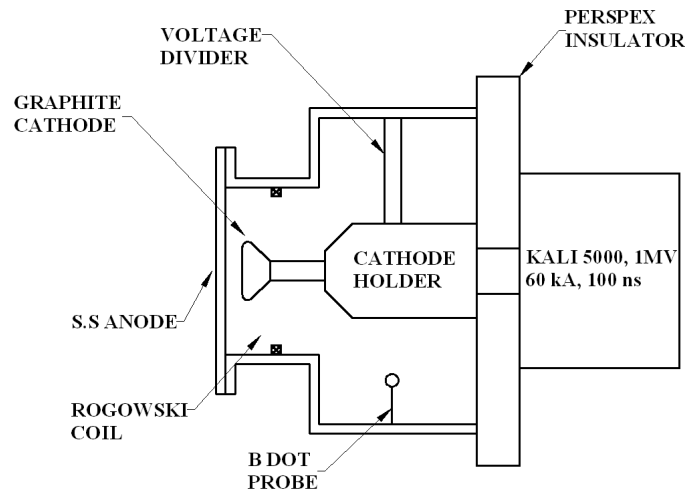


FIG. 3.5 Schematic of the planar electron beam diode with the beam diagnostics.

The schematic of the cylindrical electron beam diode is shown in Fig. 3.7. A graphite cathode with outer diameter of 13.7 cm and a copper mesh anode of 8.6 cm diameter were used for the cylindrical diode. The graphite cathode has a 2 cm emission length. The diameter of the anode was fixed. The inner diameter of the cathode varies from 11 cm to 12.3 cm. The radial AK gap varies from 1.2 cm to 1.85 cm. The diode diagnostics employed were aqueous copper sulphate

resistive divider for the diode voltage, Rogowski coil and B-Dot probe for the diode current measurement. Fig. 3.8 shows annular graphite cathodes of various diameters.



FIG. 3.6 A planar graphite cathode.

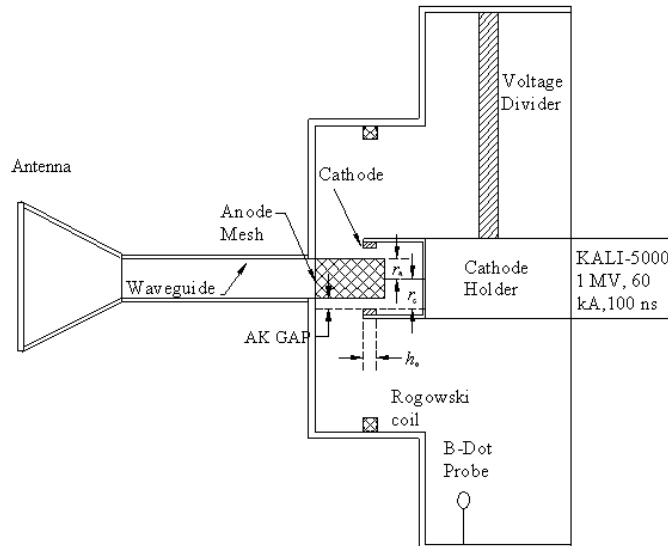


FIG. 3.7 Schematic of the cylindrical electron beam diode and coaxial vircator.



FIG. 3.8 Annular graphite cathodes of various diameters.

3.4 BEAM DIAGNOSTICS

3.4.1 Rogowski Coil

For many years the self-integrating Rogowski coil has been used to measure the currents in pulsed power experiments [102]. The Rogowski coil can measure the current of the pulsed electron beam that has a pulse length of tens of nanoseconds, a rise time of a few nanoseconds, and a magnitude of tens of kiloamperes. The advantages of these coils are (1) reliability, (2) ease of installation, (3) an output voltage independent of current distribution, (4) long term stability, and (5) non frequency-dependent output voltage. Rogowski coils are wound either on a rigid toroidal core form or on a flexible belt-like core form. While these coils are termed “air core,” the core is normally plastic. These coils have been routinely used to measure pulsed currents in excess of 1 MA in plasma, electron beam, and high radiation field environments.

For toroidal coils having a rectangular cross section such as that shown in Fig.3.9, the mutual inductance is [103]

$$M = \frac{\mu_o N w}{2\pi} \ln\left(\frac{b}{a}\right), \quad (3.1)$$

where M is the mutual inductance (in henry); μ_o is the permeability of air, which equals $4\pi \times 10^{-7}$ H/m; N is the number of turns of coils; w is the width of the toroid in meters; a is the inside diameter in meters; and b is the outside diameter in meters.

To achieve ns-response of Rogowsky coils matching resistors should be placed in order to avoid amplification of resonance frequencies.

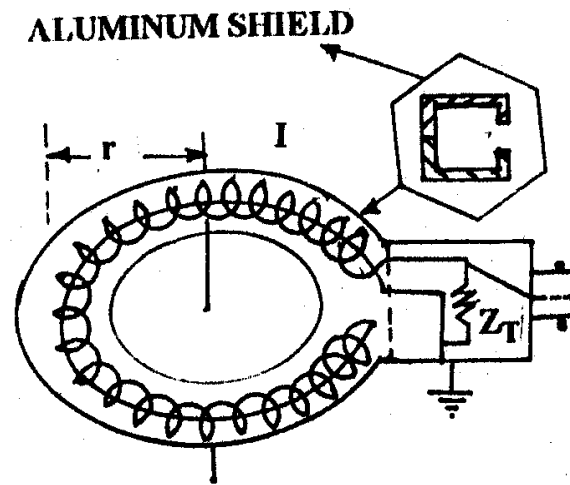


FIG.3.9 Schematic of the rogowski coil.

Rogowski coils may be wound having a single- or multiple layer windings. Multilayer coils will have higher values of mutual inductance, series self-inductance, series resistance, and distributed capacitance. A typical single-layer Rogowski coil is shown in Fig.3.9. To prevent the influence of magnetic fields crossing the coils, a return loop is necessary. The existing conductor through the core center serves as the return (second) loop, just as shown in Fig. 3.9.

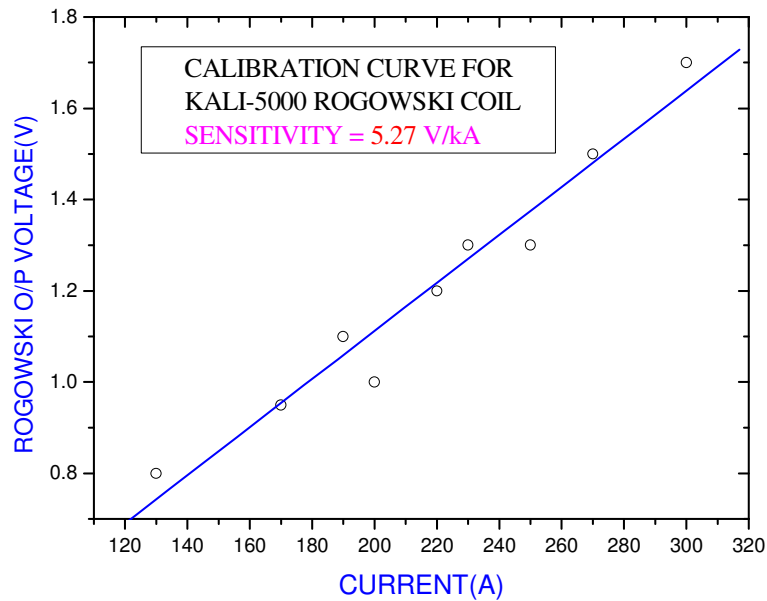


FIG. 3.10 Calibration curve of the KALI 5000 rogowski coil.

The Rogowski coil has been calibrated by the most convenient method of calibration (so called “cable pulser method”) which uses a cable pulser that consists of a high voltage charged cable as pulse forming line (PFL) coupled to a cable as pulse transmission line through a air spark gap of nanosecond rise time and delivers a rectangular voltage pulse onto the load [104]. The measured sensitivity of the Rogowski coil used in the KALI 5000 electron beam diode is 5.27 V/kA and for KALI 1000 diode it is 7.5 V/kA. Fig. 3.10 displays the calibration curve of KALI 5000 Rogowski coil.

3.4.2 B-Dot Probe

Small wire loop probes have routinely been used in plasmas to measure the time varying magnetic flux density $B(t)$. These small wire loop probes, generally known as B -dot (shown in the Fig.3.11) or dB/dt probes, produce a voltage that is proportional to the component of the time varying

magnetic flux (loop area $\times dB/dt$) that is directed normal to the plane of the loop. For a constant driving frequency, magnetic flux density is readily determined by dividing the measured (loop) voltage by the driving frequency ω , the number of turns in the loop, and the area of the loop. From the B -dot voltage and relative phase, the spatially dependent electric field and the current density can be determined through Maxwell's equations [105].

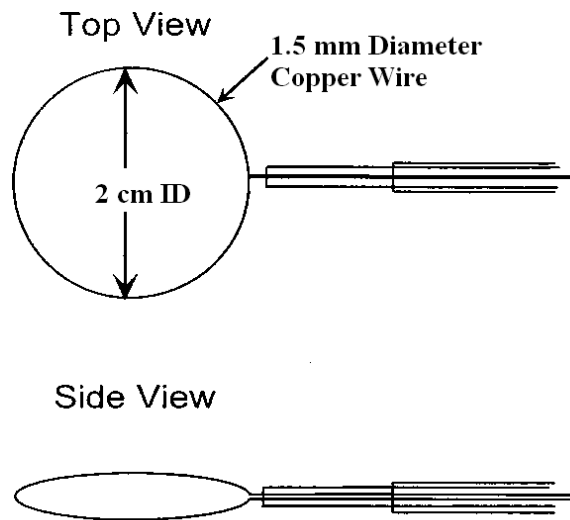


FIG. 3.11 B-Dot Probe.

As shown in the Fig. a thin wire probe has been designed and used without an insulating shell. The wire material is 1.5 mm diameter copper. Output of the B -dot probe has been fed directly to the oscilloscope after suitable attenuation. To get the actual beam current profile the B -dot probe signal has been integrated numerically with the help of software provided with the oscilloscope.

The sensitivity of B -dot probes is defined by the loop radius, the number of turns, the transmission characteristics of the lead and the connectors, and the lead lengths from the loop to the connectors. In principle, all these factors can be accounted for and probe sensitivity can be calculated; however, it is more practical and accurate to avoid calculating these parameters and instead to calibrate the probe through direct comparison with an independent

measurement. In our case the B-Dot probe has been calibrated *in situ* inside the KALI 5000 diode chamber with the help of a calibrated Rogowski coil.

3.4.3 Voltage Divider

There are several well-known methods in the measurements of short duration (10s nanosecond level) high-voltage pulses. A capacitive or inductive divider often suffers from high frequency oscillatory noise due to the existence of the stray capacitance and self-reactances of the dividing elements. It may also act as an undesired reactive load to the measured circuit. Simple aqueous resistive voltage dividers usually provide a better choice [106]. The more familiar resistive voltage divider has the advantage of an easy structure, less noise, and simple electrical properties. However, special techniques are needed to reduce the rise time of the divider, i.e., to improve the frequency response of the probe, especially in the measurement of high voltage (>100 kV) pulses with a requirement of a high load impedance of more than a few kV. In such a case two parasitic parameters, i.e., self-capacitance and stray capacitance of the resistive elements, mainly limit the frequency response of the probe [107].

The voltage divider consists of a tube of aqueous copper sulfate solution acting as a high voltage arm and a 1Ω lower arm made of 10 parallel low inductance commercial carbon resistors. The aqueous copper sulfate resistor was chosen for its proven ability to withstand large electric fields. The solution has the advantage of being readily shaped by varying the container shapes, providing good contacts and being self-healing in the event of a voltage breakdown. The copper sulfate container made of a Perspex tube of sufficient length to prevent voltage breakdown across the surface and the divider is placed inside the diode chamber (in vacuum) only the lower arm of the divider is placed in air outside the diode chamber. A 3 cm diameter Perspex tube has been inserted into the copper sulfate column to reduce the thickness

of the copper sulfate column. The thickness of the copper sulfate column of 5 mm was to minimize the effect of skin depth which was estimated to be ~10 mm for the highest frequency component in the pulse.

The voltage divider is calibrated by two methods, the first method is to connect the divider to a 15 V, 50 Hz line current and measure the voltage and current across the column. The second method uses a cable pulsar that consists of a high voltage charged cable as pulse forming line (PFL) coupled to a cable as pulse transmission line through a air spark gap of nanosecond rise time and delivers a rectangular voltage pulse onto the load. The voltage divider has been calibrated using the pulsar and a commercial high voltage probe. The copper sulfate column resistance can also be measured by an LCR meter.

3.5 VIRTUAL CATHODE OSCILLATOR FOR HIGH POWER MICROWAVE GENERATION

In KALI 1000 system the intense electron beam is injected into the axial vircator chamber of diameter 25 cm and length 25 cm to generate HPM. The vircator region was also maintained at a pressure of 2.0×10^{-5} mbar. The electron beam diode consists of a graphite cathode of diameter 70 mm and a copper mesh anode of diameter 24 cm. HPM is extracted from a Perspex window at the end of the vircator chamber. The axial vircator for the KALI 5000 system also has similar geometry and material but with different dimension.



FIG. 3.12 Coaxial vircator graphite annular cathode.



FIG. 3.13 Coaxial vircator copper anode mesh.

Fig.3.12 shows the graphite annular cathode along with the Rogowski coil for KALI 5000 coaxial vircator. Fig.3.13 shows the anode mesh for the same vircator.

A coaxial vircator also has been designed for the KALI 5000 pulse power system. It consists of a cylindrical electron beam diode as described in section 3.4. The HPM is extracted from a circular waveguide of 9 cm diameter with a conical horn antenna at the end.

3.6 HPM DIAGONSTICS

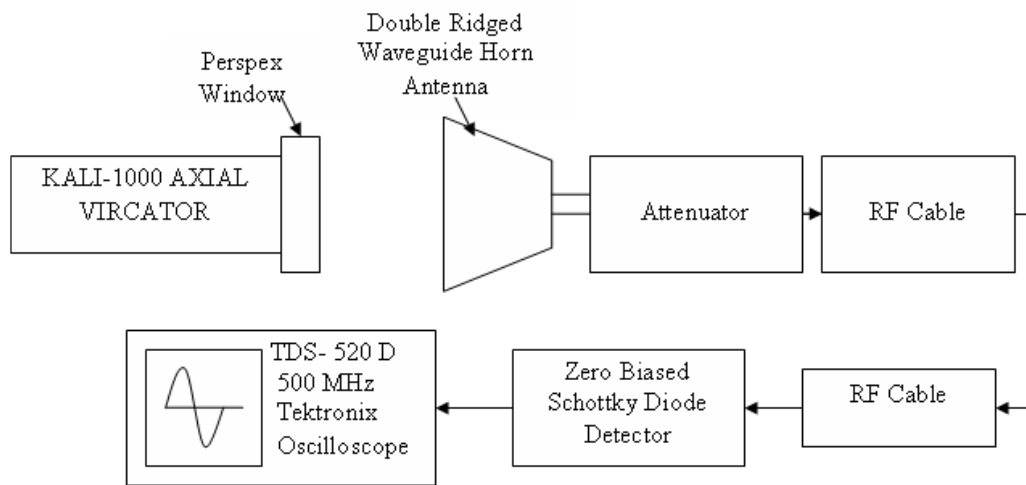


FIG. 3. 14 HPM diagnostics setup.

Diagnosing intense single microwave pulses with powers greater than 100 MW and pulse widths between 5 and 100 ns has been an area of active research for several years. Different experimenters have tried various techniques to measure ns pulse duration HPM power and frequency [108]. Diagnostics are usually frequency sensitive; thus the more accurately the frequency is measured the more accurate the power measurement. Typically the HPM power measurement is accurate within 20% (± 1 dB), the pulse energy to within 20 %, and the frequency to within 1%. These diagnostics techniques are not limited to use on any one type of HPM sources, but can be applied to a variety of HPM sources. HPM frequency can be measured directly on a high sampling rate oscilloscope [109].

For HPM power measurement most widely used apparatus is the transmitting-receiving systems. Transmitting-receiving systems are useful at high power levels because all the HPM energy is broadcast into an anechoic chamber where a receiver picks up a known small fraction of the transmitted power. In this case, the amount of external attenuation required can be minimized. These measurements rely on the radar equation

$$P_T = P_R (4\pi r / \lambda)^2 / G_R G_T, \quad (3.2)$$

where the subscript T refer to the transmitter, the subscript R refer to the receiver, P is the power, G is the antenna gain, r is the transmitter to receiver separation distance, and λ is the free space wavelength. The $(r / \lambda)^2$ characteristics allows large attenuations. For the radar equation to be accurate, the separation of the transmitter and the receiver must obey the far-field criterion: $r > 2D^2 / \lambda$, where D is the diameter of the larger of the transmitter or the receiver. It should be noted that this equation may still be inaccurate even though the far-field equation is obeyed if the phasing of the transmitted antenna is poor. In this case, the far-field limit can be several times larger than $2D^2 / \lambda$.

The HPM signal was captured by the double-ridged horn antenna placed a few meters from the vircator window. A shielded room was situated approximately 20 m away from the KALI-1000 system and 5 m away from KALI-5000 system. All the oscilloscope measurements were carried out inside the shielded room. For each shot, the beam parameters were recorded using a Lecroy model WS 454 (500 MHz, 2 GS/s) oscilloscope. The microwave detector output was recorded using a Tektronics model TDS 520 D (500 MHz, 1 GS/s) oscilloscope. Various components used in the diagnostics were calibrated using a standard modulated (few milliseconds to nanoseconds) RF source. Fig.3.14 shows a typical HPM diagnostics setup used for KALI-1000 axial vircator experiment.

CHAPTER 4

INTENSE RELATIVISTIC ELECTRON BEAM GENERATION STUDIES IN THE PRESENCE OF PREPULSE

4.1 INTENSE GIGAWATT RELATIVISTIC ELECTRON BEAM GENERATION IN THE PRESENCE OF PREPULSE

Intense gigawatt relativistic electron beam generation studies were carried out in a planar diode configuration in the presence of prepulse. It was found that with 400 kV on the diode a bipolar Prepulse of 60 kV peak and more than 800 ns duration arrives on the diode. The negative peak occurred about 600 ns before the main pulse and the positive peak about 200 ns before the main pulse [17]. Usually 100 kV/cm electric field is required to initiate plasma formation on the cathode surface. But due to poor vacuum and surface condition on the graphite cathode plasma formation can occur much below 100 kV/cm electric field. Also during the positive half of the Prepulse voltage some plasma can be generated at the anode surface. Because of the plasma expansion from the anode and cathode surfaces, the diode either short circuited before the main pulse arrived or the effective shape of the cathode changes which lowers the impedance of the diode. Increasing the AK gap reduces the prepulse electric field and eventually drops it below the explosive emission threshold and eliminates its creation. As this threshold is approached, what plasma that is turned on may well be non-uniform as explosive sites become few and far between. This will make the cathode plasma very dependent on surface preparation and the resulting plasma will be wispy, spotty, and very nonreproducible. Cathode plasma can consist of a mixture with hydrocarbons on the

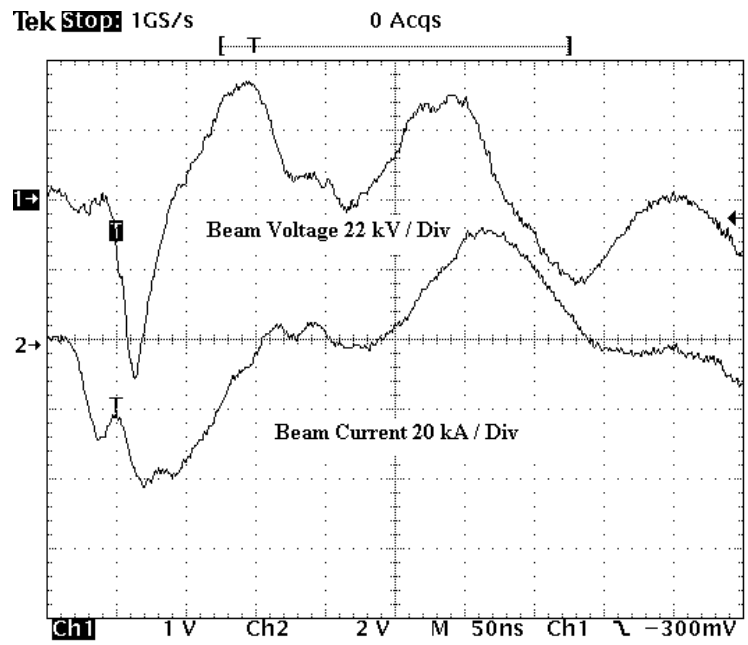


FIG. 4.1 Waveform of the electron beam voltage and current for 11.3 mm Gap, 70 mm dia cathode.

surface contributing significantly to its constitution [38]. Protons make up the majority the ion beam that is observed in most diodes.

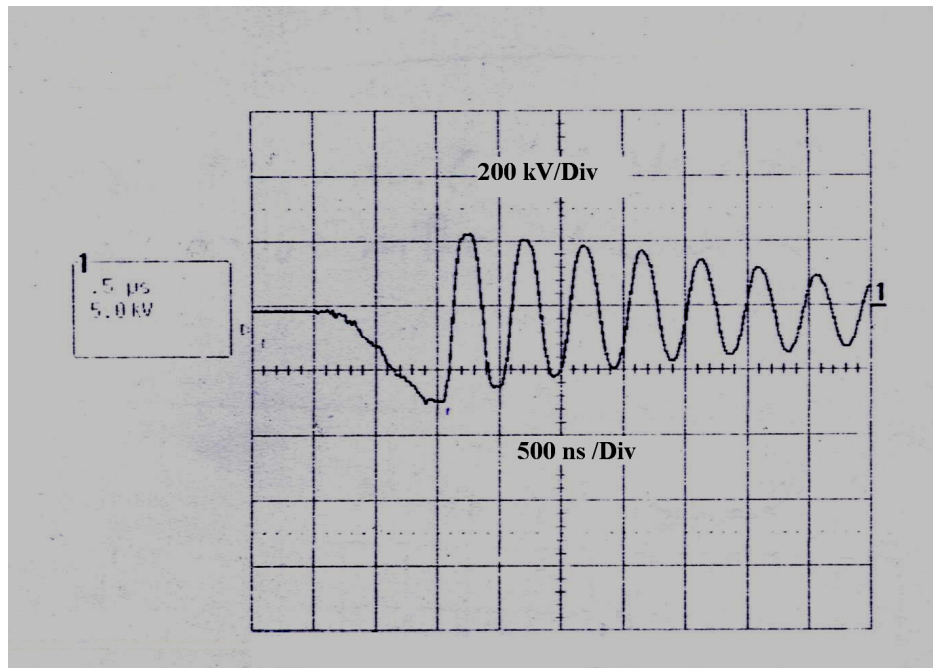


FIG. 4.2 Marx generator output voltage with impedance mismatch.

Details of the experimental set up is given in Chapter 3.3. IREB generation studies have been carried out for graphite cathode of 70 mm diameter and AK gap ' d ' was varied from 11 mm to 31 mm. A 30 cm diameter SS flange was used as an Anode. Pressure in the diode region was maintained at 4×10^{-5} m.bar by a diffusion pump backed by rotary pump. Beam voltage was measured by a copper sulphate voltage divider of ratio (2K: 1) and beam current was measured by a self integrating Rogowski coil (5 V/kA) and B-dot probe.

Initially ' d ' was kept at 11.3 mm for 70 mm diameter cathode. At this gap diode impedance should match with the impedance of the Blumlein ($\sim 19 \Omega$) for 300 kV beam voltage and can be calculated from Child-Langmuir Law. In this configuration the

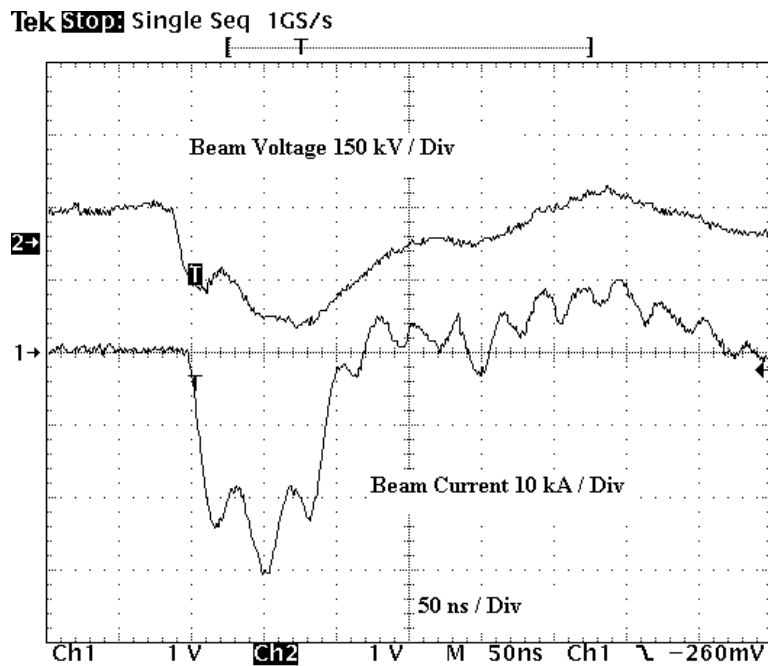


FIG. 4.3 Waveform of the electron beam voltage and current for 21 mm Gap 70 mm dia cathode.

measured beam voltage was 57 kV [Fig. 4.1] though the Marx generator output voltage was 300 kV and beam current was as high as 40 kA. Also a large reversal seen in the Marx generator output voltage due to impedance mismatch between the diode and the Blumlein line [Fig. 4.2]. In this case the diode remains in the conduction phase for 30 ns duration then suddenly voltage rises to 57 kV. So the diode behaves as plasma filled diode but the impedance is much less than vacuum impedance. The Prepulse generated plasma completely covers the AK gap during the conduction phase. There was not much shot to shot variation in this case.

In order to avoid the prepulse effect the AK gap was increased much more than that given by the Child Langmuir Law. For 70 mm diameter cathode and 21 mm gap an IREB of 150 kV and 30 kA could be generated [Fig. 4.3] for 320 kV Marx generator voltage.

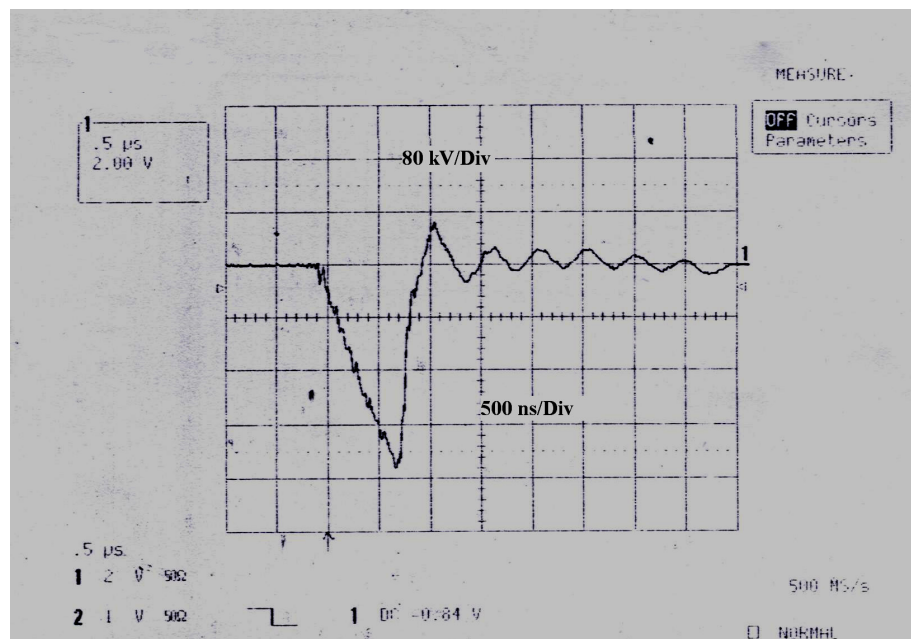


FIG. 4.4 Marx generator output voltage with matched impedance.

In this case the short circuit phase is not seen but diode voltage still remains less than Marx generator voltage and reversal in the Marx generator voltage remains but less. Marx generator voltage was varied from 250 kV to 380 kV. It was seen that as we increase the Marx generator voltage diode voltage decreases and current increases with the consequent increase of Marx generator voltage reversal. For the same Marx generator voltage there is lot of shot to shot variation in the diode voltage and current due to the nonreproducibility of Prepulse generated plasma. In this case Prepulse generated plasma expands and reduces the effective AK gap consequently reducing the diode impedance [17].

For 70 mm diameter cathode and 23 mm gap similar behavior observed in the diode voltage and current. Various shots were taken varying the Marx voltage from 300 kV to 400 kV. For a constant 400 kV Marx voltage diode voltage varies from 100 kV to 225 kV and diode current from 25 kA to 40 kA for different shots.

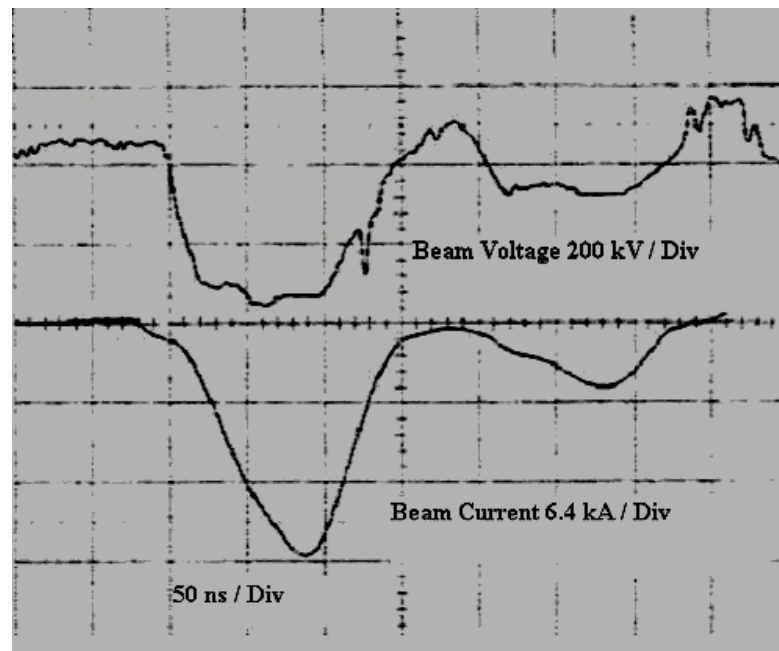


FIG. 4.5 Waveform of the electron beam voltage and current for 31 mm Gap 70 mm diameter cathode.

At 31 mm gap the beam parameters obtained are 420 KeV, 22 kA, 100 ns [Fig. 4.5]. Reversal in the Marx generator voltage also decreases [Fig. 4.4]. There is no shot to shot variation in the diode voltage and current. Typical IREB diode waveforms are shown in Fig. 4.5 In this case the diode gap is large enough to eliminate the creation of Prepulse generated plasma. Electron beam diode impedance and Perveance values (as shown in Fig. 4.6) were obtained from the diode voltage and current waveforms. It has been observed that the time varying perveance increases and diode impedance decreases with elapsed time. This is due to the fact that the effective AK gap decreases due to cathode and anode plasma expansion. Till 115 ns beam perveance does not increase so rapidly, but after that perveance increase very rapidly also there is a distinct change in the impedance curve. We conclude that diode closes at that point. The perveance value at that point is around $200 \mu\text{Perv}$ ($1 \mu\text{Perv} = 1 \times 10^{-6} \text{ A/V}^{3/2}$). So we can consider the diode as a short if perveance value is more than $200 \mu\text{Perv}$. By the word short means impedance of the diode is much less than the Blumlein impedance.

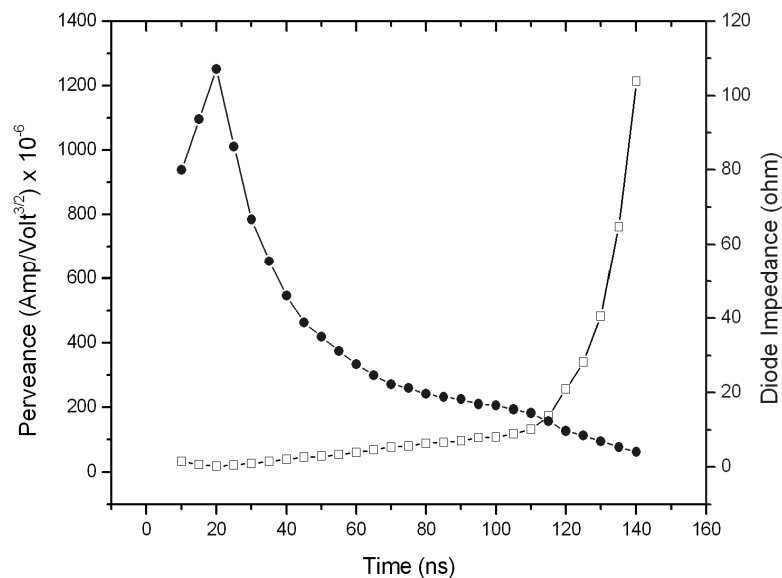


FIG. 4.6 Diode impedance and beam perveance with time.

As the Marx generator voltage increase the prepulse voltage also increases. If we change the AK gap keeping the Marx generator voltage same, the field due to prepulse at the diode gap increases. Preveance of the diode scales as $1/(\text{Anode Cathode Gap})^2$ as seen from Eq. 2.4. We have plotted the diode impedance and perveance values for various Marx Voltage / $(\text{Anode Cathode Gap})^2$ in Figs. 4.7 and 4.8 These values are obtained for 21, 23 and 31 mm AK gap and the Marx generator voltage was varied from 275 kV to 420 kV and calculated at the peak of diode voltage and current.

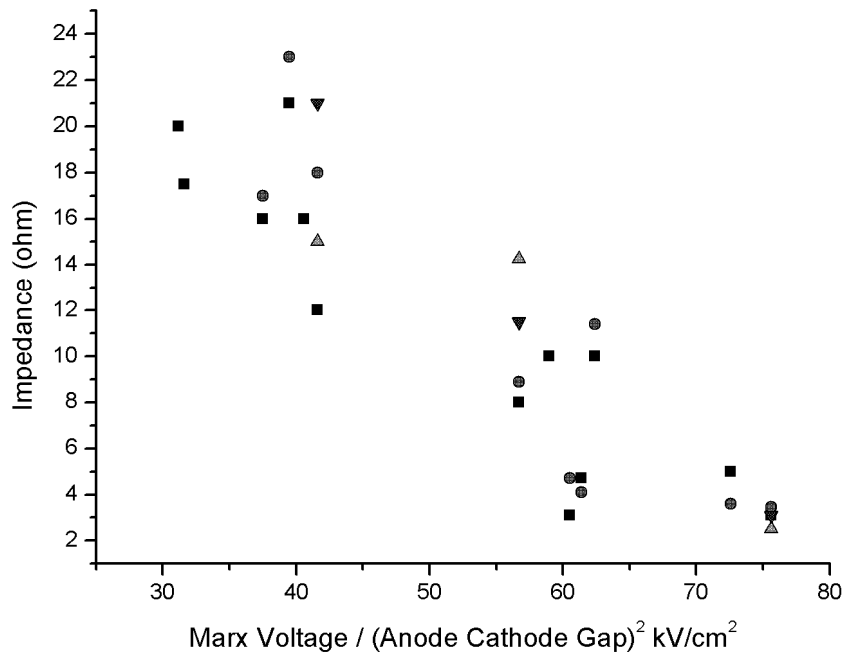


FIG. 4.7 Diode impedance for various Marx Voltage / $(\text{Anode Cathode Gap})^2$ at the diode.

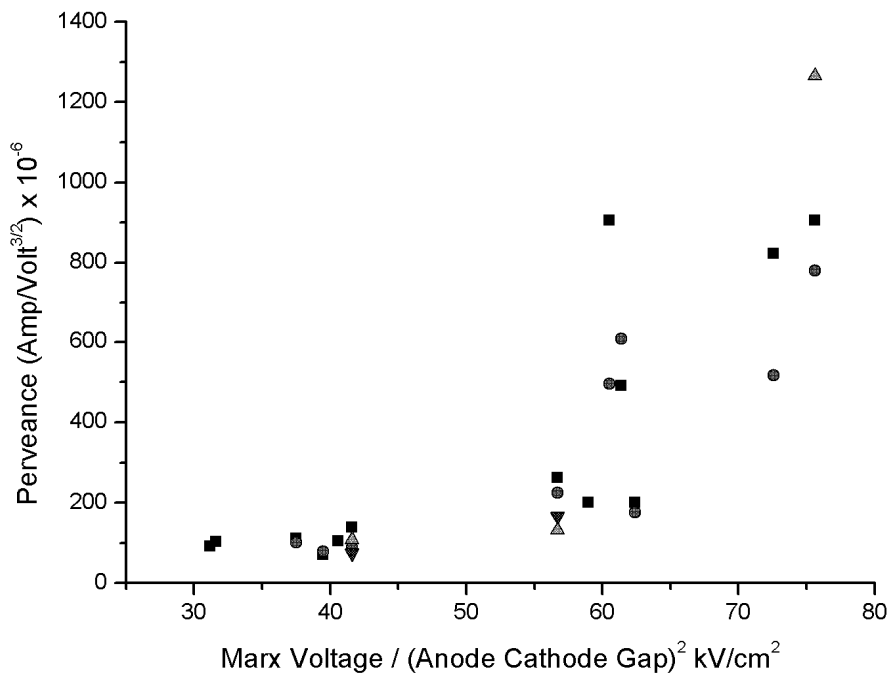


FIG 4.8 Diode perveance for various Marx Voltage / (Anode Cathode Gap)² at the diode.

It can be seen from Fig 4.8 that the perveance is more than $200 \mu\text{Perv}$ when the Marx Voltage / (Anode Cathode Gap)² is more than 56 kV/cm^2 . So in order to avoid the short-circuit condition the value of Marx Voltage / (Anode Cathode Gap)² has to be kept below 56 kV/cm^2 . Below 56 kV/cm^2 effect of Prepulse will be less and the diode can be operated with a better shot to shot reproducibility.

4.2 EFFECT OF CATHODE DIAMETER ON IREB GENERATION IN THE PRESENCE OF PREPULSE

To understand the effect of the cathode diameter on intense relativistic electron beam generation in the presence of a prepulse, we have carried out experiments with same AK gap but with various cathode diameters and diode voltages. Experiments were carried out with planar and annular graphite cathodes. Annular cathodes are used in self-magnetically pinched diodes to produce smaller diameter electron beams at the anode [28]. We have also investigated the shot to shot reproducibility of the diode voltage and current versus the prepulse generated plasma.

The electron space charge limited current in bipolar flow for an annular cathode is given by [11]

$$I_A(t) = 1.86 \times 2\pi \frac{\epsilon_o m_e c^3}{e} \left(\frac{r_c}{d - 2vt} \right)^2 (\sqrt{\gamma_o} - 0.8471)^2, \quad (4.1)$$

where c is the speed of light, $r_c = [R_c^2 - (R_c - x)^2]^{1/2}$ is an effective radius of the cathode, x is the thickness of the annular cathode, γ_o is the relativistic factor evaluated at the anode. So for both the planar and annular cathode the diode impedance decreases with the increase of cathode radius.

To study the prepulse effect on beam generation, the experiments were carried out in two phases. In phase I the beam generation experiments were carried out with planar cathodes of diameters 67 mm and 98 mm respectively.

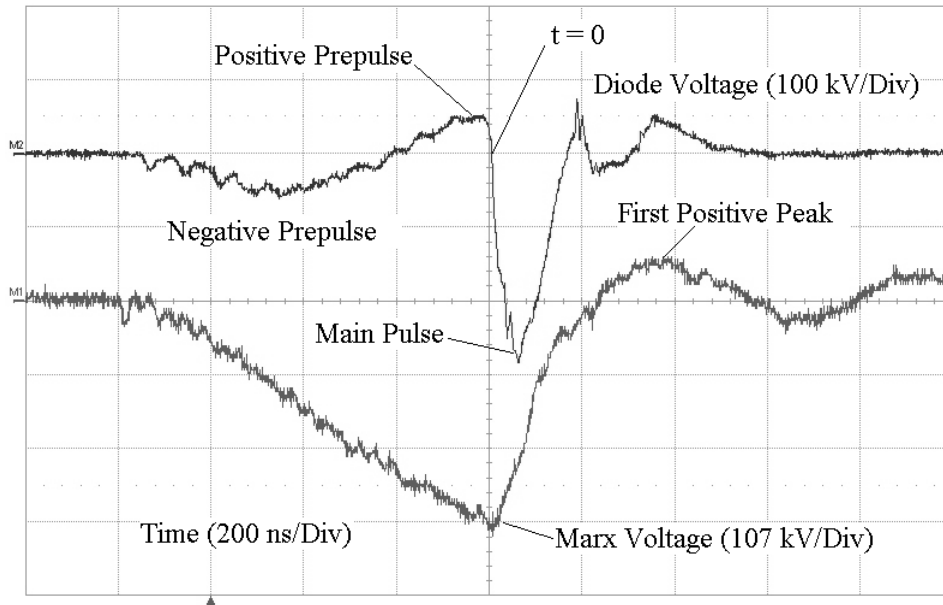


FIG. 4.9 Marx generator output and Prepulse waveform along with the main voltage pulse for 280 kV diode voltage in Phase I experiment with 67 mm diameter planar cathode.

In the phase II experiment, the planar cathodes have been replaced by annular cathodes of 40 mm and 70 mm diameters. Thickness of the annular cathode was $x = 5$ mm. The cathode material was graphite and a 30 cm diameter SS plate was used as an anode.

The diode voltage waveform along with the Marx Generator output voltage waveform in the phase I with 67 mm diameter cathode is shown in Fig. 4.9. One can see a negative prepulse of peak voltage ~ 60 kV, ~ 500 ns duration and a positive prepulse of peak voltage ~ 50 kV, ~ 200 ns duration during the Marx generator erection or the Blumlein line charging. Let us define the diode voltage as φ_D , current as I_D and the Marx generator voltage as φ_M .

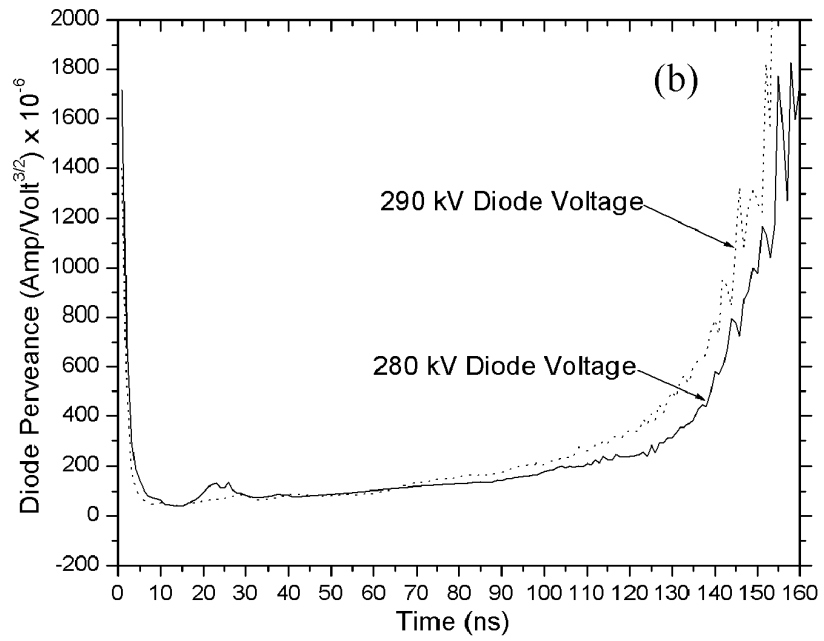
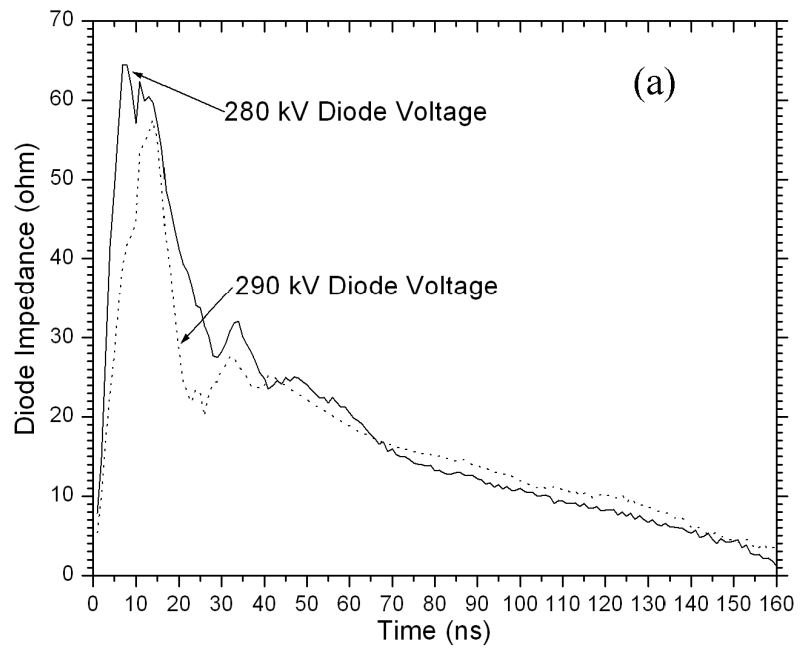


FIG. 4. 10 (a) The temporal behavior of the diode impedance in Phase I experiment with 67 mm diameter planar cathode. (b) Experimental perveance for Phase I experiment.

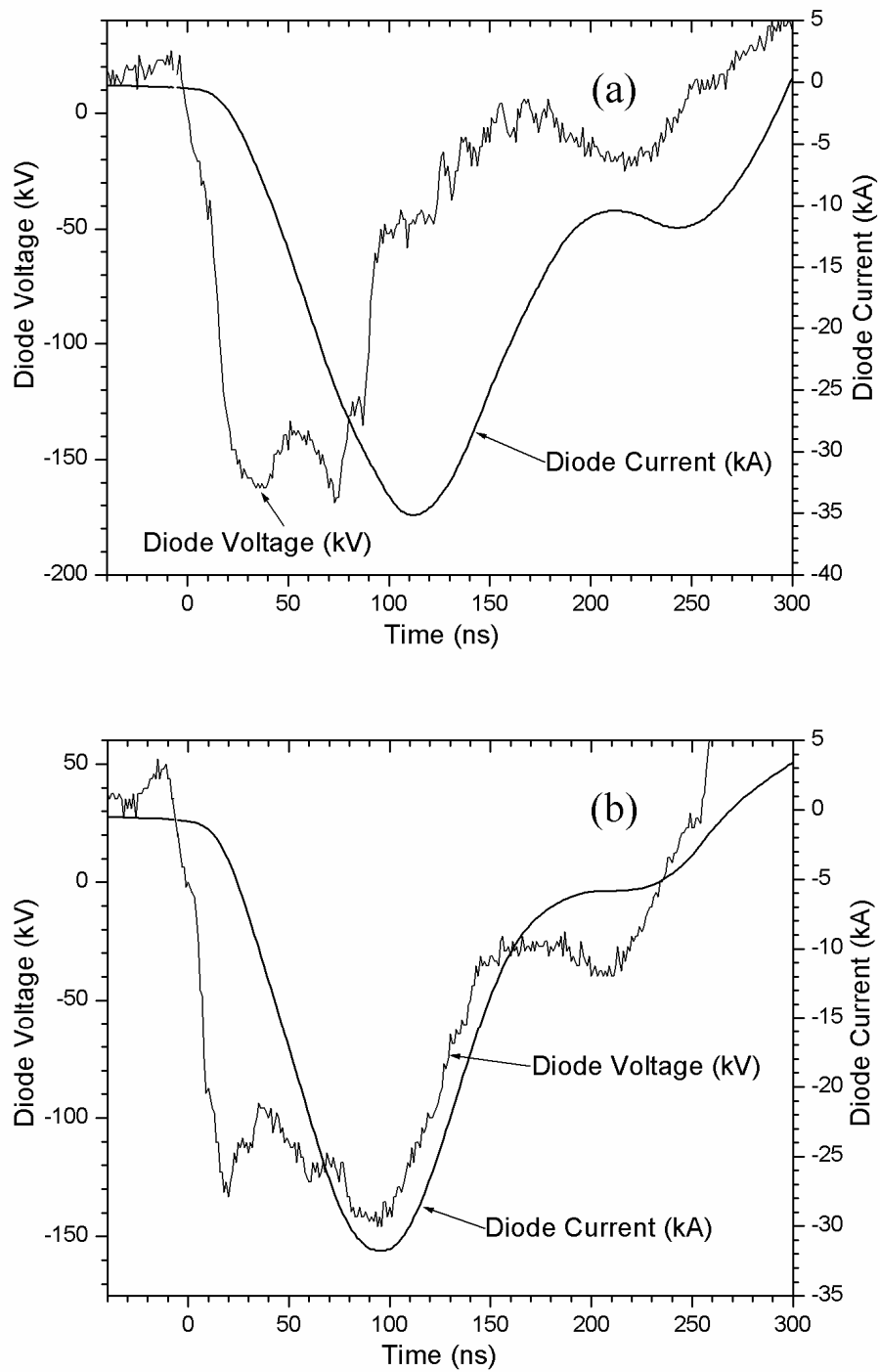


FIG. 4.11 The diode voltage and current waveform in Phase I experiment with 98 mm diameter planar cathode for (a) $\phi_M = 334$ kV, (b) $\phi_M = 306$ kV.

For phase I there was no shot to shot variation in the diode voltage and current for the same Marx generator voltage. Electron beam diode time varying impedance and perveance values were calculated using the voltage and current waveforms. The starting point or the zero time for perveance calculations was taken when the main voltage pulse is zero.

TABLE I. Results of the phase I experiment with 67 mm diameter cathode showing prepulse voltages and time durations for three different shots.

Marx output		Negative prepulse		Positive prepulse		Diode	
Voltage (kV)	Reversal (%)	Voltage (kV)	Duration (ns)	Voltage (kV)	Duration (ns)	Voltage (kV)	Current (kA)
320	17	67	500	53	200	290	19
320	17	53	500	53	200	280	18
362	17	90	500	20	50	340	24

Fig. 4.10(a) shows the diode impedance versus time for two different shots. The diode perveance for two different shots is shown in Fig. 4.10(b). One can see that there is not much differences in the impedance and perveance curve for the two shots. Results of the Phase I experiments with 67 mm diameter cathode are shown in the Table I. The % reversal in the Marx generator output voltage waveform is calculated from the ratio between the first positive peak and the peak Marx generator voltage. One can see from the Fig. 4.10(a) that the initial impedance for $\phi_D = 290$ kV voltage is less than that for the case with $\phi_D = 280$ kV voltage. This is because of the fact that the negative prepulse voltage for $\phi_D = 290$ kV voltage is higher than the case with $\phi_D = 280$ kV voltage. The estimated bipolar SCL current [see chapter 5, Eq. (5.2)], with plasma velocity $v = 0$, for 290 kV diode voltage is only 3.8 kA, much less than the measured current 19 kA. This implies that the electrode plasma closure is an important effect in this experiment. It was also found that, at $\phi_M = 362$ kV, and with a corresponding negative prepulse voltage of 90 kV, the time varying diode perveance remains same as of Fig. 4.10(b).

The reversal in the Marx output voltage was $\sim 17\%$, same as the case with $\phi_M = 320$ kV. This suggests that the prepulse generated plasma expansion has little effect in this experiment.

TABLE II. Results of the phase I experiment with 98 mm diameter cathode showing prepulse voltages and time durations for two different shots.

Marx output		Negative prepulse		Positive prepulse		Diode	
Voltage (kV)	Reversal (%)	Voltage (kV)	Duration (ns)	Voltage (kV)	Duration (ns)	Voltage (kV)	Current (kA)
334	58	67	500	27	100	169	35
306	45	53	500	47	200	146	32

For 98 mm cathode diameter, the diode voltage was less than the Marx generator output voltage and some shot to shot variation in the diode voltage and current were measured for the same Marx generator voltage. Also a large reversal seen in the Marx output voltage is due to impedance mismatch between the diode and the Blumlein line. The estimated bipolar SCL current [see chapter 5, Eq. (5.2)], with plasma velocity $v = 0$, for 169 kV diode voltage is only 3.6 kA. This indicates the effect of the prepulse on the diode voltage and current. Results of the Phase I experiments with 98 mm cathode diameter is shown in the Table II.

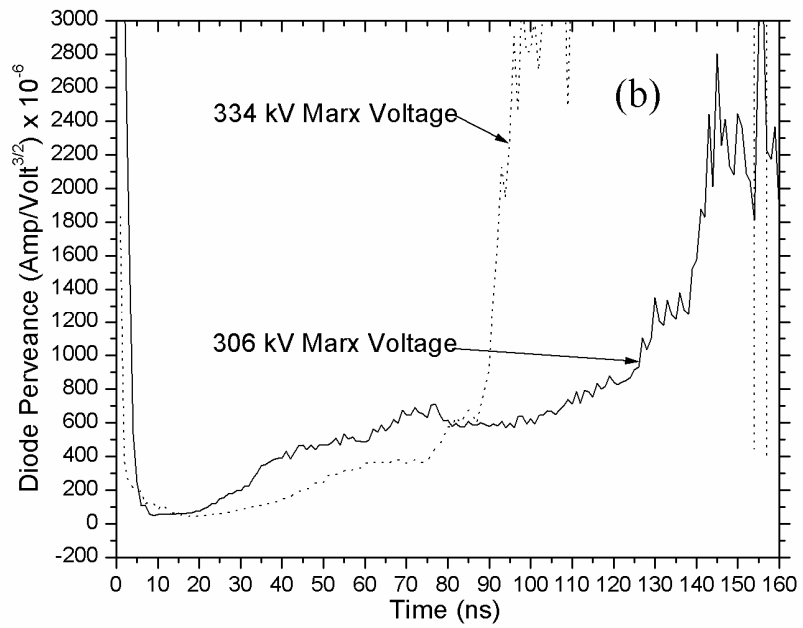
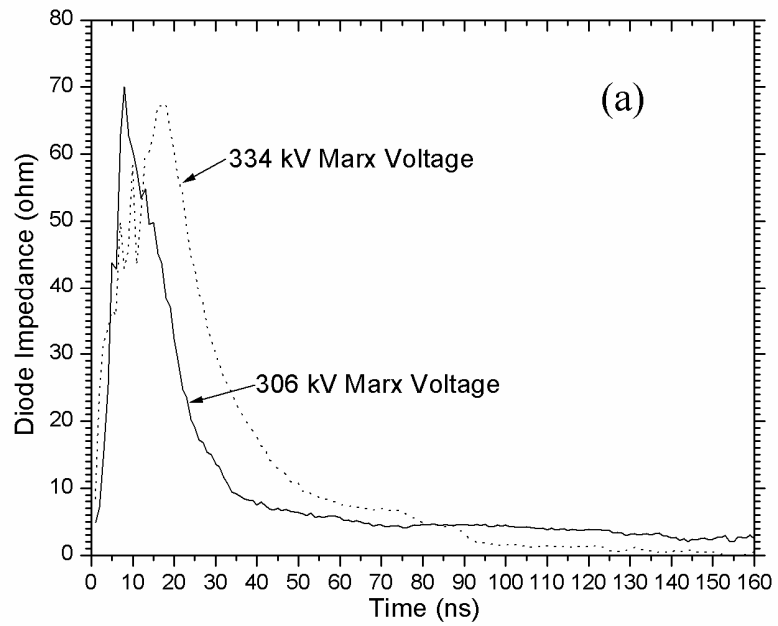


FIG. 4.12 (a) The temporal behavior of the diode impedance in Phase I experiment with 98 mm diameter planar cathode for two different Marx generator voltages. (b) Experimental perveance for Phase I experiment for two different Marx generator voltages.

The diode voltage and current waveforms for two different Marx generator voltages are shown in Fig 4.11(a) and Fig 4.11(b). Fig. 4.12 (a) shows the diode impedance versus time for the two different Marx generator voltages. Experimental perveance for two different Marx generator voltages are shown in Fig. 4.12(b). One can see from the Fig.4.12 (b) and Fig 4.11(a) that for the shot with $\phi_M = 334$ kV voltage the diode closes at much earlier time ~ 90 ns as compared to $\phi_M = 306$ kV. Fig. 4.12(a) shows that till ~ 15 ns from the beginning of the diode voltage rise the diode impedance for $\phi_M = 334$ kV is less than for $\phi_M = 306$ kV. This is probably due to the fact that the negative prepulse voltage is large for $\phi_M = 334$ kV voltage and the prepulse generated cathode plasma expanded to a larger distance than it expands at $\phi_M = 306$ kV, even though the positive prepulse voltage amplitude and duration was more for $\phi_M = 306$ kV. This implies that the positive prepulse voltage has little effect on the diode perveance.

TABLE III. Results of the phase II experiment with 40 mm diameter cathode showing prepulse voltages and time durations for two different shots.

Marx output		Negative prepulse		Positive prepulse		Diode	
Voltage (kV)	Reversal (%)	Voltage (kV)	Duration (ns)	Voltage (kV)	Duration (ns)	Voltage (kV)	Current (kA)
320	30	80	500	33	150	300	25
278	25	53	500	60	250	346	10

Also the reversal in the Marx generator output voltage is less for the case $\phi_M = 306$ kV due to the smaller negative prepulse voltage. The reason for the shot to shot variation in this experiment may be because of a decrease in the uniformity of the prepulse generated plasma with the corresponding increase in the cathode diameter.

In the phase II, for both the cathode diameter some shot to shot variation in the diode voltage and current were measured for the same Marx generator voltage. But the diode peak voltage

obtained for 40 mm diameter cathode is much larger than the 70 mm diameter cathode. Results of the Phase II experiments are shown in the Table III and Table IV. The estimated bipolar SCL current from Eq. (4.1), with plasma velocity $v = 0$, for 346 kV diode voltage is only 0.9 kA. The diode voltage and current waveforms for two different Marx generator voltages are shown in Fig. 4.13(a) and Fig. 4.13(b). One can see from the Fig. 4.13(b) that the voltage waveform is associated with few spikes which can be considered as noise. Fig. 4.14 shows the diode impedance versus time for two different Marx generator voltages. One can see from the Fig. 4.14 that the diode impedance obtained for $\phi_M = 278$ kV is much higher than that for $\phi_M = 320$ kV as the prepulse voltage is much higher for the second case.

TABLE IV. Results of the phase II experiment with 70 mm diameter cathode showing prepulse voltages and time durations for two different shots.

Marx output		Negative prepulse		Positive prepulse		Diode	
Voltage (kV)	Reversal (%)	Voltage (kV)	Duration (ns)	Voltage (kV)	Duration (ns)	Voltage (kV)	Current (kA)
320	48	67	500	27	100	210	31
348	48	67	500	33	150	231	35

The estimated bipolar SCL current for 70 mm cathode diameter from Eq. (4.1), with plasma velocity $v = 0$, for 231 kV diode voltage is only 1.1 kA.

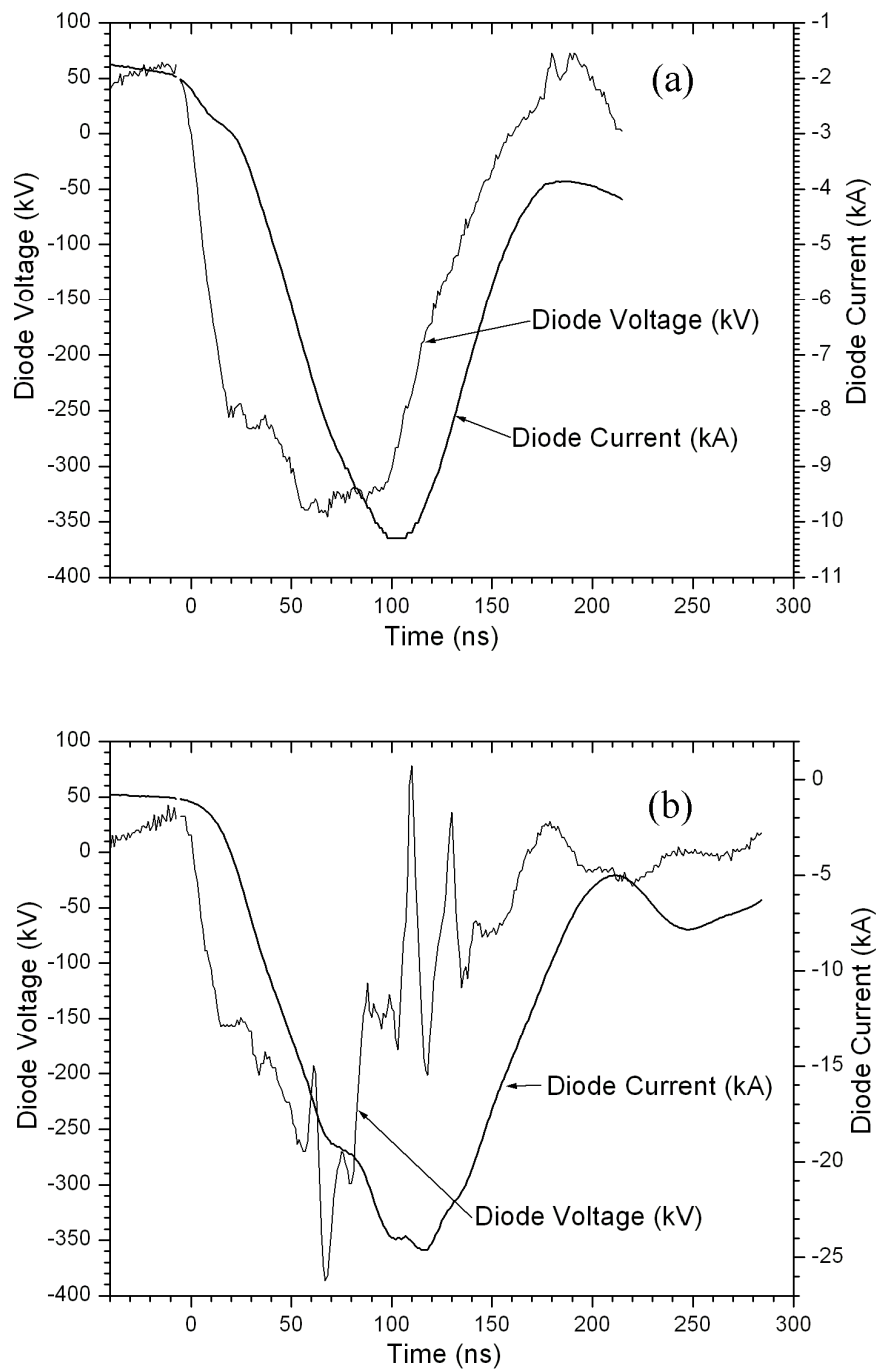


FIG. 4.13 The diode voltage and current waveform in Phase II experiment with 40 mm diameter annular cathode for (a) $\phi_M = 278$ kV, (b) $\phi_M = 320$ kV.

The diode voltage and current waveforms for two different Marx generator voltages are shown in Fig 4.15(a) and Fig 4.15(b). The diode voltage waveform for this case is always noisy. Fig. 4.16 shows the diode impedance versus time for two different Marx generator

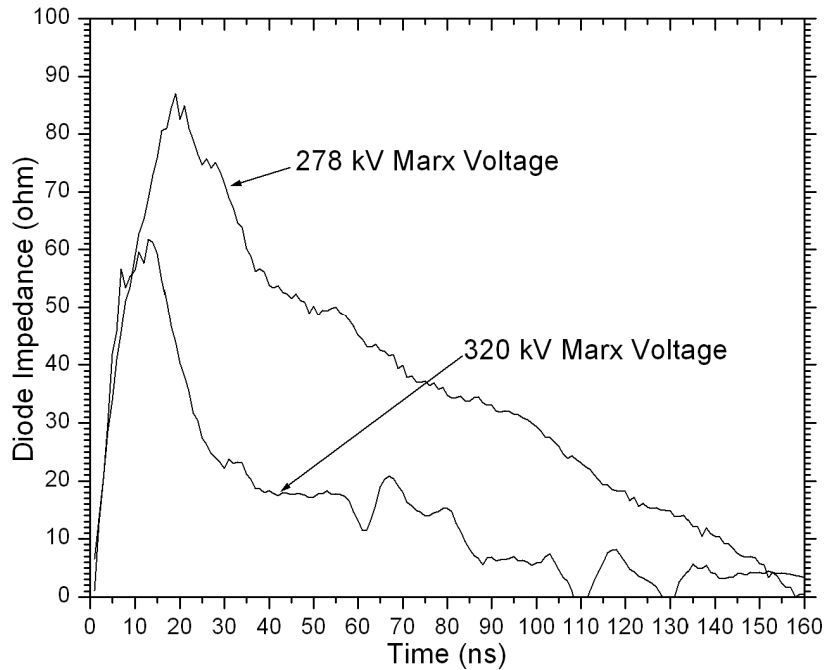


FIG. 4.14 The temporal behavior of the diode impedance in Phase II experiment with 40 mm diameter annular cathode for two different Marx generator voltages.

voltages. One can see that till ~ 15 ns from the beginning of the diode voltage rise the diode impedance for $\phi_M = 348$ kV is less than for $\phi_M = 320$ kV, even though the negative prepulse voltages were same. Probably because of the fact that the uniformity of the prepulse generated plasma was not similar for both the cases. It is interesting to note that the reversal in the Marx generator output voltage is same for the two cases. But the reversal is large as compared to the 40 mm diameter annular cathode.

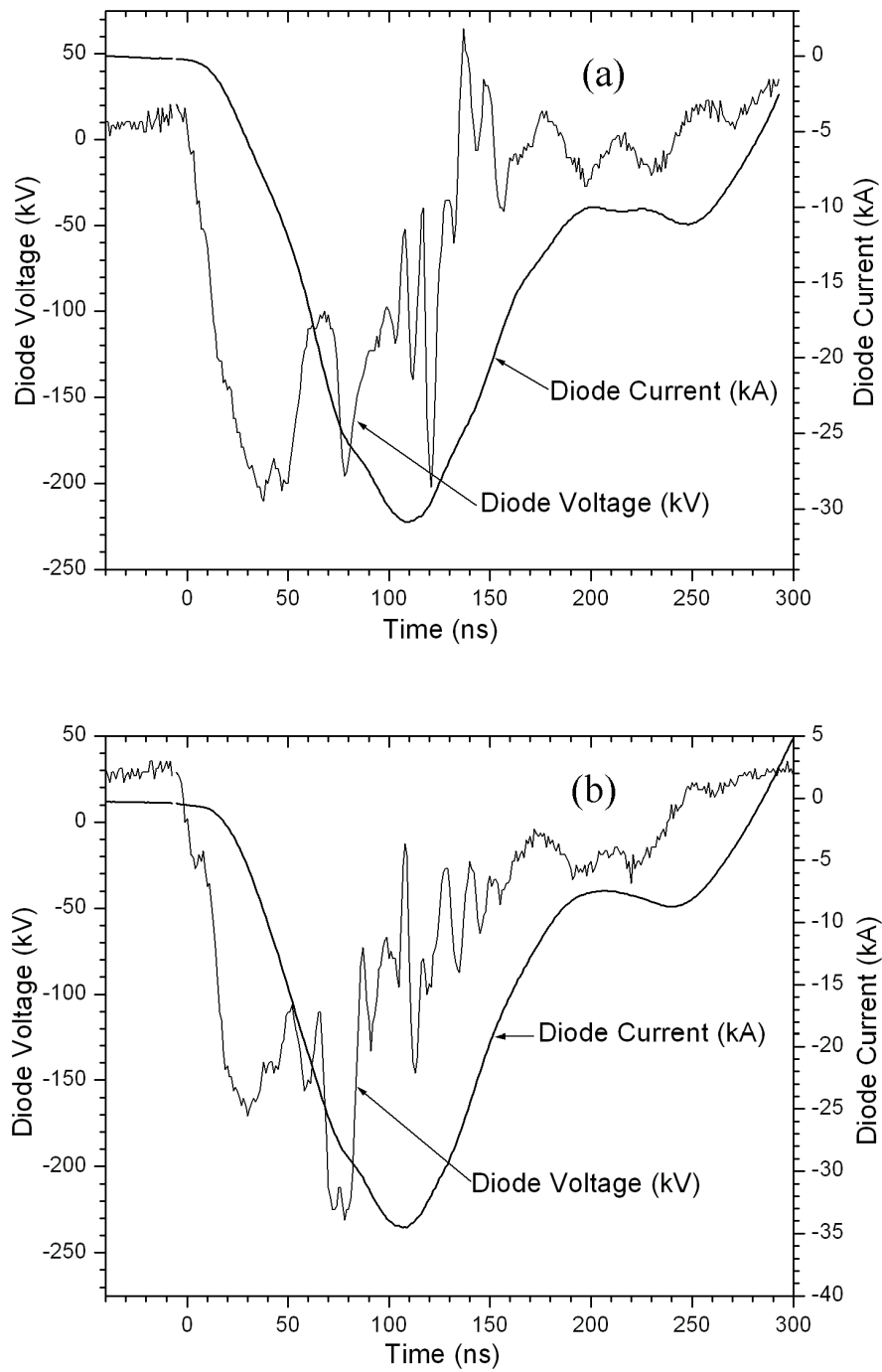


FIG. 4.15 The diode voltage and current waveform in Phase II experiment with 70 mm diameter annular cathode for (a) $\phi_M = 320$ kV, (b) $\phi_M = 348$ kV.

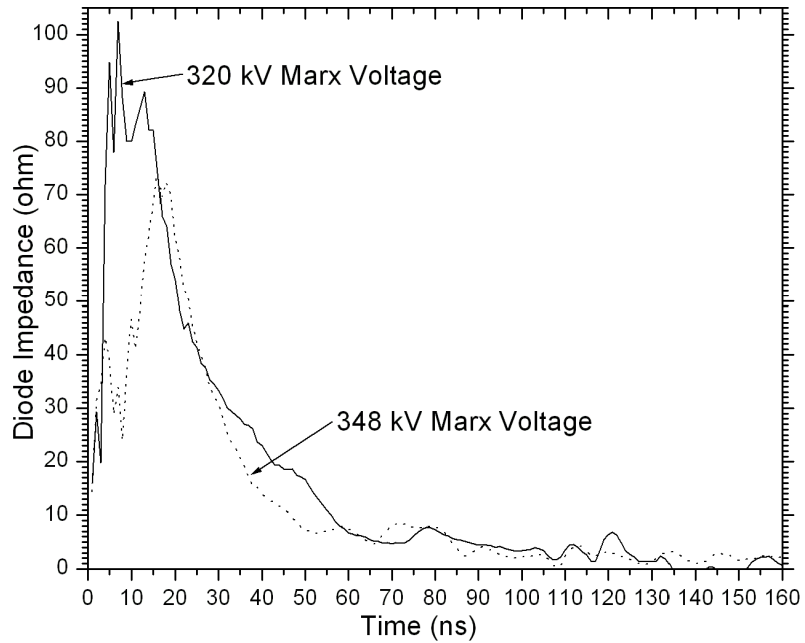


FIG. 4.16 The temporal behavior of the diode impedance in Phase II experiment with 70 mm diameter annular cathode for two different Marx generator voltages.

4.3 IREB GENERATION IN HIGH POWER CYLINDRICAL DIODE IN THE PRESENCE OF PREPULSE

The experimental setup used is shown in Chapter 3.3. The cylindrical diode consists of an annular cathode and grounded mesh anode. A graphite cathode with outer diameter of 13.7 cm and a copper mesh anode of 8.6 cm diameter were used for the cylindrical diode. The graphite cathode has a 2 cm emission length. To study the prepulse effect on beam generation in a high power cylindrical diode, the experiments were carried out in three phases. In phase I the cathode inner diameter was set to 12.3 cm with the radial AK gap of 1.85 cm. The diode chamber was evacuated using a diffusion pump backed by a rotary pump. The vacuum in the diode chamber was $\leq 6 \times 10^{-5}$ mbar. In the phase II experiment,

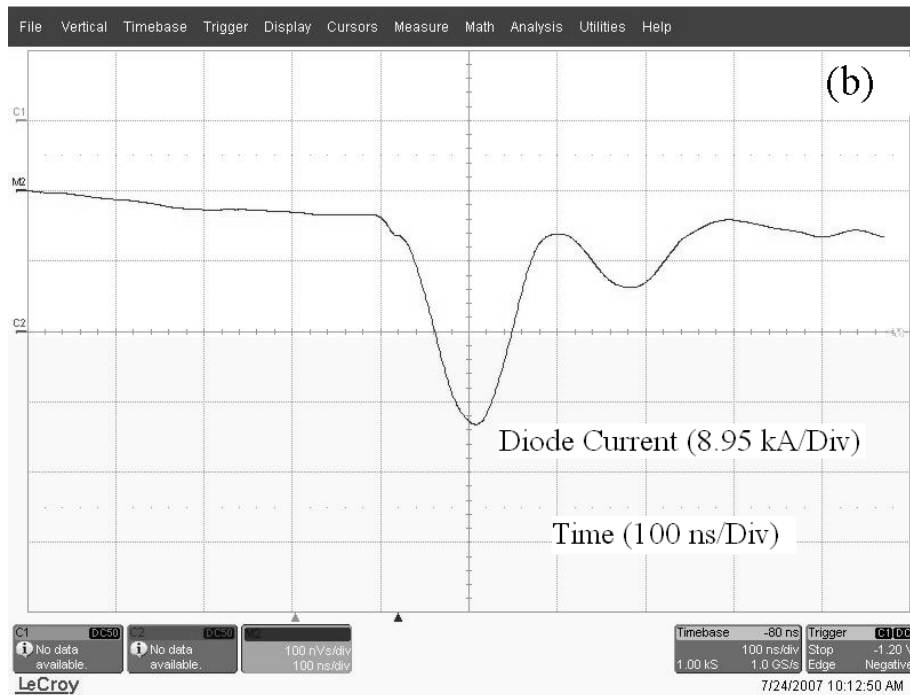
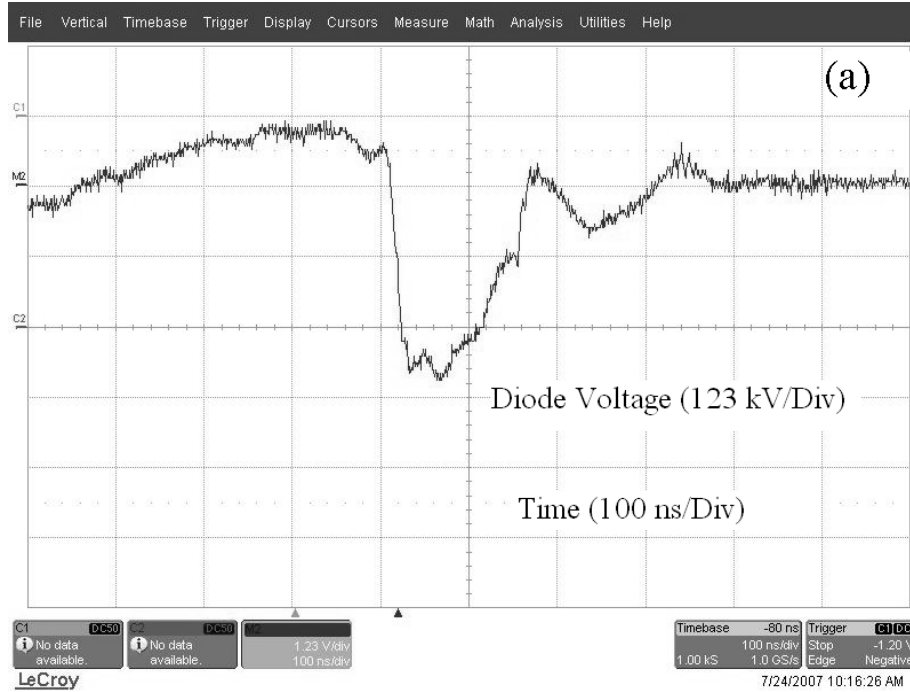


FIG. 4.17 (a) Voltage waveform in the Phase I experiment. (b) Current waveform in the Phase I experiment.

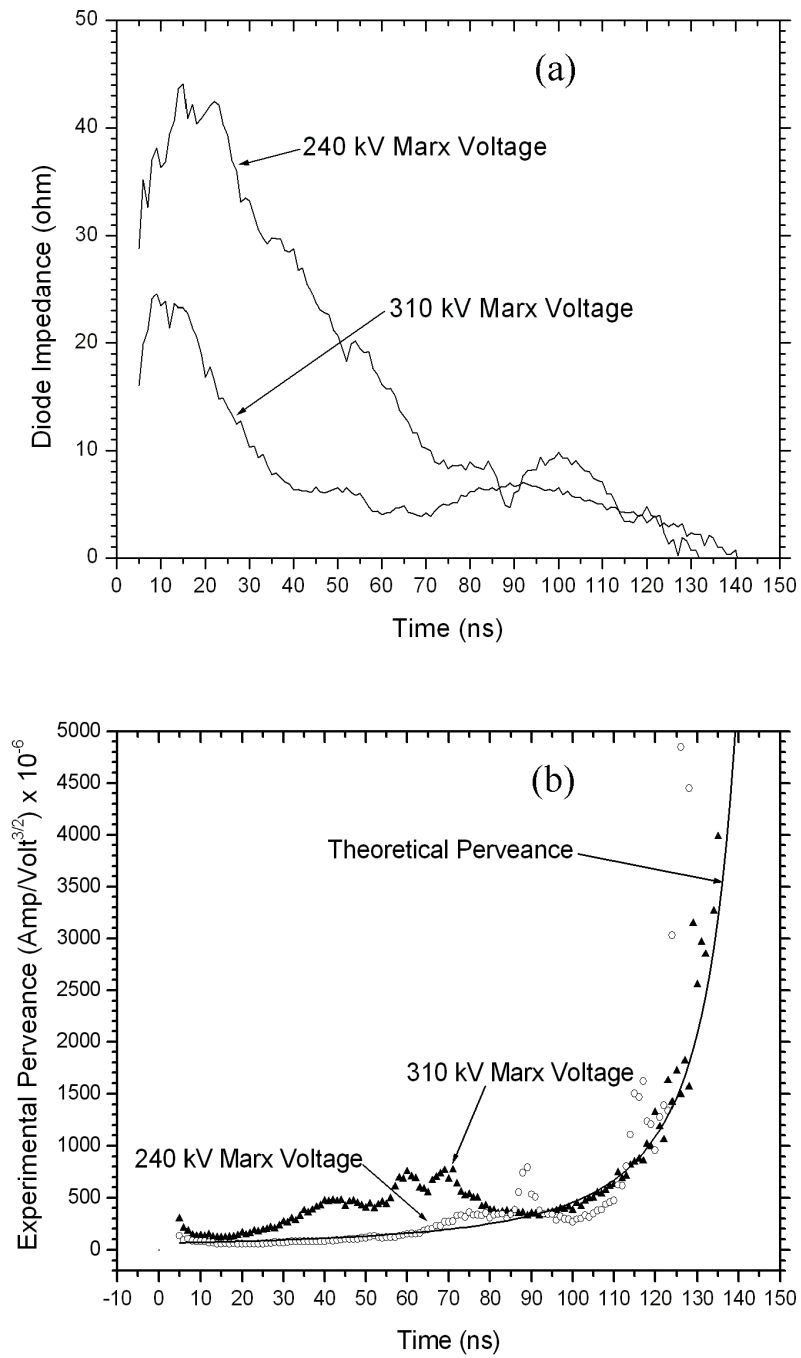


FIG. 4.18 (a) The temporal behavior of the diode impedance in Phase II experiment. (b) Experimental and theoretical perveance for Phase II experiment. Solid triangle represent perveance for 310 kV Marx voltage and open circles represent 240 kV Marx voltage. Continuous line represents theoretical perveance.

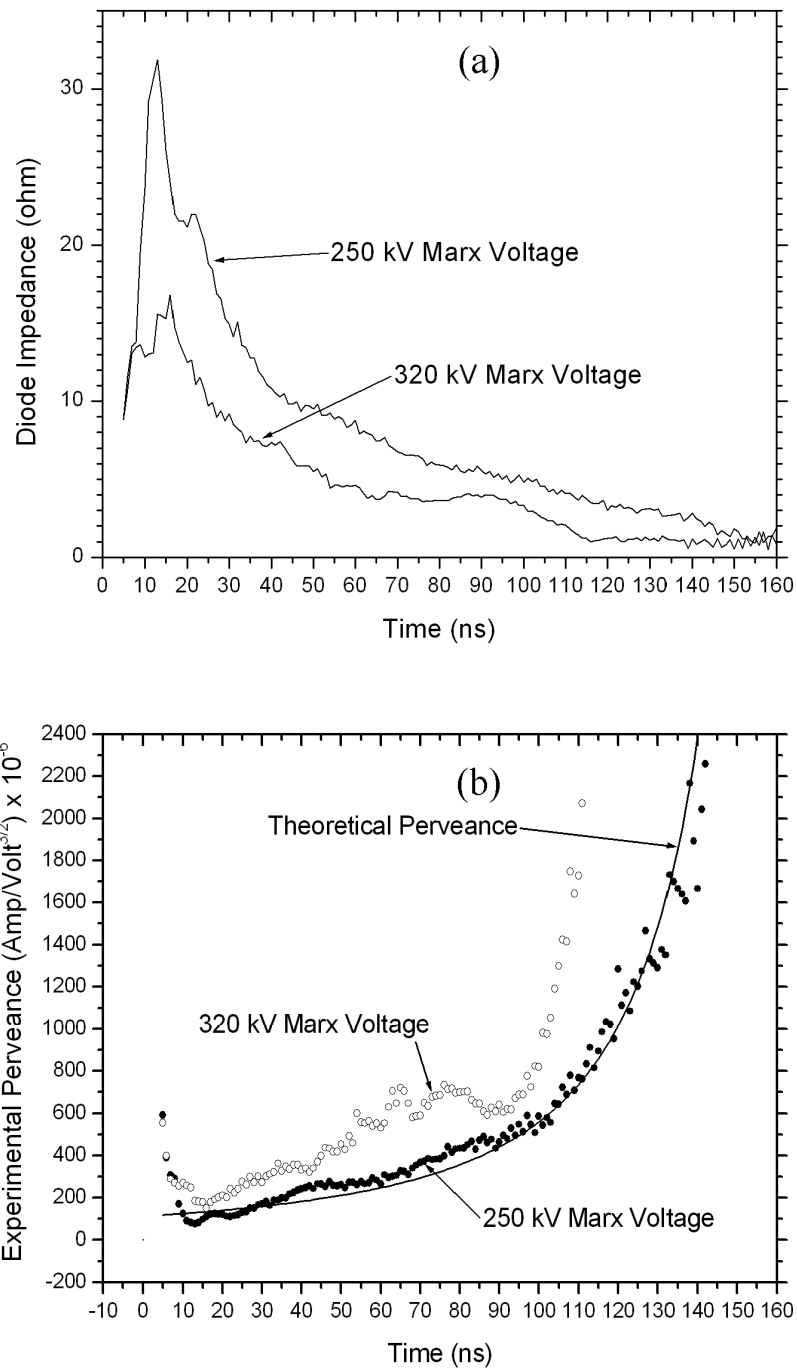


FIG. 4.19 (a) The temporal behavior of the diode impedance in Phase III experiment. (b) Experimental and theoretical perveance for Phase III experiment. Solid circles represent perveance for 250 kV Marx voltage and open circles represent 320 kV Marx voltage. Continuous line represents theoretical perveance.

the cathode inner diameter was set to 11.9 cm with the radial AK gap of 1.65 cm. In phase III experiment, the cathode inner diameter was set to 11 cm with the radial AK gap of 1.2 cm. For the phase I there was no shot to shot variation in the voltage and current for the same Marx generator voltage. One can see from Fig. 4.17 (b) that the diode current starts at positive prepulse, i.e., there is a plasma formation at the cathode during the prepulse with negative polarity. Also, one can see the rise in the impedance at the beginning of the accelerating pulse, which indicates on plasma prefilled mode of the diode operation with a fast plasma erosion.

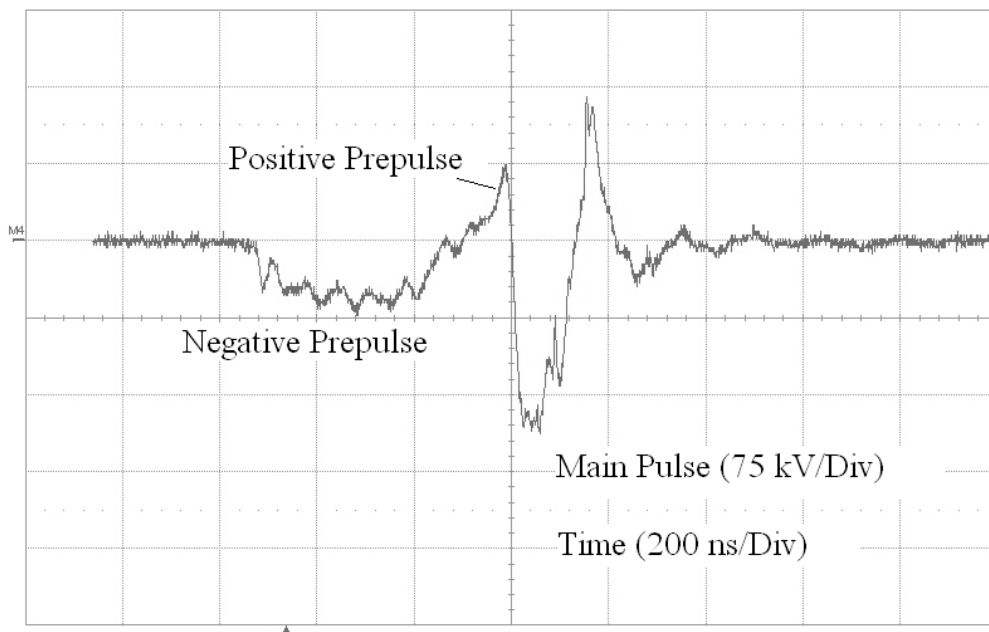


FIG. 4.20 Prepulse waveform along with the main voltage pulse for 240 kV Marx voltage in Phase II experiment.

In the phase II, the diode voltage was less than the Marx generator output voltage and some shot to shot variation in the diode voltage and current were measured for the same Marx voltage. This indicates the effect of the prepulse on the diode voltage and current. Results of the Phase II experiments are shown in the Table I. Fig. 4.18 (a) shows the diode impedance

versus time for two different Marx generator voltages. Experimental perveance for two different Marx generator voltages is shown in Fig. 4.18 (b). One can see that after 110 ns, the perveance increases rapidly as compared to the case of the phase

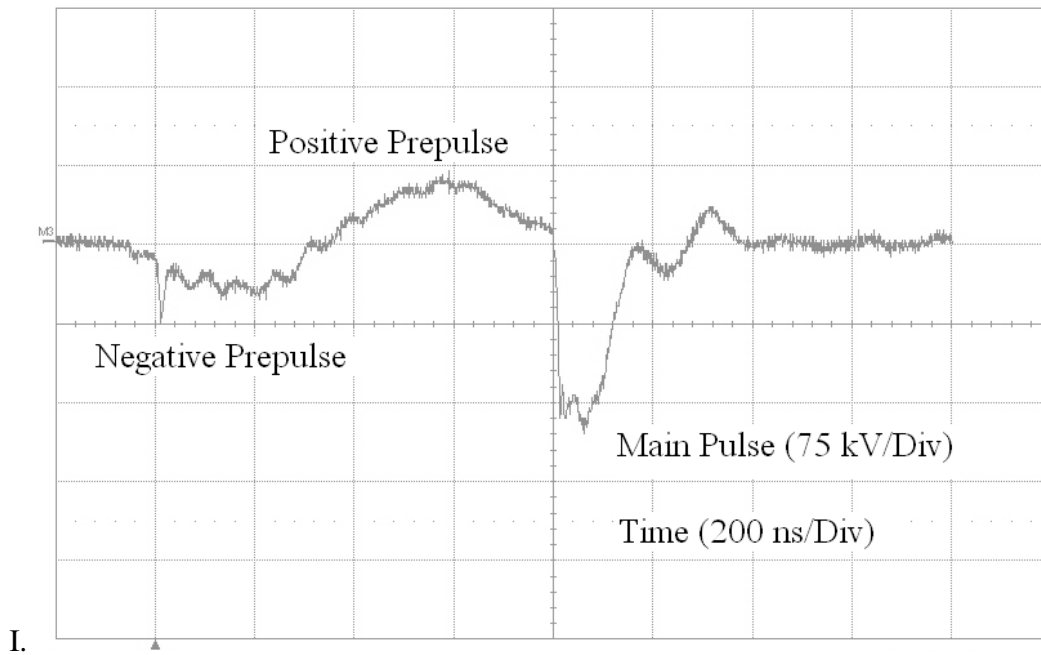


FIG. 4.21 Prepulse waveform along with the main voltage pulse for 250 kV Marx voltage in Phase III experiment.

This shows that AK gap closure occurs after 110 ns. It is interesting to note that the time varying experimental perveance values were the same for the two shots except their values between 20 ns and 80 ns of the diode voltage. Since the prepulse voltages were similar for the two cases, the effective diode geometry did not changed much due to the prepulse generated plasma expansion. Fig. 4.20 shows the prepulse waveform for 240 kV Marx generator voltage.

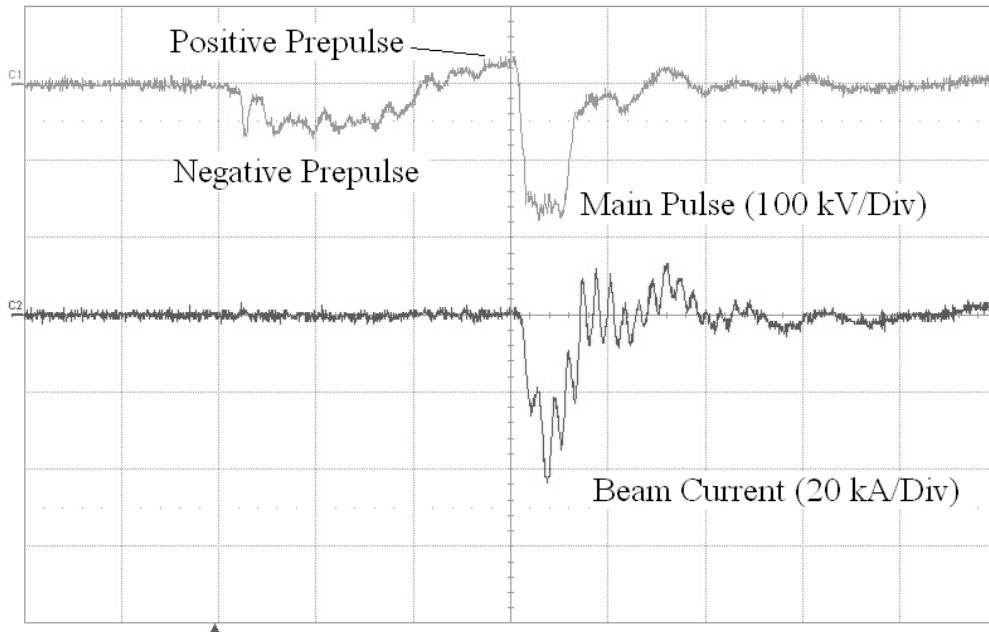


FIG. 4.22 Prepulse waveform along with the main voltage and current waveform for 320 kV Marx voltage in Phase III experiment.

Results of the Phase III experiments are shown in the Table II. For the Phase III, the diode voltage obtained was less than the Marx generator output voltage also some shot to shot variation in the diode voltage and current were measured for the same Marx generator voltage. Fig. 4.19 (a) shows the diode impedance versus time for the two different Marx generator voltages. Experimental perveance for two different shots, one with $\varphi_M = 320$ kV and another with $\varphi_M = 250$ kV are shown in Fig. 4.19 (b). One can see from the Fig. 4.19 (b) that already at the beginning of the main voltage pulse the initial perveance for $\varphi_M = 320$ kV is larger than for case $\varphi_M = 250$ kV.

TABLE I. Results of the phase II experiment showing prepulse voltages and time durations for two different Marx generator output voltages.

Marx output voltage (kV)	Negative prepulse		Positive prepulse		Diode	
	Voltage (kV)	Duration (ns)	Voltage (kV)	Duration (ns)	Voltage (kV)	Current (kA)
310	60	400	60	160	190	30
240	70	400	70	100	185	16

This is due to the fact that the negative prepulse voltage is large for $\varphi_M=320$ kV voltage and the prepulse generated cathode plasma expanded to a larger distance than it expands at $\varphi_M=250$ kV, even though the positive prepulse voltage amplitude and duration was more for $\varphi_M=250$ kV (Fig. 4.21 and Fig. 4.22). This implies that the positive prepulse voltage has little effect on the diode perveance. The reason for this may be that the explosive emission threshold for copper anode mesh is higher than for the graphite cathode. After ~ 100 ns, the perveance for $\varphi_M=320$ kV increases rapidly showing AK gap closure.

TABLE II. Results of the phase III experiment showing prepulse voltages and time durations for two different Marx generator output voltages.

Marx output voltage (kV)	Negative prepulse		Positive prepulse		Diode	
	Voltage (kV)	Duration (ns)	Voltage (kV)	Duration (ns)	Voltage (kV)	Current (kA)
320	60	400	30	150	170	42
250	45	400	60	450	175	26

The comparison of the Phase III experiment with previous planar diode experiment with 1.13 cm AK gap, shows that in the case of the planar diode the prepulse generated plasma completely fills the AK gap and the diode behaves as plasma filled diode. For the cylindrical diode the prepulse generated plasma decreases the impedance of the diode and, respectively, increases the diode perveance. However, one can conclude that the plasma dose not

completely fill the diode gap, resulting in ≥ 170 kV diode voltage. Let us note, that the current density in the planar diode experiment was in the range $0.2 - 1.0$ kA/cm², similar to the measured peak current density for the present cylindrical diode experiment, $0.2- 0.6$ kA/cm². The effect of the prepulse is less pronounced in the cylindrical diode as compared to planar diode that allows one to operate the cylindrical diode with the AK gap ≤ 1.85 cm.

4.4 ELECTRON BEAM GENERATION WITH A BIPOLAR PULSE IN A HIGH POWER CYLINDRICAL DIODE

In the present experiment, KALI 5000 system has been operated without a prepulse switch which results in generation of the bipolar high-voltage prepulse.

The experimental setup used is shown in Chapter 3.3. The cylindrical diode consists of an annular cathode and grounded mesh anode. A graphite cathode with outer diameter of 13.7 cm and a copper mesh anode of 8.6 cm diameter were used for the cylindrical diode. The graphite cathode has a 2 cm emission length. The inner diameter of the graphite cathode is 11 cm with the radial AK gap of 1.2 cm. The diode diagnostics employed were aqueous copper sulphate resistive divider for the diode voltage, and B-Dot probe for the diode current measurement. The inductive correction due to the transmission line inductance of 14 nH from the resistive divider to the cathode edge is less than a few percent since the di/dt is typically $0.14-0.27$ kA/ns in the present experiment. The diode chamber was evacuated to $\leq 8 \times 10^{-5}$ mbar using a diffusion pump backed by a rotary pump. During the positive voltage pulse the copper mesh act as an explosive emission electron source. Whereas during the negative voltage pulse the outer graphite electrode acts as a cathode.

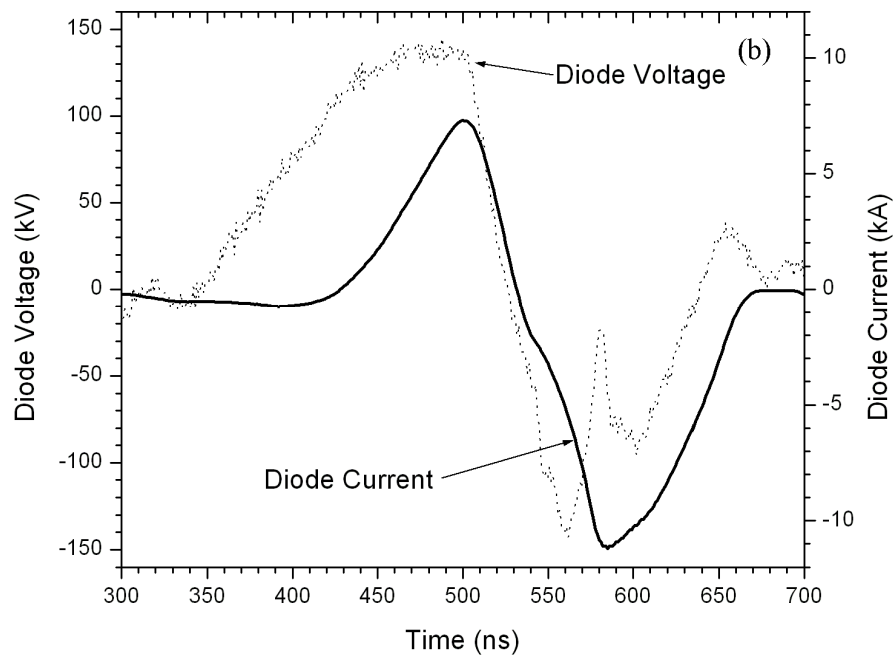
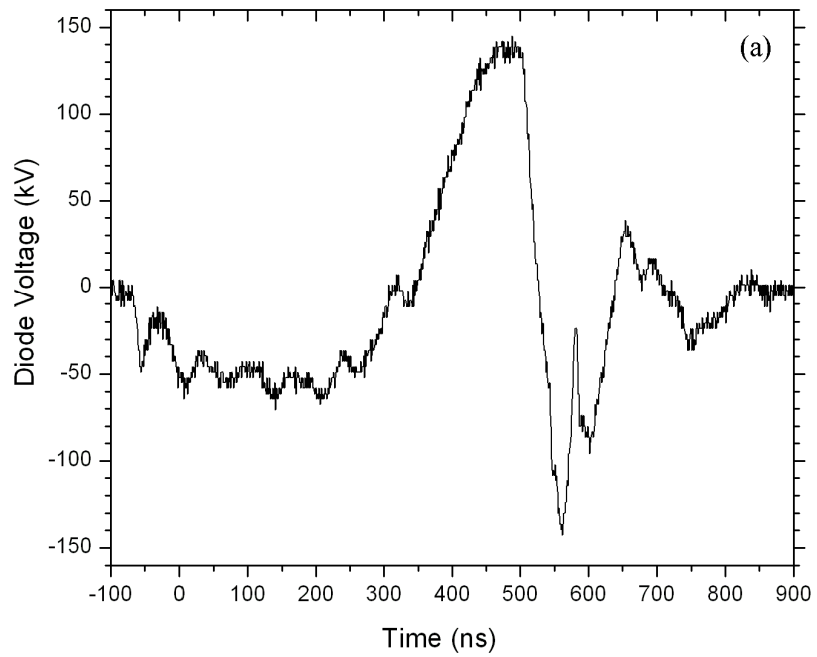


FIG. 4.23 (a) The diode voltage waveform. (b) The diode positive and the second negative voltage waveform with the corresponding current waveform.

The diode voltage waveform is shown in Fig. 4.23 (a). During the first ~ 400 ns the diode voltage is negative with the peak voltage of ~ 70 kV, then the diode voltage changes to positive for ~ 200 ns duration and again negative for ~ 100 ns duration.

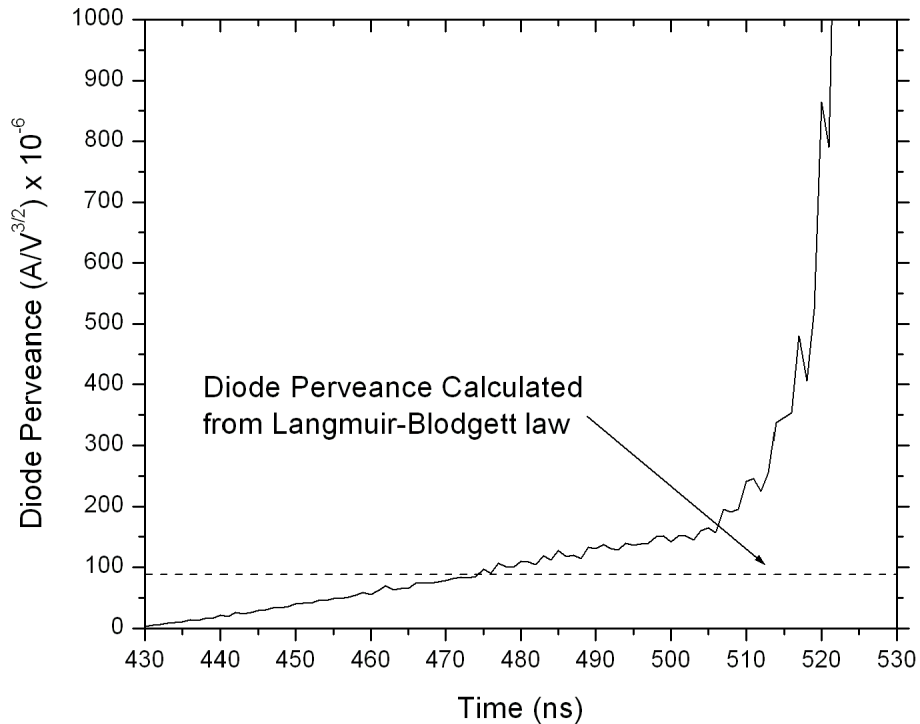


FIG. 4.24 The temporal behavior of the diode perveance for positive voltage pulse. The dashed line is the perveance calculated from Langmuir-Blodgett law.

No detectable current is recorded in the diode during the initial negative diode voltage. Fig. 4.23 (b) shows the diode positive, and the second negative voltage waveform along with the corresponding current wave form. The diode peak voltage and current obtained in the positive and negative voltage pulse were 142 kV, 7.3 kA and 143 kV, 11.2 kA, respectively. One can see a sharp decrease and increase in the negative voltage pulse [Fig. 4.23 (b)]. At the same time, however, there are no changes in the current waveform. It may be due to a partial surface

breakdown either along the voltage divider surface or along the interface insulator. It is understood that this partial surface breakdown introduces error in the voltage measurement of the negative voltage pulse.

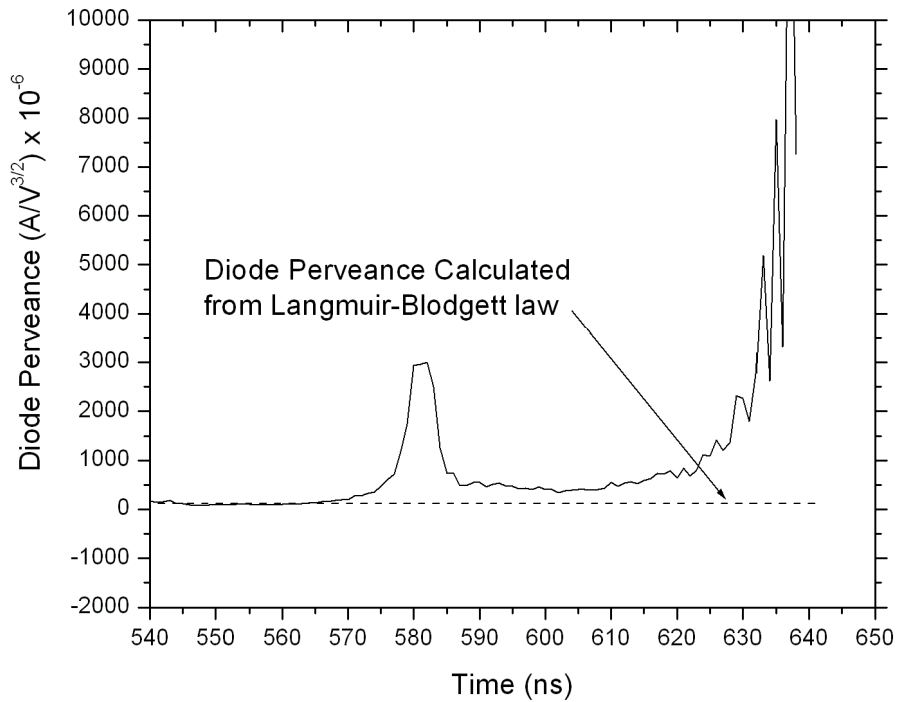


FIG. 4.25 The temporal behavior of the diode perveance for negative voltage pulse. The dashed line is the perveance calculated from Langmuir-Blodgett law.

One can see from Fig. 4.23 (b) that the diode current starts at the positive voltage pulse after ~ 80 ns from the initial rise in the diode voltage. This indicates that the explosive emission threshold for the copper mesh is ~ 95 kV/cm and the plasma formation occurs after ~ 80 ns. Because of this high explosive emission threshold, ~ 70 kV positive

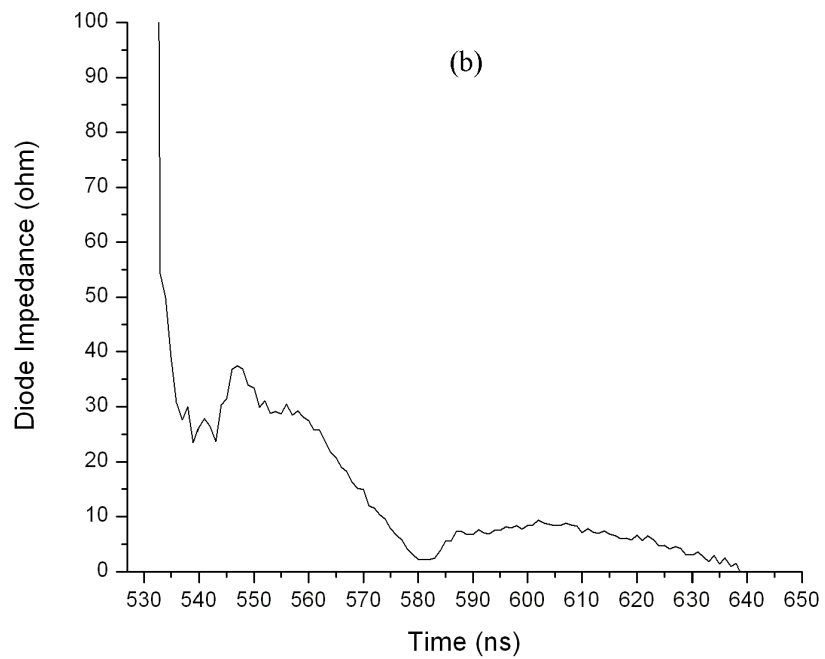
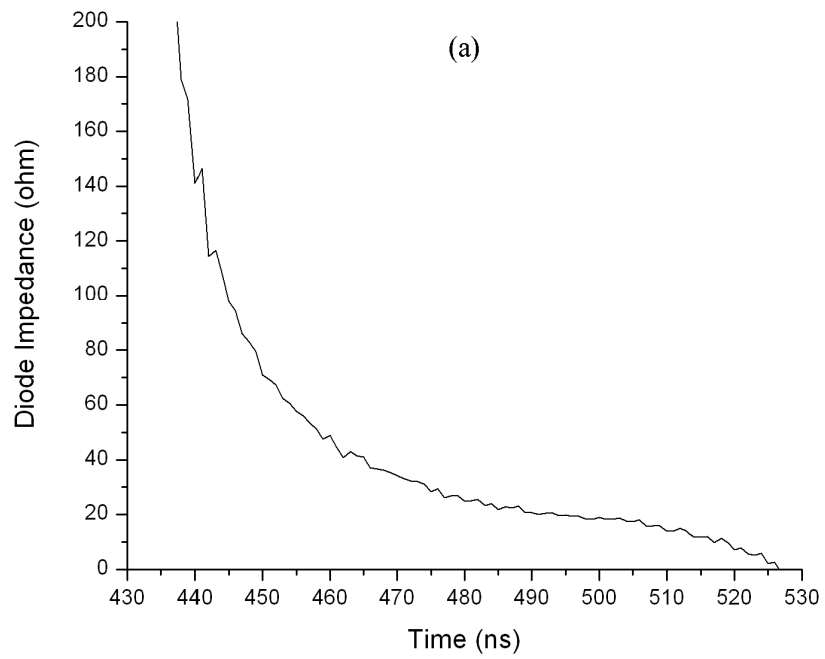


FIG. 4.26 (a) The temporal behavior of the diode impedance for positive voltage pulse. (b) The temporal behavior of the diode impedance for negative voltage pulse.

prepulse voltage had no significant effect on the diode perveance in our earlier experiment described in the previous section. One can also see from Fig. 4.23 (b) that before the onset of positive current, the diode current is slightly negative. The latter indicates that there is a plasma formation at the graphite cathode during the first negative voltage pulse. In the subsequent discussion, the negative voltage pulse refers to second negative voltage pulse only. At the time of maximum current during the positive pulse, the diode voltage $V = 130$ kV, if we use the initial radii of the electrodes (with no gap closure) and assume a 2 cm emission length (the length of the anode during the positive pulse). The SCL current from Langmuir-Blodgett law (See chapter 5) for these parameters is 5 kA, close to the measured value of 7.3 kA. This indicates that electrode plasma closure is a small effect in the positive voltage pulse.

The diode perveance P is defined as, $I = PV^{3/2}$ where I is the diode SCL current. The experimental perveance derived from the positive diode voltage and current is shown in Fig. 4.24 where it is compared with the perveance calculated according to Langmuir-Blodgett law. One can see that perveance increases linearly with time. Initially the diode gap is close to 1.2 cm, but the emission occurs over only a fraction of the cathode area. This area increases as the current increases and the perveance increases due to the increase of the emission area.

During the negative pulse, the diode voltage is about -100 kV at the time of peak current. The estimated SCL current from Langmuir-Blodgett law is 2.9 kA, much less than the measured peak current 11.2 kA. So during the negative voltage pulse diode current increases due to the plasma expansion. The time varying perveance for negative diode voltage and current is shown in Fig. 4.25. Fig. 4.26 (a) and Fig. 4.26 (b) shows the diode impedance versus time for positive and negative voltage pulses, respectively. During the positive voltage pulse, the diode

impedance decrease with time due to the increase in the emission area. But during the negative voltage pulse, the diode impedance decreases with time due to the plasma expansion.

Therefore even though there is a plasma formation on the anode during the positive voltage pulse, the electron beam can be generated from the graphite cathode in the negative voltage pulse with a modest perveance ($\sim 1.1 \times 10^{-4} \text{ A/V}^{3/2}$).

4.5 PREPULSE SUPPRESSION TECHNIQUES

4.5.1 Prepulse Suppression using a dielectric cathode holder

In general, the best method to avoid prepulse is the use of spark gap switch or additional transmission line. The magnitude and polarity of the prepulse allowed are a function of the type of application of the electron beam diode. In order to reduce prepulse voltage to an acceptable level prepulse switches are used after the pulse forming line [16]. Depending upon the particular diode, various low capacitance prepulse switches have been used, for example, water, oil and gas switches. It is also possible to reduce prepulse by introducing a surface flashover switch into the conductor feeding the diode in vacuum [110], [56]. It can reduce prepulse by a factor of a few or so up to about 10, depending upon the geometry [16]. In order to see the feasibility of a surface flashover prepulse switch in the KALI 5000 electron beam diode we have operated the diode with corrugated Perspex cylinder at the cathode holder.

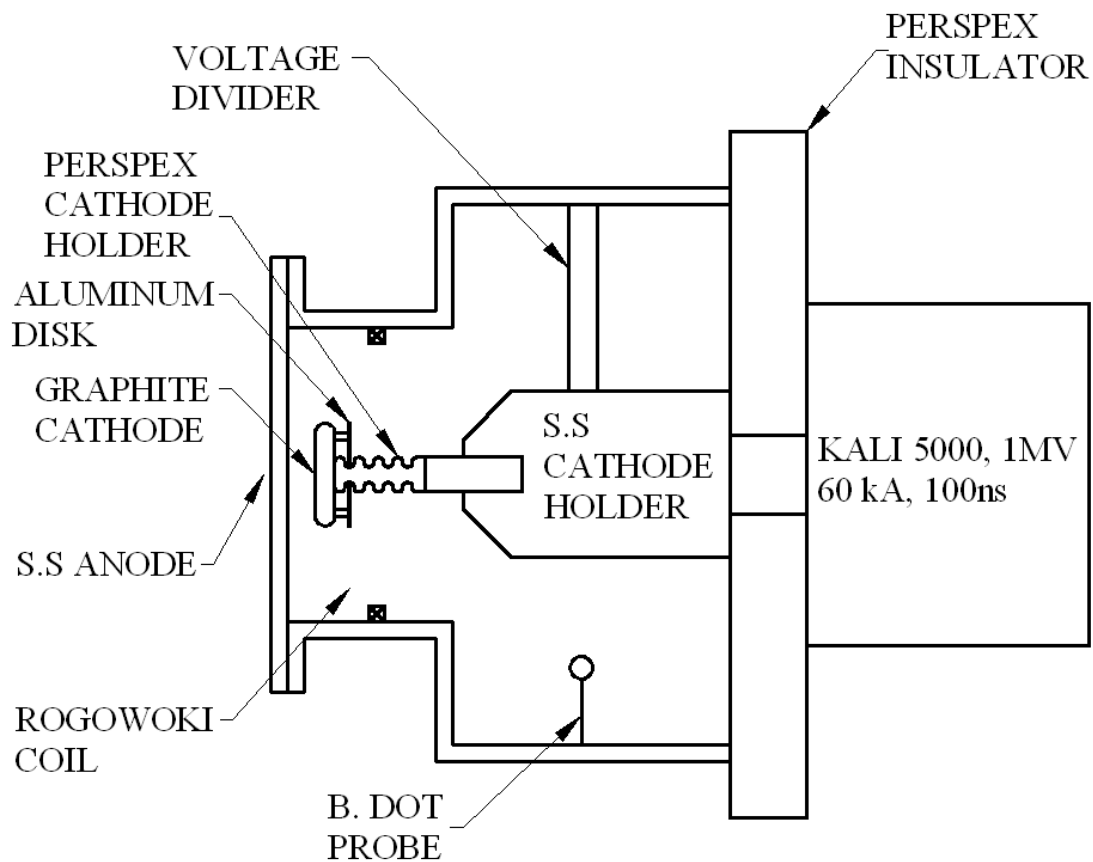


FIG. 4.27 Schematic of the experimental setup showing Perspex cathode holder and the electron beam diode.

The experimental setup used is shown in Fig.4.27. A cylindrical graphite cathode has been connected to the SS cathode holder by a corrugated Perspex cylinder of 26 mm maximum diameter and 10 mm minimum diameter. The cathode diameter was 66 mm. An aluminum disk of 1.5 mm thickness was connected to the backside of the cathode by metal screws. Effective length of the Perspex cylinder can be changed by changing the position of the aluminum disk with respect to the cathode. The location of the prepulse switch is very important, if the switch is placed too close to the cathode prepulse could couple through the capacitance of the switch and would not be reduced enough. If the switch were placed too far

backward, the diode insulator and voltage divider would be exposed to UV from the flashover, resulting in a breakdown [56].

TABLE I. Results of the experiment with 66 mm diameter cathode showing diode voltage and current for various AK gaps and Perspex insulator length.

Anode-Cathode Gap (mm)	Perspex Insulator Length(mm)	Diode Voltage (kV)	Diode Current (kA)
6	24	20	40
9	27	26	39
12	28	43	42
14	29	59	42
15	30	100	32
18	35	180	26
25	40	180	15

Intense relativistic electron beam generation studies have been carried out for 66 mm diameter graphite cathode and the AK gap has been varied from 6 mm to 25 mm and the Perspex insulator length has been varied from 24 mm to 40 mm. Results of the experiments are shown in Table I. Fig. 4.9 shows the Marx generator output and the bipolar prepulse waveform along with the main voltage pulse when the cathode is connected to the pulse forming line by a conducting rod. For 9 mm AK gap with 27 mm Perspex length there is no prepulse voltage in the diode voltage waveform, but the diode voltage is less ~ 26 kV and the current is quite large ~ 39 kA. Also some prepulse current is recorded before the main current pulse. Also at 6 mm AK gap and 24 mm Perspex length similar prepulse current has been observed though there was no prepulse voltage. This suggests that the 27 mm length Perspex is not sufficient to stop the prepulse arriving at the diode and during the prepulse voltage itself the diode AK gap has been filled with cathode plasma resulting in a very low voltage at the diode. Usually a 60 kV bipolar prepulse voltage has been seen at the diode at 300 kV Marx generator voltage [17].

Therefore surface flashover can occur at an electric field < 20 kV/cm due to the bipolar nature of the prepulse voltage [111]. At 12 mm AK gap and 28 mm Perspex length similar prepulse current has been recorded but a negative prepulse voltage of peak 40 kV and 200 ns duration was also present at the diode voltage. For 14 mm AK gap with 29 mm Perspex a negative prepulse of peak voltage ~ 16 kV with ~ 300 ns duration arrives at the diode either due to capacitive coupling or due to the surface flashover at the Perspex insulator. At 15 mm AK gap and 30 mm Perspex length a 30 kV peak bipolar prepulse voltage has been recorded at the diode.

To get a higher voltage at the diode we increase the diode gap to 18 mm and increase the Perspex length to 35 mm. The diode peak voltage and current obtained in this experiment were 180 kV and 26 kA [Fig. 4.28]. No prepulse voltage or current has been observed in this case. One can see from the Fig. 4.28 that till $t = 50$ ns the diode voltage rises slowly to ~ 40 kV then suddenly rises to ~ 350 kV then the diode current also started rising at $t = 70$ ns. This indicates that till $t = 70$ ns, surface flashover did not occur at the 35 mm length Perspex insulator. But before the breakdown of the Perspex insulator diode voltage rises slowly to ~ 50 kV due to the capacitive coupling. Also little current is recorded in this low voltage phase of the diode, showing plasma formation on the cathode surface. With the increase of the Marx generator voltage, diode current increases up to ~ 40 kA but the diode voltage remains almost same. Fig. 4.29 shows the diode voltage and current waveform for 18-mm AK gap with a higher Marx generator voltage.

Fig.4.30 shows the diode voltage and current waveform for 25 mm AK gap with 40 mm Perspex. In this case diode voltage has been measured before the dielectric cathode holder but inside the diode chamber only. One can see from the Fig. 4.30 that at $t = 60$ ns diode voltage

suddenly drops to ~ 150 kV. This is because of the fact that the diode voltage, measured before the Perspex insulator, increase to 330 kV, since by that time surface flashover has not taken place. At $t = 60$ ns the voltage breakdown takes place across the Perspex surface and the diode current started rising at the same time.

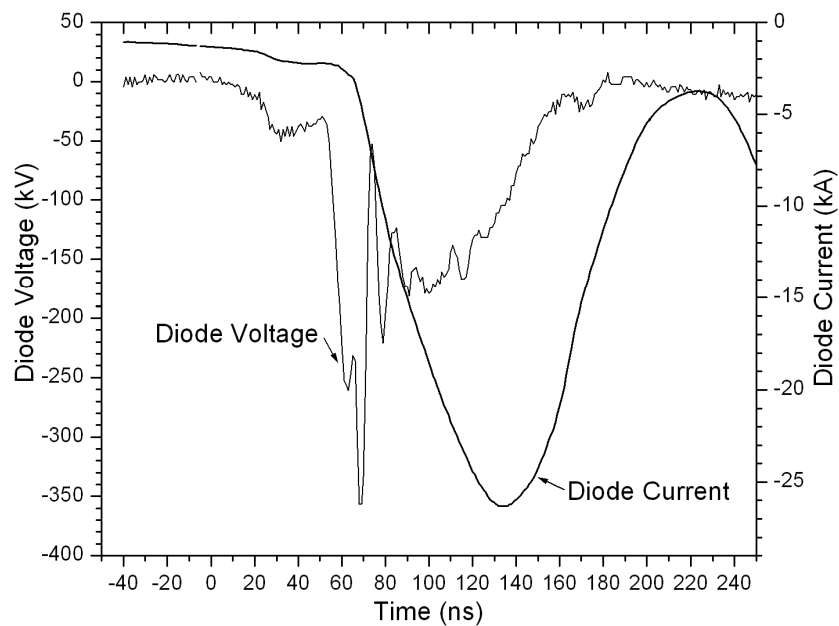


FIG. 4.28 Diode voltage and current waveform for 18 mm AK gap and 35 mm Perspex insulator.

With the increase of the Marx generator voltage both the diode current and voltage increases. Fig. 4.31 shows the diode voltage and current waveform for 25 mm AK gap with a higher Marx generator voltage. One can see from the Fig. 4.31 that in this case breakdown across the Perspex insulator occurs at an earlier time $t = 40$ ns and consequently the diode current started rising earlier than the previous case.

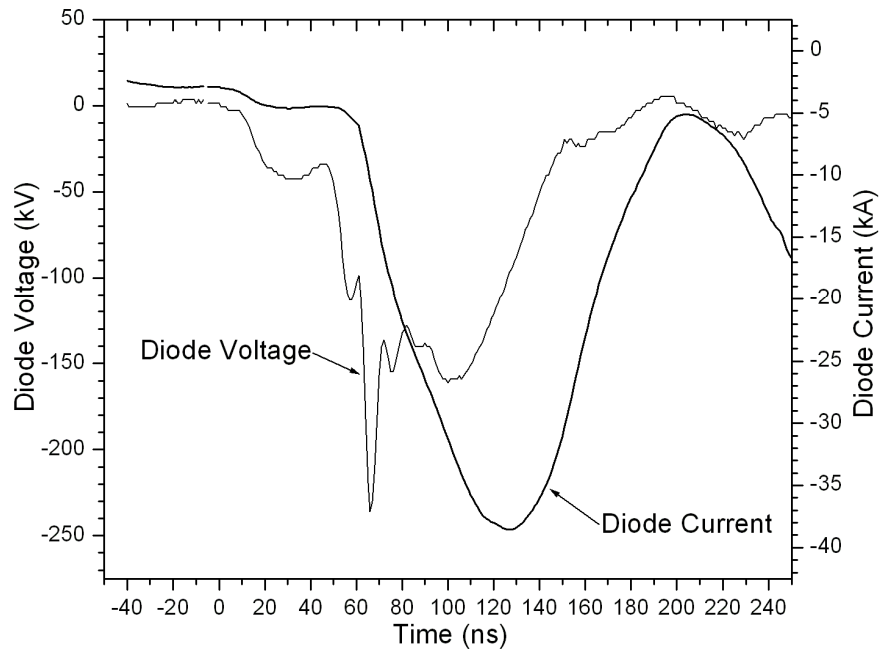


FIG. 4.29 Diode voltage and current waveform for 18 mm AK gap and 35 mm Perspex insulator with a higher Marx generator voltage.

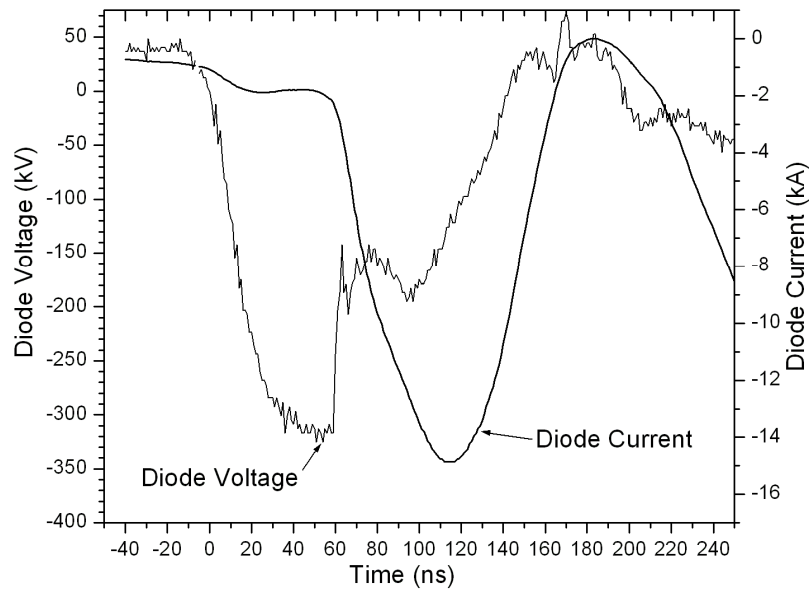


FIG.4.30 Diode voltage and current waveform for 25 mm AK gap and 40 mm Perspex insulator.

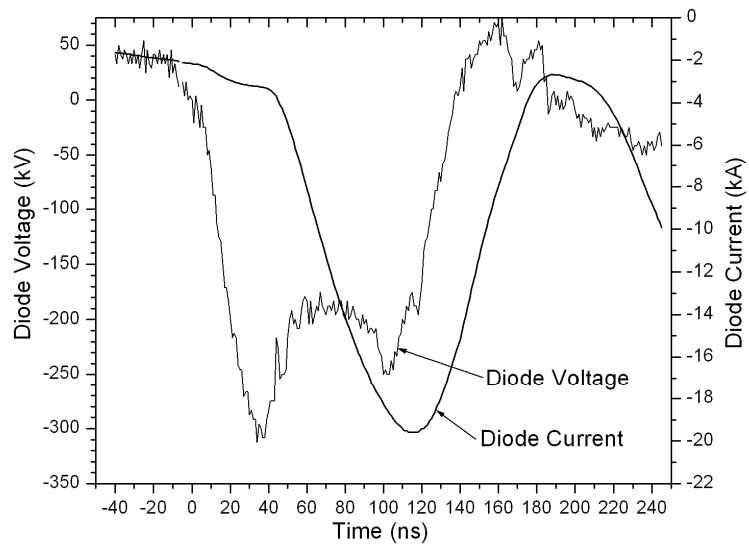


FIG. 4.31 Diode voltage and current waveform for 25 mm AK gap and 40 mm Perspex insulator with a higher Marx generator voltage.

Therefore inserting a dielectric at the cathode holder could be a very effective method to reduce prepulse voltage at the electron beam diode, but it increases the rise time of the diode voltage and reduces the effective electron beam pulsewidth.

4.5.2 Prepulse Suppression by adding an Extra Inductance to the Charging Circuit of the Blumlein Line

To compare the diode operation with other technique of prepulse mitigation an inductance has been added to the charging circuit of the Blumlein line. In the case of the added inductance to the Blumlein circuit, the slower rise time reduces the prepulse voltage from 32% to $\leq 10\%$. In this case a 67 mm diameter graphite cathode and a Tantalum disk has been used as an anode.

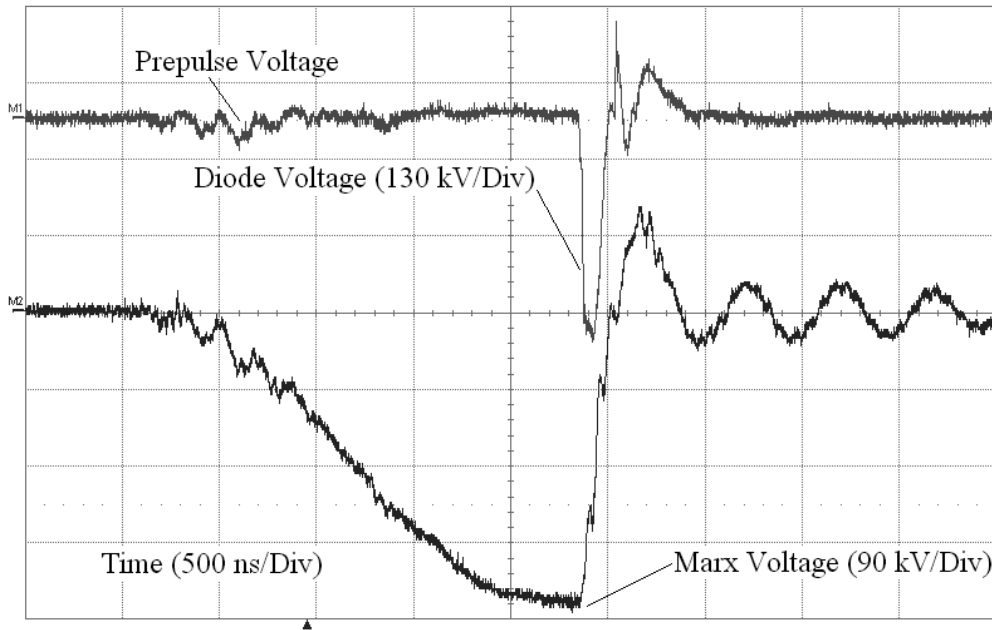


FIG. 4.32 Marx output and Prepulse waveform along with the main voltage pulse with an inductance added to the charging circuit of the Blumlein line.

One can see from the Fig. 4.32 that in this case the Blumlein charging time has increased from 800 ns (Fig. 4.9) to $\sim 2 \mu\text{s}$ and there is no significant prepulse voltage. Some prepulse voltage is recorded during the beginning of the Blumlein charging but this prepulse voltage appears around $1.7 \mu\text{s}$ prior to the main voltage pulse and will have no effect on the diode operation.

4.6 CONCLUSIONS

An intense relativistic electron beam has been generated without a prepulse switch. Electron beam generation mechanism in the presence of the prepulse has been analyzed by the expansion of the prepulse generated plasma and plasma filled diode. Increasing the AK gap reduces the prepulse voltage and eventually drops it below the explosive emission threshold and eliminates its creation. For the same Marx generator voltage there is lot of shot to shot variation in the diode voltage and current due to the nonreproducibility of prepulse generated

plasma. For perveance more than 200 μPerv we can consider the diode as short. The diode can be considered short if the Marx voltage/(Anode Cathode Gap)² is more than 56 kV/cm². Below 56 kV/cm² the effect of the prepulse will be less and the diode can be operated with a better shot to shot reproducibility

An intense relativistic electron beam has been generated from planar and annular graphite cathodes at a fixed 25 mm AK gap in the presence of prepulse. For the planar cathode, the beam parameters obtained are 340 keV, 24 kA, and 100 ns at a 680 A/cm² current density. With an annular cathode, 346 keV, 10 kA, and 100 ns electron beam could be generated at a 3.4 kA/cm² current density. The peak electric field in the diode varies from 58 to 138 kV/cm. A bipolar prepulse voltage has been recorded at the diode. The amplitude of the negative prepulse voltage increases with the Marx generator voltage but the time duration remains the same. A maximum of 32% negative prepulse voltage has been recorded at the diode. Both the time duration and the amplitude of the positive prepulse voltage decrease with the increase in the Marx generator voltage. The highest positive prepulse voltage is 17% of the peak diode voltage. The voltage reversal in the Marx generator output signal is higher for the 98 mm diameter planar cathode compared to that for the 67 mm diameter cathode. Also there is no shot to shot variation for the 67 mm diameter planar cathode. It was found that the positive prepulse voltage has no significant effect on the diode perveance and impedance. Reversal in the Marx generator output voltage is higher for the annular cathode compared to the planar cathode. Also the Marx reversal increases with the cathode diameter for both types of cathodes due to a decrease in the diode impedance. For the same Marx generator voltage, there is lot of shot to shot variation in the diode voltage and current in the annular cathode. Annular graphite cathodes of 40 and 70 mm diameters and 98 mm diameter planar graphite cathodes are not

very suitable for reliable operation in the presence of prepulse. The effect of prepulse is more pronounced in the cathode of higher diameter due to a decrease in the uniformity of the prepulse generated plasma with the corresponding increase in the cathode diameter.

Intense relativistic electron beam has been generated in a high power cylindrical diode in the presence of prepulse. A bipolar prepulse voltage has been recorded at the diode. The amplitude and the time duration of the prepulse voltage vary with the Marx generator voltage. It was found for the AK gap ≤ 1.65 cm that there is some shot to shot variation in the cylindrical diode voltage and current for the same Marx generator voltage. It was shown that the positive prepulse voltage has no significant effect on the diode perveance. The effect of the prepulse is less pronounced in the cylindrical diode as compared to planar diode that allows one to operate the cylindrical diode with the AK gap ≤ 1.85 cm.

Studies have been carried out to generate intense electron beam in the cylindrical electron beam diode when subjected to a high voltage bipolar pulse. In the positive voltage pulse, a copper mesh acts as a source of electrons. The diode perveance in the positive voltage pulse linearly increases with time due to the increase in the emission area. The electrode plasma closure is a small effect on the positive voltage pulse. During the negative voltage pulse, the diode impedance decreases with time due to the plasma expansion. Thus, even though there is a plasma formation on the anode during the positive voltage pulse, the electron beam can be generated from the graphite cathode in the negative voltage pulse with a modest perveance ($\sim 1.1 \times 10^{-4} \text{ A/V}^{3/2}$).

Intense relativistic electron beam has been generated in a planar diode with a dielectric cathode holder. Electron beam generation studies have been carried out for various AK gaps. The length of the Perspex insulator has been varied from 24 mm to 40 mm. It was found that for

the Perspex length < 35 mm prepulse voltage appears at the diode either due to capacitive coupling or surface flashover at the Perspex insulator surface at the prepulse voltage itself. This surface flashover occurs at an unexceptionally low flashover fields could be because of the bipolar nature of the prepulse voltage. No prepulse voltage has been recorded at the diode for the Perspex length ≥ 35 mm. But due to the pre breakdown time delay in the surface flashover across the insulator the rise time of the diode voltage increases. The diode current started rising after ~ 50 ns from beginning of the diode voltage, this reduces the effective pulse width by 50 ns. Inserting a dielectric at the cathode holder could be a very effective method to reduce prepulse at the electron beam diode, but it increases the rise time of the diode voltage and reduces the effective electron beam pulse width. The prepulse voltage reduces significantly ($\leq 10\%$) when an inductance is added to the charging circuit of the Blumlein line and much higher diode voltage has been obtained for the same AK gap.

CHAPTER 5

PLASMA CLOSURE VELOCITY MEASUREMENT IN HIGH POWER ELECTRON BEAM DIODE

5.1 SPACE CHARGE LIMITED ELECTRON FLOW IN A PLANAR DIODE

For shorter pulse duration <100 ns and at the comparatively low current density $\sim 10 \text{ A/cm}^2$ electron flow remains unipolar [14]. However at the higher current density greater than few hundreds of A/cm^2 electron flow becomes bipolar [15]. Our observation can be described by a model for the bipolar space-charge limited flow in the presence of the plasma expanding from the cathode and anode surfaces. The anode plasma could be generated by either melting and subsequent evaporation of the anode material or by electron stimulated desorption of the contaminants on the anode surface [30]. The charge neutralizations of the electrons by the ions allow ~ 1.86 times the current to flow as compared to single species Child–Langmuir with the limiting electron current independent of the ion mass [6]. The combination of a very few ions and of a secondary emission of $1/42.8$ for hydrogen causes the diode to be in space-charge limited bipolar flow [30]. Both the anode and cathode plasmas are assumed to expand with equal velocity v .

The diode current density j at time t during the pulse, and the total current I are given by the Child Langmuir law. For a plane parallel diode consisting of a cathode of radius ' r ' and a AK gap ' d ' the j and I are given by [6],

$$j(t) = 1.86 \times \frac{4\epsilon_0}{9} \left(\frac{2e}{m_e} \right)^{1/2} \frac{V(t)^{3/2}}{(d-2vt)^2} = 1.86 \times 2.33 \times 10^{-6} \frac{V(t)^{3/2}}{(d-2vt)^2}, \quad (5.1)$$

and

$$I(t) = j(t) \pi r^2 = 1.86 \times 2.33 \times 10^{-6} \frac{\pi r^2 V(t)^{3/2}}{(d - 2vt)^2}, \quad (5.2)$$

where V is the applied voltage, t is the time during pulse at which j and I are measured; e and m_e are electron charge and mass and ϵ_0 is the free space permittivity.

In fact, it could be some time delay in the anode plasma formation with respect to the cathode plasma generation [11]. A delay of 10 ns has been measured experimentally between cathode and anode plasma generation [11]. In that case Eqs. (5.1) and (5.2) should be modified with respect to the value of $(d - 2vt)$.

The diode impedance Z_d is given by,

$$Z_d(t) = \frac{V(t)}{I(t)} = \frac{73}{V(t)^{1/2}} \frac{(d - 2vt)^2}{r^2}, \quad (V \text{ in MV}). \quad (5.3)$$

The perveance expression for the electron flow in the planar region of the diode can be defined by

$$P_{\text{planar}} = \frac{I(t)}{V(t)^{3/2}} = 1.86 \times 2.33 \times 10^{-6} \frac{\pi r^2}{(d - 2vt)^2}. \quad (5.4)$$

A perveance expression for the cathode surface must also include the effect of electron flow from the cathode circumferential edge. Contribution due to edge can be accounted for by using Langmuir Compton equation [2, 40] for cylindrically symmetric space charge limited electron flow. Edge effects in finite area diodes may significantly increase the value of space-charge limited current relative to the prediction of 1D Child–Langmuir Law [40, 33]. Edge contribution is particularly important for $r/d < 1$ and can be neglected for $r/d > 1$.

$$P_{\text{edge}} = \frac{14.66 \times 10^{-6}}{8} \frac{2\pi r}{d \alpha^2}, \quad (5.5)$$

where $\alpha = \ln(d/vt) - 0.4[\ln(d/vt)]^2 + 0.0917[\ln(d/vt)]^3 - 0.0142[\ln(d/vt)]^4 + \dots$.

The perveance of the total bipolar electron flow from the cathode edge and face is equal to the sum of two components. Thus the diode perveance in the generalized form can be expressed as

$$P_{diode} = P_{planar} + P_{edge} \quad (5.6)$$

Thus, the cathode emission area, the effective diode separation, and the beam envelope are the only parameters that can affect the diode perveance. These interpretations are strictly valid only in the nonrelativistic limit. But the error associated will be small if the electron kinetic energy is less than 500 keV [40]

5.2 PLASMA EXPANSION VELOCITY MEASUREMENT IN A HIGH POWER PLANAR DIODE

To measure the electrode plasma expansion velocity of the IREB planar diode, beam generation experiments were carried out at 18 mm, 25 mm and 31 mm AK gap respectively. For 18 mm AK gap a Tantalum disk has been used as an anode. Also for this case an inductance has been added to the charging circuit of the Blumlein line. In the case of the added inductance to the Blumlein circuit, the slower rise time reduces the prepulse voltage from 32% to $\leq 10\%$. For other experiments beam generation studies has been carried out in the presence of prepulse and a SS plate has been used as an anode.

Fig. 5.1 (a) shows the diode voltage and current waveform for 18 mm AK gap. The diode peak voltage and current obtained in this experiment were 270 kV and 33 kA, respectively. Electron beam diode time varying impedance and perveance values were calculated using the voltage and current waveforms. The starting point or the zero time for perveance calculations was taken when the main voltage pulse is zero. Fig 5.1 (b) shows corresponding impedance and perveance derived from the diode voltage and current waveform. One can see that the diode impedance decreases with time showing impedance collapse. The diode perveance increases

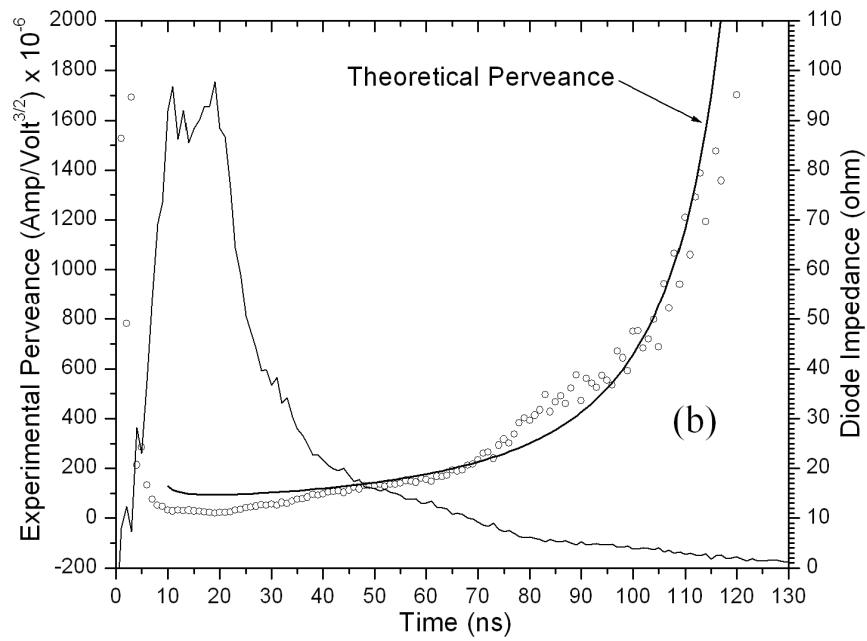
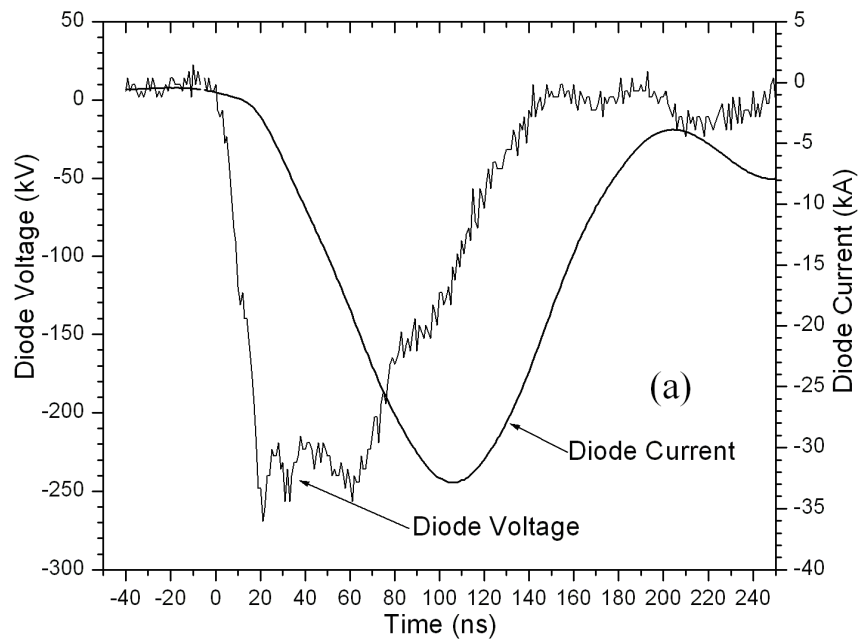


FIG. 5.1 (a) Diode voltage and current waveform for 18 mm AK gap. (b) The temporal behavior of the diode impedance and perveance for 18 mm AK gap. Continuous line represents theoretical perveance.

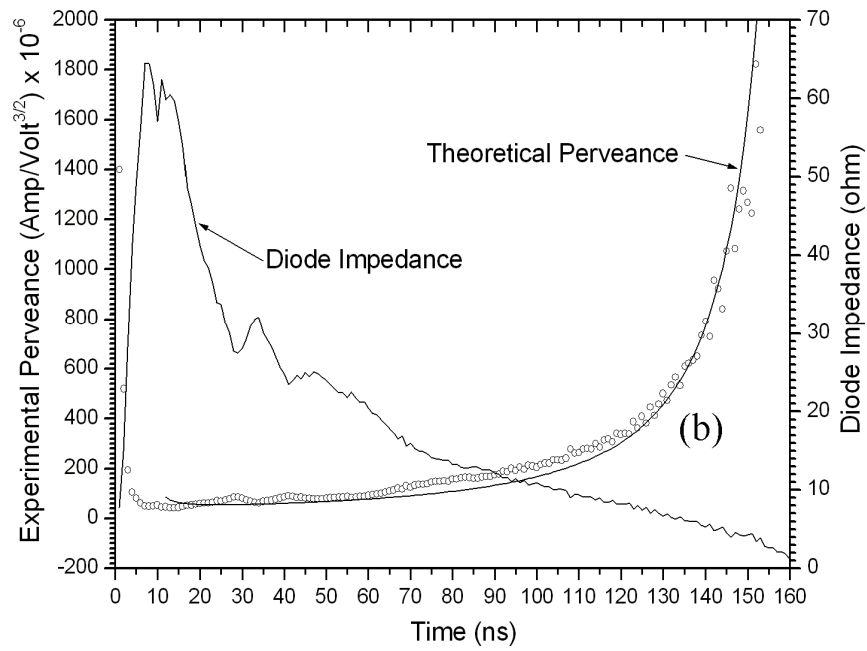
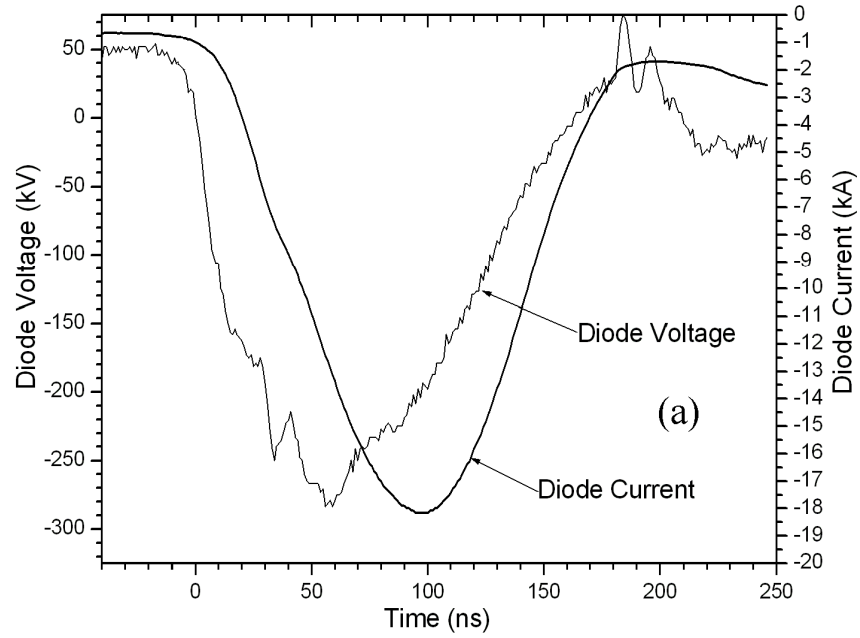


FIG. 5.2 (a) Diode voltage and current waveform for 25 mm AK gap. (b) The temporal behavior of the diode impedance and perveance for 25 mm AK gap. Continuous line represents theoretical perveance.

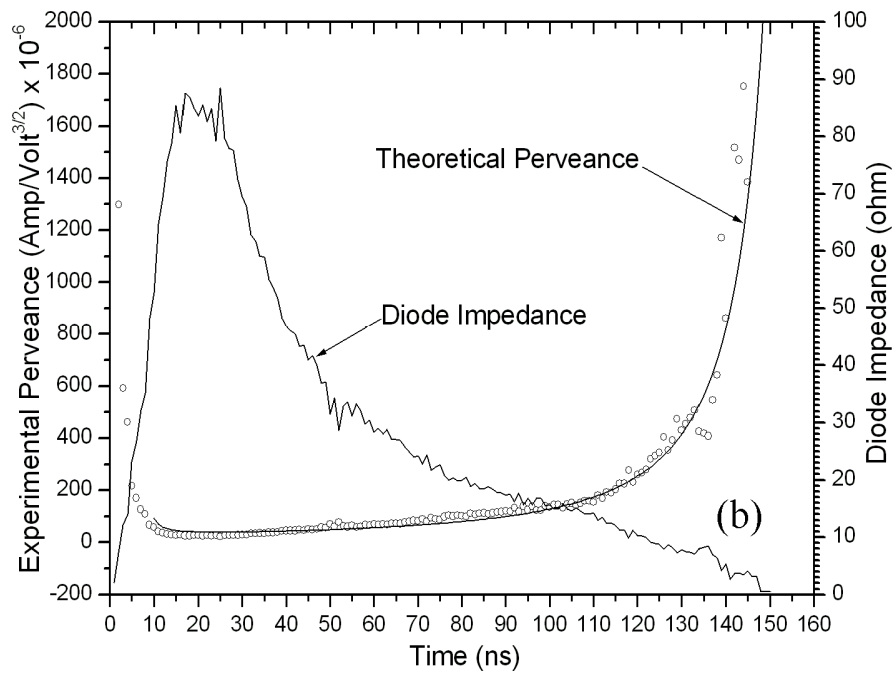
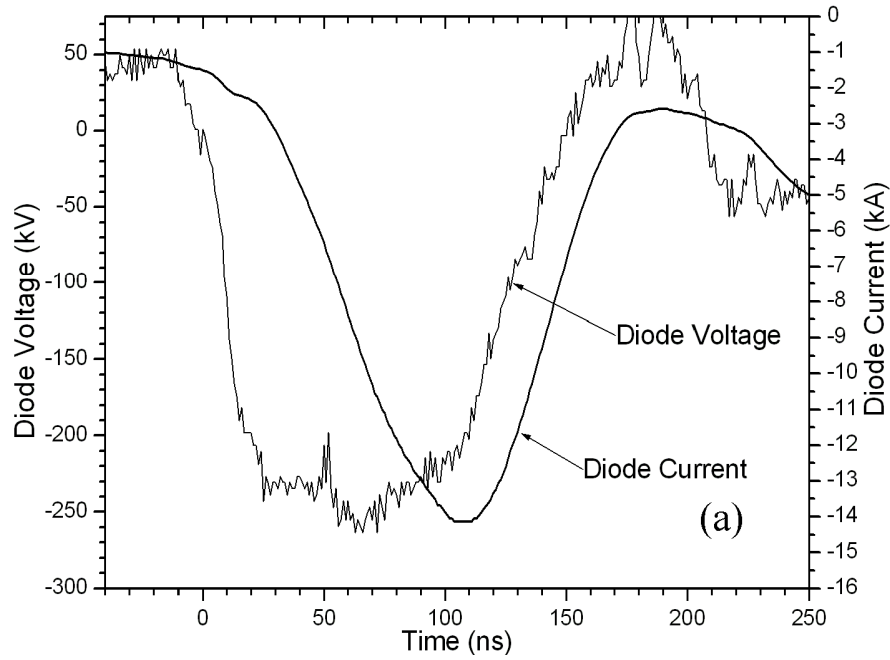


FIG. 5.3 (a) Diode voltage and current waveform for 31 mm AK gap. (b) The temporal behavior of the diode impedance and perveance for 31 mm AK gap. Continuous line represents theoretical perveance.

rapidly after ~ 110 ns showing gap closure. The best fit for the theoretical model [Eq. (5.6)] was obtained assuming the plasma expansion velocity to be 6.5 cm/ μ s. The peak current density was $j = 936$ A/cm².

The diode voltage and current waveforms for 25 mm AK gap is shown in Fig. 5.2 (a). The diode peak voltage and current obtained in this experiment were 280 kV and 18 kA, respectively. The experimental impedance and perveance derived from the diode voltage and current is shown in Fig. 5.2 (b). The diode perveance increases rapidly after ~ 130 ns showing gap closure. In this case the best fit for the theoretical model [Eq. (5.6)] was obtained assuming the plasma expansion velocity to be 7.3 cm/ μ s. The peak current density was $j = 515$ A/cm².

The diode voltage and current waveforms for 31 mm AK gap is shown in Fig. 5.3 (a). The diode peak voltage and current obtained were 270 kV and 14 kA, respectively. Fig 5.3 (b) displays the time varying impedance and perveance. As can be seen in Fig 5.3 that the diode impedance decreases and perveance increases with time. The best fit for the theoretical model was obtained assuming the plasma expansion velocity to be 9.5 cm/ μ s. The peak current density in this case was $j = 401$ A/cm². Such a high plasma expansion velocity has also been observed with carbon nanotube cathode [112] with a high current density $j = 309$ A/cm² (the plasma velocity reported $v = 9.1$ cm/ μ s). The plasma expansion velocity for 31 mm AK gap is higher than the 25 mm AK gap, even though the current density is less for 31 mm AK gap. The peak current density for 31 mm AK gap has been calculated using the actual cathode diameter. But usually a large percentage of the cathode fails to take part in the emission process. So if we account for the actual emission area, the current density for 31 mm AK gap could be higher than the 25 mm AK gap, resulting in higher plasma expansion velocity. But

the increase in the plasma velocity with the AK gap cannot be explained only by the surface ratio argument. It may also be possible that the higher electric field at lower AK gap is slowing one of the two plasmas.

So the electron beam emission mechanism in a high power planar diode can be explained by the bipolar space-charge limited flow model. Summary of the beam generation experiments for three different AK gaps are shown in Table I.

TABLE I. Results of the experiment with 67 mm diameter cathode showing diode voltage and current for various AK gaps.

Anode-Cathode Gap (mm)	Diode Voltage (kV)	Diode Current (kA)	Electrode Plasma Expansion Velocity (cm/ μ s)	Current Density (A/cm ²)
18	270	33	6.5	936
25	280	18	7.3	515
31	270	14	9.5	401

One can see from the Table I that as we increase the AK gap the diode current and the current density reduces but the electrode plasma expansion velocity increases.

5.3 PLASMA EXPANSION VELOCITY MEASUREMENT IN A HIGH POWER PLANAR DIODE WITH A DIELECTRIC CATHODE HOLDER

Plasma closure velocity has been measured when the planar electron beam diode has been operated with a dielectric cathode holder. Experimental setup used has been described in the Section 4.5.2. Electron beam diode time varying impedance and perveance values were calculated using the voltage and current waveforms. The starting point or the zero time for

perveance calculations was taken when the main voltage pulse is zero. The experimental impedance and perveance derived from the diode voltage and current for 18-mm AK gap and 35-mm Perspex insulator are shown in Fig. 5.4. The best fit for the theoretical model [Equation (5.6)] was obtained assuming the plasma expansion velocity to be $5.1 \text{ cm}/\mu\text{s}$. The peak current density was $j = 760 \text{ A}/\text{cm}^2$. The plasma expansion velocity deduced from the fit is valid over only one part of the shot and really approximate. It is clear from the Fig. 5.4 that, till 70 ns, the experimental and the theoretical perveance are not matching but after that perveance match nicely. With the increase of the Marx generator voltage diode current increases upto $\sim 40 \text{ kA}$ but the diode voltage remains almost same. Fig 5.5 shows impedance and perveance with a higher Marx generator voltage. In this case the best fit for the theoretical model [Equation (5.6)] was obtained assuming the plasma expansion velocity to be $5.7 \text{ cm}/\mu\text{s}$. The peak current density was $j = 1 \text{ kA}/\text{cm}^2$. The plasma velocity increases with the increase of the Marx generator voltage because of the increase in the current density.

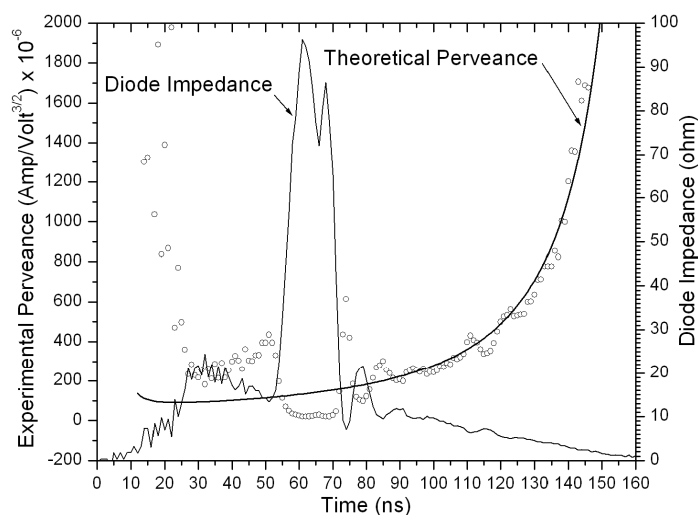


FIG. 5.4 The temporal behavior of the diode impedance and perveance for 18 mm AK gap and 35 mm Perspex insulator. Continuous line represents theoretical perveance.

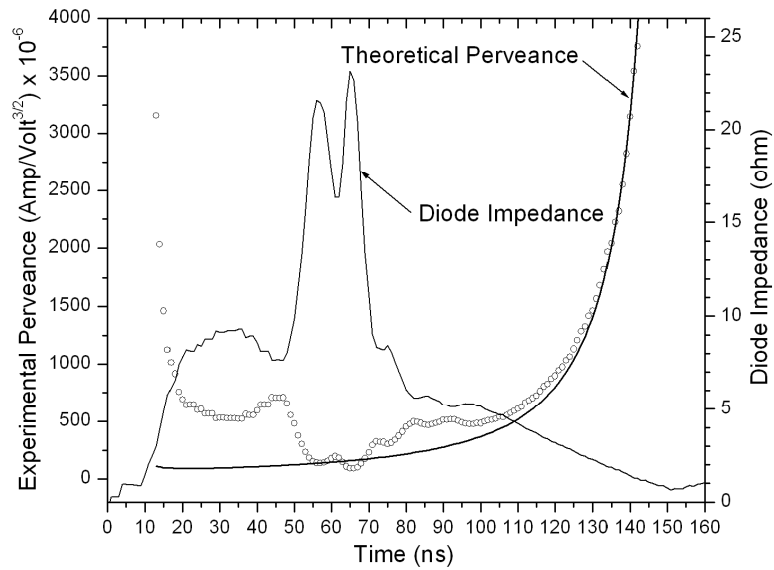


FIG. 5.5 The temporal behavior of the diode impedance and perveance for 18 mm AK gap and 35 mm Perspex insulator with a higher Marx generator voltage. Continuous line represents theoretical perveance.

The temporal behavior of the diode impedance and perveance for 25 mm AK gap were shown in Fig. 5.6. It is clear from the Fig. 5.6 that, till 70 ns, the experimental and the theoretical perveance are not matching, but after that it matches nicely. In this case the plasma expand at a higher speed of $7.9 \text{ cm}/\mu\text{s}$ with $j = 439 \text{ A}/\text{cm}^2$.

With the increase of the Marx generator voltage both the diode current and voltage increases. Fig 5.7 shows corresponding impedance and perveance derived from the diode voltage and current waveform for 25 mm AK gap with a higher Marx generator voltage. In this case the best fit for the theoretical model [Equation (5.6)] was obtained assuming the plasma expansion velocity to be $8.1 \text{ cm}/\mu\text{s}$. The peak current density was $j = 573 \text{ A}/\text{cm}^2$. One can see that for all the cases, the plasma expansion velocity increases with the AK gap. It may be possible that the higher electric field at lower AK gap is slowing one of the two electrode plasmas

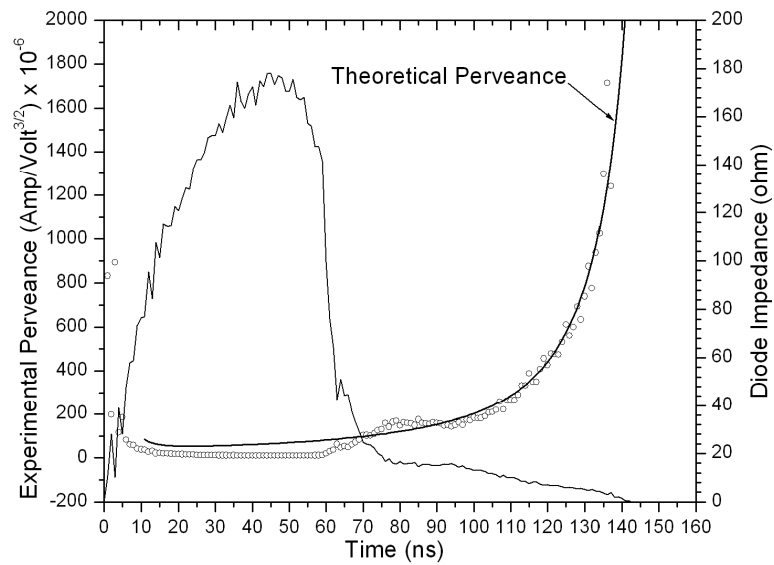


FIG. 5.6 The temporal behavior of the diode impedance and perveance for 25 mm AK gap and 40 mm Perspex insulator. Continuous line represents theoretical perveance

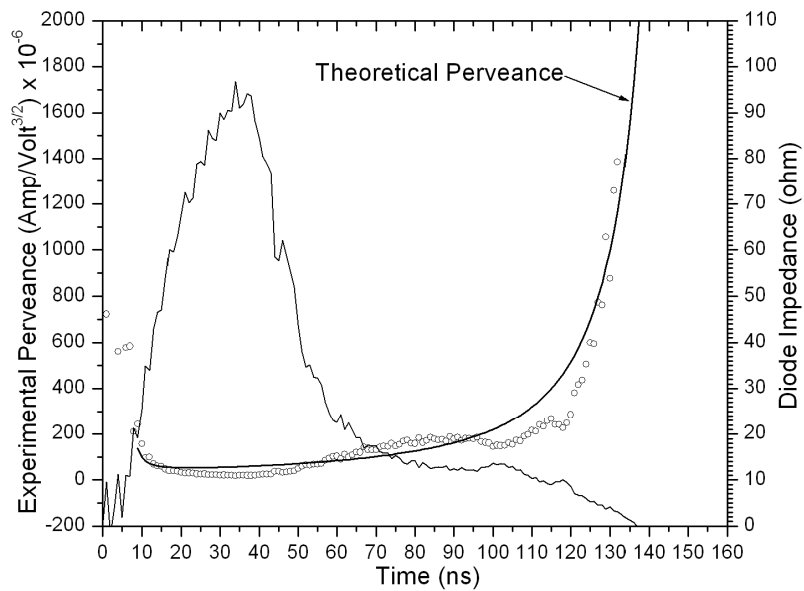


FIG. 5.7 The temporal behavior of the diode impedance and perveance for 25 mm AK gap and 40 mm Perspex insulator. Continuous line represents theoretical perveance.

5.4 SPACE CHARGE LIMITED ELECTRON FLOW IN A CYLINDRICAL DIODE

For cylindrical diode in the idealized case of 1D electron flow between long coaxial cylinders the space charge limited electron current per unit length j_{1D} at some radial position r between two coaxial cylinders is given by the Langmuir-Blodgett law [94].

$$j_{1D} = \frac{8\pi\epsilon_0}{9} \left(\frac{2e}{m_e} \right)^{1/2} \frac{V^{3/2}}{r\beta^2}, \quad (5.7)$$

where V is the potential, and $\beta = f\left(\frac{r}{r_c}\right)$ is a function expressed by the infinite series,

$$\beta = \mu - \frac{2\mu^2}{5} + \frac{11\mu^3}{120} - \frac{47\mu^4}{3300} + \dots, \quad (5.8)$$

with $\mu = \ln \frac{r}{r_c}$.

Here r_c is the cathode radius, e is the electron charge, m_e is the electron mass, and ϵ_0 is the free space permittivity.

The Langmuir-Blodgett law has been extended to two dimensions by performing 2D particle in cell simulations [95]. But the results obtained using these simulations were limited to low voltage and current regime (few kilovolts and few Amps). Approximate analytical solutions for the space-charge limited current in 1D and 2D cylindrical diodes are also have been calculated by various authors [96, 97].

Our observation can be described by a simple model for the electron space-charge limited current in the presence of the plasma expanding from the cathode and anode surfaces. The anode plasma is formed from the desorbed and ionized gases [11]. Also during the positive half of the prepulse voltage, the explosive emission plasma can be generated at the anode surface. Both the anode and cathode plasmas are assumed to expand with equal velocity v_p . In

this case the time-dependent cathode and anode radius becomes $r_c - v_p t$ and $r_a + v_p t$ respectively. Thus, the value of μ in Eq. (5.8) is replaced by $\mu = \ln \frac{r_a + v_p t}{r_c - v_p t}$ and β becomes time dependent parameter. Then the time dependent Langmuir-Blodgett law can be written as

$$j_{1D}(t) = \frac{8\pi\epsilon_0}{9} \left(\frac{2e}{m_e} \right)^{1/2} \frac{V^{3/2}}{(r_a + v_p t)\beta(t)^2}, \quad (5.9)$$

if the cathode width is h then the time dependent $P(t)$ of the cylindrical diode reads:

$$P(t) = \frac{8\pi\epsilon_0}{9} h \left(\frac{2e}{m_e} \right)^{1/2} \frac{1}{(r_a + v_p t)\beta(t)^2}. \quad (5.10)$$

In fact, it could be some time delay in the anode plasma formation with respect to the cathode plasma generation [11]. In that case Eqs. (5.9) and (5.10) should be modified with respect to the value of r_a .

It was shown that in the Space Charge Limited (SCL) regime many of the results from planar diodes provide reasonably good estimates for cylindrical diodes [98]. Also when the AK gap distance d , is very small compared with the cathode radius, $r_c \gg d$ the approximate analytical solutions for SCL current density [96] becomes proportional to $\frac{V^{3/2}}{d^2}$. So if $d(t)$ is the time

dependent AK gap the approximate value of $P(t)$ reads:

$$P(t) \propto \frac{1}{d(t)^2}. \quad (5.11)$$

The proportionality constant is determined by the initial AK gap and the measured perveance at the time of the initial rise in the diode voltage [65].

5.5 PLASMA EXPANSION VELOCITY MEASUREMENT IN A HIGH POWER CYLINDRICAL DIODE

To study the plasma expansion and impedance collapse in a high power cylindrical diode, the experiments were carried out in three phases. The experimental setup used is described in the Section 3.3. In phase I the cathode inner diameter was set to 12.3 cm with the radial AK gap of 1.85 cm. The diode chamber was evacuated using a diffusion pump backed by a rotary pump. The vacuum in the diode chamber was $\leq 6 \times 10^{-5}$ mbar. In the phase II experiment, the cathode inner diameter was set to 11.9 cm with the radial AK gap of 1.65 cm. In phase III experiment, the cathode inner diameter was set to 11 cm with the radial AK gap of 1.2 cm.

The diode voltage and current waveforms in the phase I is shown in Fig. 4.17 (a) and Fig. 4.17 (b). The diode peak voltage and current obtained in this experiment was 340 kV and 30 kA, respectively, at 340 kV Marx generator voltage. Electron beam diode time varying impedance and perveance values were calculated using the voltage and current waveforms. The starting point or the zero time for perveance calculations was taken when the main voltage pulse is zero. The experimental impedance and perveance derived from the diode voltage and current is shown in Fig. 5.8. The best fit for the theoretical model [Eq. (5.10)] was obtained assuming the plasma expansion velocity to be $5 \text{ cm} / \mu\text{s}$.

In phase II the best fit for the theoretical model was obtained assuming the plasma expansion velocity to be $5.3 \text{ cm} / \mu\text{s}$ [Fig. 4.18]. This plasma velocity measurement may not be very accurate because of the modification in the diode geometry by the expansion of the prepulse generated plasma prior to the main voltage pulse.

In phase III experiment the best fit for $\phi_M = 250 \text{ kV}$ was obtained assuming the plasma expansion velocity to be $3.4 \text{ cm} / \mu\text{s}$ [Fig. 4.19]. Where ϕ_M is the Marx generator voltage. Again

this plasma velocity measurement may not be very accurate because of the expansion of the prepulse generated plasma prior to the main voltage pulse.

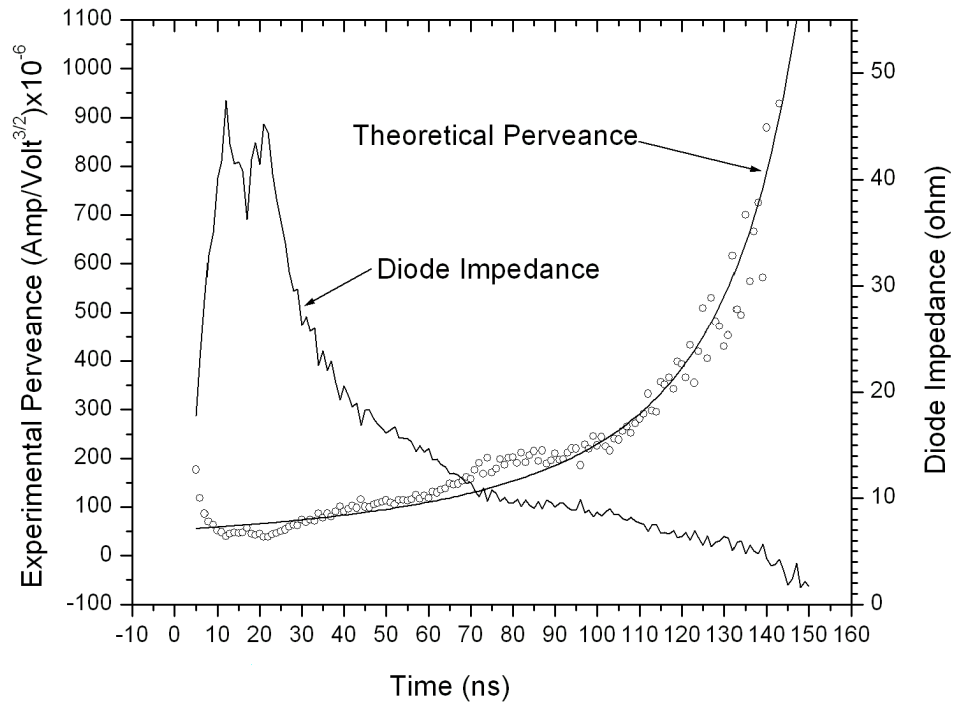


FIG. 5.8 The temporal behavior of the diode impedance and perveance for Phase I experiment. Continuous line represents theoretical perveance.

The time dependence of the diode gap is calculated using Eq. (5.11). The temporal behaviors of the diode gaps are shown in Fig. 5.9. One can see that in the initial stage of the Phase I and Phase III the plasma expansion velocity is very fast but after around 40 ns, the plasma expansion becomes relatively slow. In the case of Phase II experiment the plasma expansion velocity is very fast for the entire pulse duration [Fig. 5.9 (b)].

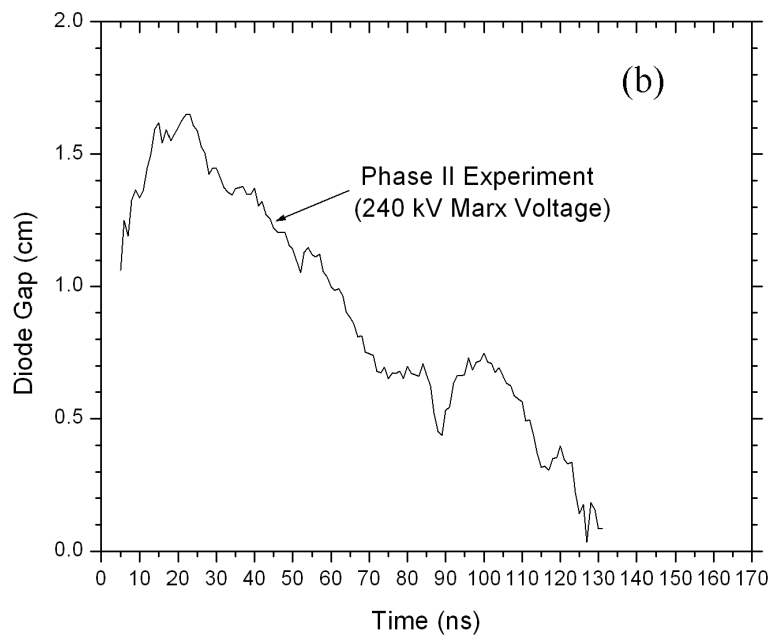
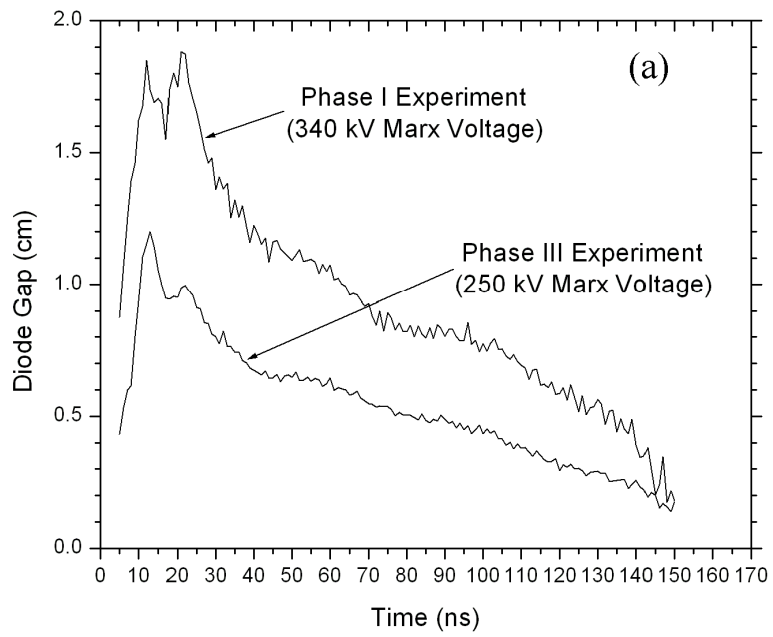


FIG. 5.9 (a) The temporal behavior of the diode gap in Phase I and Phase III experiment. (b) The temporal behavior of the diode gap in Phase II experiment.

The closure rate calculated from Eq. 5.11 overestimates the gap closure rate since any increase in measured current is attributed to a decrease in the AK gap due to plasma expansion across the gap and does not take into account the possibility of radial plasma expansion [65]. Equation (5.11) also neglects the effect of electron flow from the cathode circumferential edge and the cathode edge contribution.

5.6 CONCLUSIONS

Electron beam emission mechanism can be explained by the bipolar space-charge limited flow model. The time varying electron beam diode impedance and perveance were measured for 18, 25 and 31 mm AK gaps. It was found that the diode impedance collapse due to plasma expansion from the cathode and anode surfaces. For 31 mm AK gap the anode and cathode plasmas expand at $9.5 \text{ cm}/\mu\text{s}$ toward each other. Plasma expansion velocity decreases for 25 mm AK gap.

Electrode plasma expansion velocity has been measured when the planar diode is operated with a dielectric cathode holder to suppress prepulse. It was found that for 18-mm AK gap, the anode and cathode plasmas expand at $5.1 \text{ cm}/\mu\text{s}$ toward each other. Plasma velocity increases with the current density. Plasma expansion velocity increases for 25-mm AK gap.

Cylindrical electron beam diode perveance was measured for 1.85, 1.65, and 1.2 cm AK gaps. The anode and cathode plasma expansion velocities were measured using the perveance data. For 1.85 cm radial AK gap the anode and cathode plasmas expand at $5 \text{ cm}/\mu\text{s}$ toward each other. Plasma expansion velocity decreases for 1.2 cm AK gap.

The time dependence of the diode gap is calculated for cylindrical diode. It was found that in the initial stage of the 1.85 cm and 1.2 cm accelerating gap the plasma expansion velocity is

very fast but after around 40 ns, the plasma expansion becomes relatively slow. In the case of 1.65 cm diode gap the plasma expansion velocity is very fast for the entire pulse duration

It was found that almost for all the cases, the plasma expansion velocity increases with the AK gap. It may be possible that the higher electric field at lower AK gap is slowing one of the two electrode plasmas.

The faster plasma expansion velocity obtained for larger anode cathode gaps is related to smaller number of the cathode plasma spots and respectively to larger current densities for larger anode-cathode gaps. This results in larger plasma density and temperature and, respectively, to larger plasma expansion velocity.

CHAPTER 6

HIGH POWER MICROWAVE GENERATION FROM VIRTUAL CATHODE OSCILLATOR (VIRCATOR)

6.1 HPM GENERATION FROM AXIAL VIRCATOR

KALI 1000 pulse power system has been used to generate HPM from axial vircator using the planar diode described in the previous section. A vacuum explosive Emission Diode was used to generate Intense Relativistic Electron Beam (IREB). The high voltage pulse

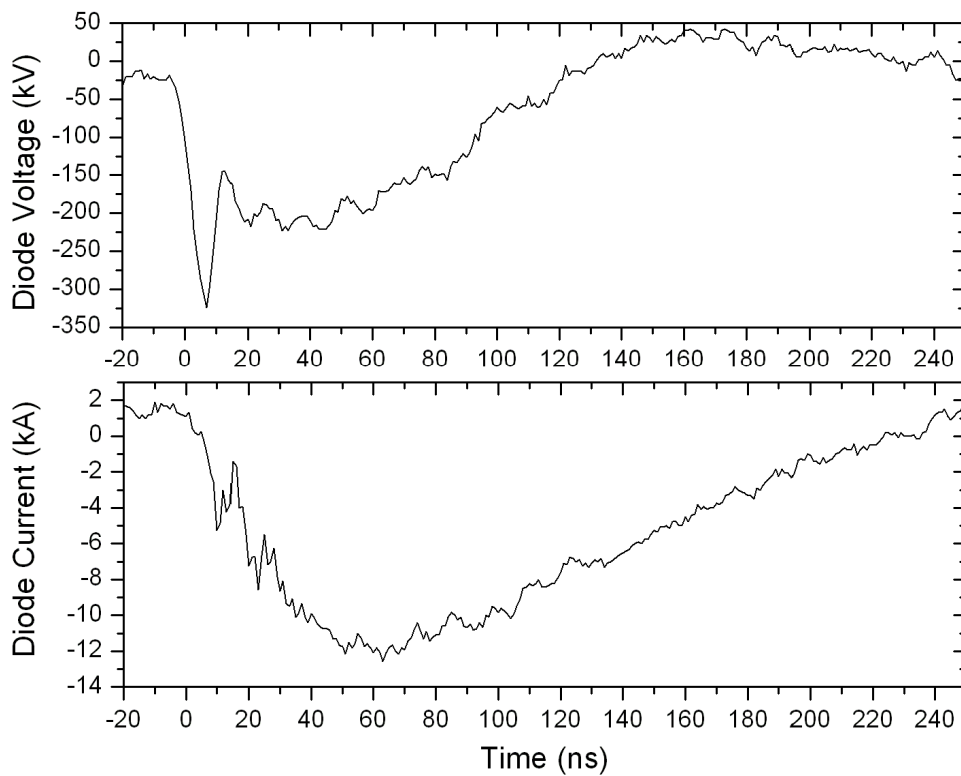


FIG. 6.1 Diode voltage and current waveform for 6 mm AK gap 70 mm diameter graphite cathode.

generated from the pulse power system is applied to the field emission diode. The diode consists of a planar graphite cathode (70 mm diameter) and copper anode mesh (240 mm diameter) at various AK gaps and various voltage levels. A resistive CuSO₄ Voltage Divider and a self integrating Rogowski Coil were used to measure the diode voltage and current pulses respectively. After the copper mesh anode flange, there is a axial virtual cathode oscillator (vircator) chamber (length 25 cm, diameter 25 cm) for microwave generation. The IREB is injected to the vircator chamber for HPM generation. In the VIRCATOR chamber, the beam front forms a virtual cathode at a distance equal to the AK gap if the injected current is greater than the space charge limiting current by four times .It is given by [6]

$$I_l = \frac{4\pi\epsilon_0 m_0 c^3 (\gamma^{2/3} - 1)^{3/2}}{e[1 + 2 \ln(R/r_b)]} , \quad (6.1)$$

where r_b is the beam radius, R is the drift column radius, γ is the relativistic factor and e and m_0 are the electron charge and rest mass respectively.

The virtual cathode reflects the electrons that follow the beam front. The electrons thus oscillate between the cathode and virtual cathode which causes microwave emission. The reflection frequency is given by

$$f_r = v/4d, \quad (6.2)$$

where v is the velocity of electrons and d the AK gap.

The virtual cathode oscillation frequency in GHz is given by

$$f_{vc} = 10(J/\beta\gamma)^{1/2} , \quad (6.3)$$

where J is the current density in kA/cm^2 .

Scaling law derived from the two dimensional oscillation of the virtual cathode and can also be derived from a harmonic one dimensional oscillator model of reflexing electrons.

$$f_s = \frac{4.77}{d} \ln[\gamma + (\gamma - 1)^{1/2}] \quad , \quad (6.4)$$

The frequency at which maximum power is emitted will be in between f_r and f_{vc} and the emission is broadband.

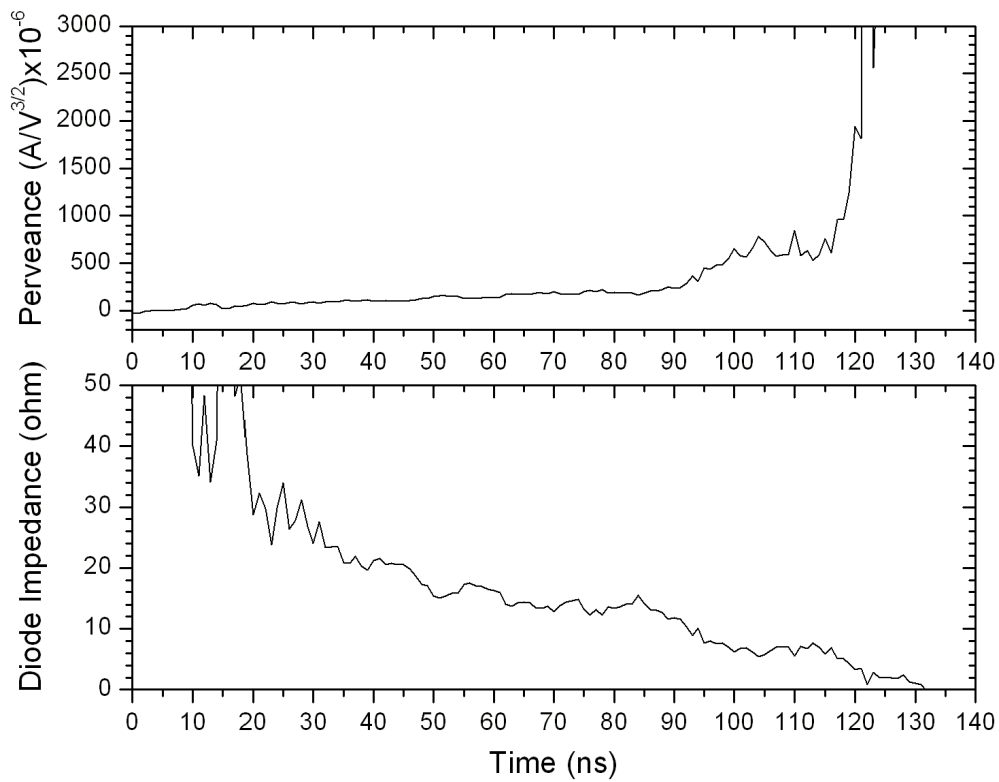


FIG. 6.2 The temporal behavior of the diode perveance and impedance for 6 mm AK gap.

A vacuum level of the order of $< 5 \times 10^{-5}$ mbar was maintained in the diode chamber as well as the vircator chamber. High power microwave has been detected by neon lamp discharge by HPM illumination when placed a few meter distances from the vircator window. Microwave power has been optimized by changing the anode-cathode gap. It was found that the peak power occur around 6 mm AK gap.

The diode voltage and current waveforms for 6 mm AK gap is shown in Fig. 6.1 As can be seen from the Fig. 6.1 that the voltage rises to a peak ~ 325 kV and then suddenly decreased to ~ 150 kV. This voltage peak is due to the fact that the explosive emission cathode plasma formation takes few ns time, during that time diode voltage rises to a peak as the pulse forming line see an open circuit load. Electron beam diode time varying impedance and perveance values were calculated using the voltage and current waveforms. The starting point or the zero time for perveance calculations was taken when the voltage pulse started rising. The experimental impedance and perveance derived from the diode voltage and current is shown in Fig. 6.2. There is an initial plateau region in time where the perveance is almost constant. At this time the diode perveance is $< P_{CL}$ indicating that the emission occurs over a fraction of the cathode area only. The cathode plasma expands both radially and axially, increasing the diode perveance. The diode perveance increases rapidly after ~ 120 ns showing gap closure.

Various components used in the diagnostics were calibrated using standard modulated RF source. For each shot, the beam parameters were recorded using Lecroy model WS 454 (500MHz, 2GS/s) scope. Microwave detector output was recorded using Tektronics make oscilloscope TDS 520D (500MHz, 1GS/s).The microwave signal after detection was carried to the scope by a BNC cable which was kept inside a metal conduit. Initially, the detector output could not be recorded due to the high noise level persisting in the ambiance. To reduce the

noise level, different techniques were tried such as grounding the conduit to the signal cable ground, to the inner wall of the shield room etc. Isolating the scope supply from the AC mains was also tried during the recording, but in vain. It was observed that ~ 300mV noise persisted throughout. To override the noise signal and to improve the microwave signal amplitude from the diode detector, a pre amplifier (BMC 1595) was used at the output of the microwave detector. This could not also help in detecting the microwave signal as the noise level too got amplified.

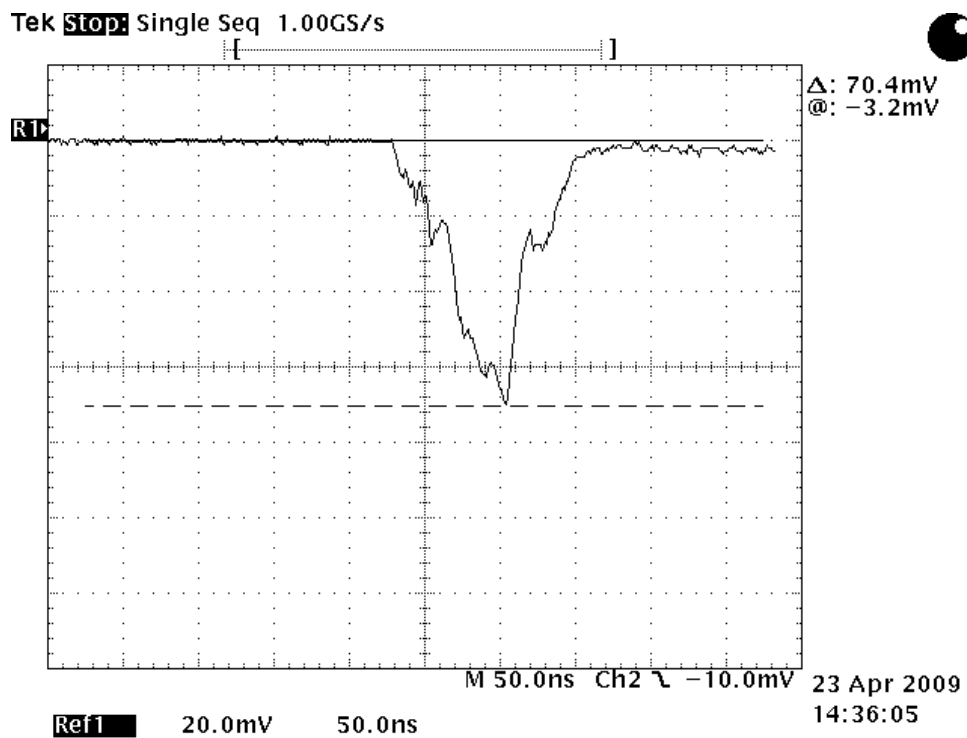


FIG. 6.3 HPM signal recorded from axial vircator.

It was observed that noise was picked up by the BNC cable when the BNC cable along with the conduit was kept inside the shield chamber, though the amplitude was low. So the use of BNC cable was avoided hence forward. Microwave signal was recorded successfully when RF

cable was used to carry the signal from the receiving antenna and the diode detector was at the scope end.

Finally HPM pulse has been successfully detected using wide band antenna RF cable and diode detector setup. Estimated microwave peak power ~ 59.8 dBm (~ 1 kW) at (within the effective aperture area of the receiving antenna) 7 m distance from the vircator window. Fig. 6.3 displays a typical HPM signal recorded by the diode detector. The corresponding beam peak voltage and current was 256 kV and 9 kA. It was observed that there was a shot to shot variation in the microwave peak power. For different shots microwave peak power at 7 m distance varied to the maximum of ~ 1 kW. Few attempts were also made to measure frequency of the radiation using YIG base tunable band pass filter. As the pass band of the filter is only ~ 100 MHz we are unable to detect any signal using the filter.

6.2 HPM GENERATION FROM COAXIAL VIRCATOR

A coaxial virtual cathode oscillator (vircator) has been designed to generate High Power Microwaves. Coaxial virtual cathode oscillators are known for better efficiency compared to the axial virtual cathode oscillators. This Coaxial vircator has been designed for the KALI-5000 pulse power system. Provision for a large anode-cathode gap has been kept to avoid the prepulse effect during the electron beam generation from the KALI-5000 system. Experimental studies are carried out to generate and characterize High Power Microwaves in the presence of significant prepulse voltages. Relativistic Electron Beams are generated by the Coaxial Explosively emitted graphite cathodes as described in the previous section. Electron beam voltage has been measured by a copper sulphate voltage divider and beam current by a B-dot probe. High Power Microwaves are detected by the glow of neon lamps placed closed to the output window.

The coaxial vircator consist of an cylindrical electron beam diode and a waveguide. The electron beam is accelerated in the coaxial direction and is injected into the waveguide. Electron beam is accelerated in the diode gap where pulsed high voltage is applied between the anode and the cathode. The beam passes through the copper mesh anode, and is injected into the area on the other side of the anode. Coaxial diode impedance calculated from the Langmuir-Blodgett law for various anode cathode radiuses is given in the Table I.

TABLE I. Coaxial diode impedance for various anode cathode radiuses.

Diode Voltage (kV)	Cathode Radius (cm)	Anode Radius (cm)	A K Gap (cm)	Cathode Width (cm)	Diode Impedance (ohm)
300	5.5	4.5	1.0	2	13
	5.9	4.5	1.4	2	25
	6.3	4.5	1.8	2	41
	6.9	4.5	2.4	2	71
400	5.5	4.5	1.0	2	11
	5.9	4.5	1.4	2	22
	6.3	4.5	1.8	2	35
	6.9	4.5	2.4	2	61

TABLE II. The calculated coaxial vircator frequency for various anode cathode radiuses and diode voltages.

Diode Voltage (kV)	Cathode Radius (cm)	Anode Radius (cm)	A K Gap (cm)	f_r (GHz)	f_{vc} (GHz)
300	5.5	4.5	1.0	5.8	4.8
	5.9	4.5	1.4	4.0	4.7
	6.3	4.5	1.8	3.0	4.5
	6.9	4.5	2.4	2.4	4.3
400	5.5	4.5	1.0	6.2	4.4
	5.9	4.5	1.4	4.4	4.3
	6.3	4.5	1.8	3.5	4.1
	6.9	4.5	2.4	2.6	3.9

HPM generation studies were carried out in the Coaxial Vircator for 1.8 cm and 1.2 cm AK gap. For 1.8 cm AK gap the peak diode voltage obtained was 350 kV and the peak current was 25 kA. For 1.2 cm AK gap the peak diode voltage was 200 kV and the peak diode current was 40 kA.

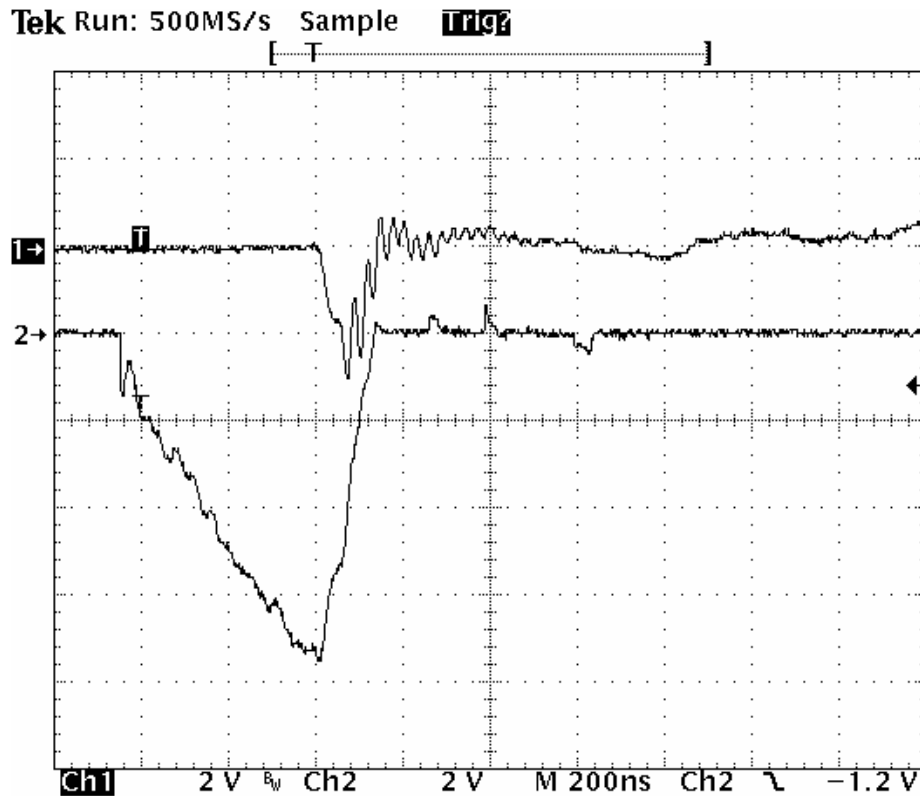


FIG. 6.5 Marx output voltage (Bottom 80 kV/Div) and diode current (Top 10 kA /Div) (Time 200 ns/Div)

The microwave pulse was measured by using the set up shown in Section 3.6. The HPM radiation was received by a double-ridge horn antenna located a distance 4 meter away from the output window and after suitable attenuation given to a diode detector. The diode detector output is shown in the Fig. 6.6. Also HPM discharge observed on Tube light and Neon Lamp placed a distance away from the output window.

For both the cases HPM generation was observed and microwave pulse recorded by the diode detector (Fig. 6.6.). For 1.2 cm diode gap HPM has got more peak power as the diode detector was getting saturated even when the antenna has been placed at around 4.5 meter distance from the vircator output window. At this place the measured HPM peak power was more than 20 dBm (within the effective aperture area of the receiving antenna). Also Neon Lamp Glow

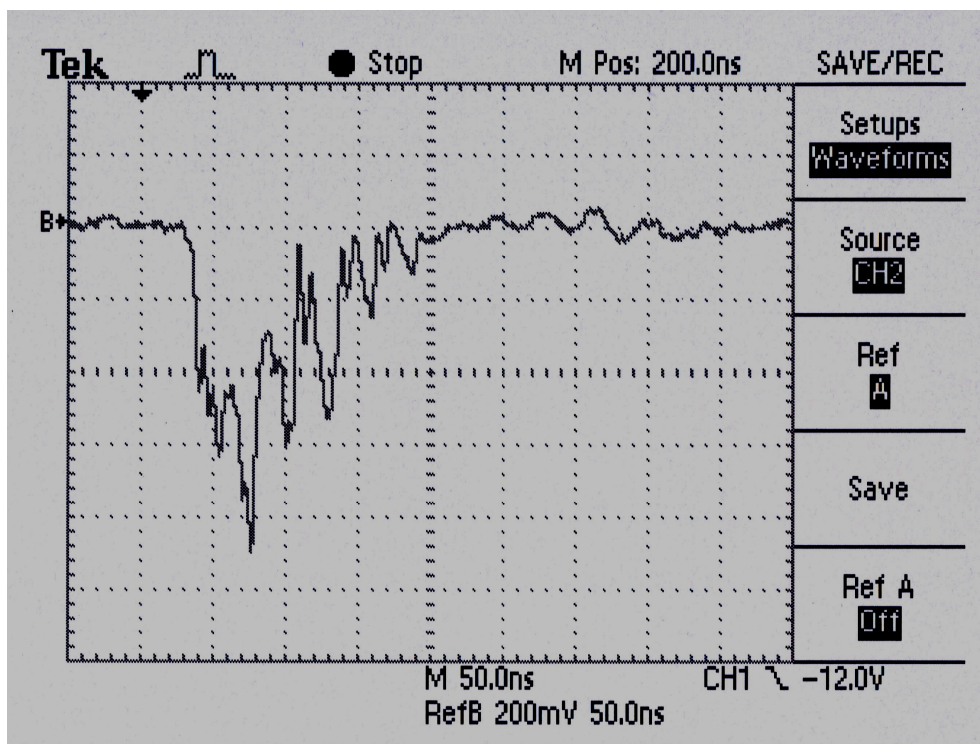


FIG. 6.6 HPM signal from coaxial vircator detected by diode detector and horn antenna setup.

was observed at a distance of 10 cm from the output window and the power density required for HPM discharge is more than 1 kW/ cm^2 . So the estimated peak power of the Coaxial Vircator was more than 1 MW. Further experiments are required to measure the HPM power more accurately.

6.3 CONCLUSIONS

HPM generation studies have been carried out using the pulsed power generator KALI 1000. The typical electron beam parameter was 200 kV, 14 kA, 100 ns. High power microwave has been detected by neon lamp discharge by HPM illumination when placed a few meter distances from the vircator window. A graphite explosive emission cathode has been used to generate intense electron beams. Microwave power has been optimized by changing the AK gap. It was found that the peak power occur around 6 mm anode cathode gap. HPM measurements were done using zero bias schottky diode detectors along with a horn antenna and sufficient attenuation so as to reduce the power level below the power rating of the diode detector. Various components used in the diagnostics were calibrated using standard modulated RF source. The estimated microwave peak power ~1 kW at 7 m distance from the vircator window (within the effective aperture area of the receiving antenna). The corresponding peak power at the vircator window was 196 MW. It was observed that there was a shot to shot variation in the microwave peak power.

HPM generation studies were carried out with a coaxial vircator using cylindrical electron beam diode in the presence of significant prepulse voltages. For 1.2 cm diode gap HPM has got more peak power as the diode detector was getting saturated even when the antenna has been placed at around 4.5 meter distance from the vircator output window. At this place the measured HPM peak power was more than 20 dBm (within the effective aperture area of the receiving antenna). The estimated peak power of the Coaxial Vircator was more than 1 MW. Further experiments are required to measure the HPM power more accurately.

CHAPTER 7

SUMMARY AND CONCLUSIONS

Based on the above studies following conclusions were made.

- a) It was shown that intense gigawatt relativistic electron beams can be generated in the presence of significant prepulse voltages in planar, annular and cylindrical diodes with a larger gap than that estimated by the space charge limited law. A maximum of 32% negative prepulse voltage has been recorded at the diode. Both the time duration and the amplitude of the positive prepulse voltage decrease with the increase in the Marx generator voltage. The highest positive prepulse voltage is 17% of the peak diode voltage. Electron beam generation mechanism in the presence of the prepulse has been analyzed by the expansion of the prepulse generated plasma and plasma filled diode. Increasing the AK gap reduces the prepulse voltage and eventually drops it below the explosive emission threshold and eliminates its creation. It was found that the positive prepulse voltage has no significant effect on the diode perveance and impedance. The effect of the prepulse is less pronounced in the cylindrical diode as compared to planar diode that allows one to operate the cylindrical diode with the AK gap ≤ 1.85 cm. Studies have been carried out to generate intense electron beam in the cylindrical electron beam diode when subjected to a high voltage bipolar pulse. In the positive voltage pulse, a copper mesh acts as a source of electrons. The diode perveance in the positive voltage pulse linearly increases with time due to the increase in the emission area. The electrode plasma closure is a small effect on the positive voltage pulse. During the negative voltage pulse, the diode impedance decreases with time due to the plasma expansion. Thus, even though there is a plasma formation on the anode during

- the positive voltage pulse, the electron beam can be generated from the graphite cathode in the negative voltage pulse with a modest perveance ($\sim 1.1 \times 10^{-4} \text{ A/V}^{3/2}$).
- b) It was found that for lesser AK gap there is shot to shot variation in the diode voltage and current for the same Marx generator voltage due to the nonreproducibility of the prepulse generated plasma. For perveance more than $200 \mu\text{Perv}$ we can consider the diode as short. The diode can be considered short if the Marx voltage/(Anode Cathode Gap)² is more than 56 kV/cm^2 . Below 56 kV/cm^2 the effect of the prepulse will be less and the diode can be operated with a better shot to shot reproducibility For the same Marx generator voltage, there is lot of shot to shot variation in the diode voltage and current in the annular cathode. Annular graphite cathodes of 40 and 70 mm diameters and 98 mm diameter planar graphite cathodes are not very suitable for reliable operation in the presence of prepulse. The effect of prepulse is more pronounced in the cathode of higher diameter due to a decrease in the uniformity of the prepulse generated plasma with the corresponding increase in the cathode diameter.
- c) Intense relativistic electron beam has been generated in a planar diode with a dielectric cathode holder. It was found that for the Perspex length $< 35 \text{ mm}$ prepulse voltage appears at the diode either due to capacitive coupling or surface flashover at the Perspex insulator surface at the prepulse voltage itself. This surface flashover occurs at an unexceptionally low flashover fields could be because of the bipolar nature of the prepulse voltage. No prepulse voltage has been recorded at the diode for the Perspex length $\geq 35 \text{ mm}$. But due to the pre breakdown time delay in the surface flashover across the insulator the rise time of the diode voltage increases. The diode current started rising after $\sim 50 \text{ ns}$ from beginning of the diode voltage, this reduces the

- effective pulse width by 50 ns. Inserting a dielectric at the cathode holder could be a very effective method to reduce prepulse at the electron beam diode, but it increases the rise time of the diode voltage and reduces the effective electron beam pulse width.
- d) In the case of the added inductance to the Blumlein circuit, the slower rise time reduces the prepulse voltage from 32% to $\leq 10\%$.
- e) It was found that during the main pulse the diode impedance collapses due to plasma expansion from the cathode and anode surfaces. Electrode plasma expansion velocities are measured from the perveance data for planar and cylindrical graphite cathodes. For 31 mm AK gap planar diode the anode and cathode plasmas expand at $9.5 \text{ cm}/\mu\text{s}$ toward each other. Plasma expansion velocity decreases for 25 mm AK gap. Electrode plasma expansion velocity has been measured when the planar diode is operated with a dielectric cathode holder to suppress prepulse. It was found that for 18-mm AK gap, the anode and cathode plasmas expand at $5.1 \text{ cm}/\mu\text{s}$ toward each other. Plasma velocity increases with the current density. Plasma expansion velocity increases for 25-mm AK gap. Cylindrical electron beam diode perveance was measured for 1.85, 1.65, and 1.2 cm AK gaps. The anode and cathode plasma expansion velocities were measured using the perveance data. For 1.85 cm radial AK gap the anode and cathode plasmas expand at $5 \text{ cm}/\mu\text{s}$ toward each other. Plasma expansion velocity decreases for 1.2 cm AK gap. The time dependence of the diode gap is calculated for cylindrical diode. It was found that in the initial stage of the 1.85 cm and 1.2 cm accelerating gap the plasma expansion velocity is very fast but after around 40 ns, the plasma expansion becomes relatively slow. In the case of 1.65 cm diode gap the plasma expansion velocity is very fast for the entire pulse duration. It was found that almost for all the cases, the plasma

expansion velocity increases with the AK gap. It may be possible that the higher electric field at lower AK gap is slowing one of the two electrode plasmas.

- f) HPM has been generated from axial and coaxial virtual cathode oscillator using the IREB and the HPM power has been measured using a diode detector and receiving horn antenna set up. High power microwave has been detected by neon lamp discharge by HPM illumination when placed a few meter distances from the VIRCATOR window. A graphite explosive emission cathode has been used to generate intense electron beams. Microwave power has been optimized by changing the AK gap. It was found that the peak power occur around 6 mm anode cathode gap. The estimated microwave peak power ~1 kW (within the effective aperture area of the receiving antenna) at 7 m distance from the VIRCATOR window. The corresponding peak power at the VIRCATOR window was 196 MW. It was observed that there was a shot to shot variation in the microwave peak power. HPM generation studies were carried out with a coaxial vircator using cylindrical electron beam diode in the presence of significant prepulse voltages. For 1.2 cm diode gap HPM has got more peak power as the diode detector was getting saturated even when the antenna has been placed at around 4.5 meter distance from the vircator output window. At this place the measured HPM peak power was more than 20 dBm (within the effective aperture area of the receiving antenna). The estimated peak power of the Coaxial Vircator was more than 1 MW.

Finally some suggested future work is being outlined.

- a) Beam generation studies should be carried out with a gas prepulse switch.

- b) Cathode and anode plasma expansion velocities should be measured more accurately with a streak camera.
- c) Plasma expansion velocities should be measured for other cathode materials like velvet and carbon fiber and CsI coated cathodes.
- d) HPM generation and measurements should be carried out with more accurate diagnostics.

Present work has contributed to a better understanding of intense gigawatt relativistic electron beam generation process and its usefulness towards HPM generation. The results of the study are useful in the design of a reliable and efficient large electron beam system and HPM devices.

REFERENCES

- [1] Steven H. Gold, Gregory S. Nusinovich, "Review of high-power microwave source research," *Rev. Sci. Instrum.* Vol. 68, pp. 3945-3974, 1997.
- [2] Lie Liu, Li-Min Li, Xiao-Ping Zhang, Jian-Chun Wen, Hong Wan, and Ya-Zhou Zhang, "Efficiency Enhancement of Reflex Triode Virtual Cathode Oscillator Using the Carbon Fiber Cathode," *IEEE Trans. Plasma Sci.* Vol. 35, pp. 361-368, 2007.
- [3] H. P. Freund, T. M. Antonsen, *Principles of free-electron lasers* Published by Springer, 1996.
- [4] Maenchen, J.; Cooperstein, G.; Oapos; Malley, J.; Smith, I., "Advances in pulsed power-driven radiography systems," *Proceedings of the IEEE*, Vol. 92, pp. 1021-1042, 2004.
- [5] L. X. Schneider, K. W. Reed, and R. J. Kaye, in *Applications of Accelerators in Research and Industry*, edited by J. L. Duggan and I. L. Morgan (AIP, New York, 1997), p. 1085.
- [6] R. B. Miller, *An Introduction to the Physics of Intense Charge Particle Beams*, (Plenum, New York, 1982, ch. 2).
- [7] J. C. Martin, AWRE Report No. SSWA/JCM/70327 (1970); and AWRE Report No. SSWA/JCM/1065/25 (1965)
- [8] S. E. Graybill and S. V. Nablo, "OBSERVATIONS OF MAGNETICALLY SELF-FOCUSING ELECTRON STREAMS," *Appl. Phys. Lett.* Vol. 8, pp. 18-20, 1966.
- [9] D. Durga Praveen Kumar, S. Mitra, K. Senthil, Archana Sharma, K. V. Nagesh, S. K. Singh, J. Mondal, Amitava Roy, and D. P. Chakravarthy, "Characterization and analysis of a pulse power system based on Marx generator and Blumlein," *Rev. Sci. Instrum.* Vol. 78, pp. 115107, 2007.

- [10] S. Mitra, D. Durga Praveen Kumar, R. Agarwal, S. R. Raul, J. Mondal, A. Roy, A. Sharma, K. V. Nagesh, G. Venugopala Rao, K. C. Mittal, and D. P. Chakravarthy, National Power Systems Conference, 2006 (unpublished).
- [11] Mitsuyasu Yatsuzuka, Masakazu Nakayama, Mitsuru Tanigawa, Sadao Nobuhara, Douglas Young, and Osamu Ishihara, "Plasma Effects on Electron Beam Focusing and Microwave Emission in a Virtual Cathode Oscillator," *IEEE Trans. Plasma Sci.* Vol. 26, pp. 1314-1321, (1998).
- [12] Peter J. Truchi, and Robert E. Peterkin, "Modeling of Impedance Collapse in High-Voltage Diodes," *IEEE Trans. Plasma Sci.* Vol. 26, pp. 1485-1491, 1998.
- [13] N. R. Pereira and A. Fisher, "Slower impedance collapse with hot anode and enhanced emission cathode," *IEEE Trans. Plasma Sci.* Vol. 27, pp. 1169-1174, 1999.
- [14] Yuri M. Saveliev, Wilson Sibbett and David M. Parkes, "On anode effects in explosive emission diodes," *J. Appl. Phys.* Vol. 94, pp. 5776-5781, 2003.
- [15] Donald A. Shiffler, John W. Luginsland, Ryan J. Umstattd, M. LaCour, K. Golby, Michael D. Haworth, M. Ruebush, D. Zagar, A. Gibbs, and Thomas A. Spencer, "Effects of anode materials on the performance of explosive field emission diodes," *IEEE Trans. Plasma Sci.* Vol. 30, pp.1232-1237, 2002.
- [16] Ian D. Smith, "Induction voltage adders and the induction accelerator family," *Phys. Rev. ST Accel. Beams* Vol. 7, pp. 064801, 2004.
- [17] J. Mondal, D. D. P. Kumar, A. Roy, S. Mitra, A. Sharma, S. K. Singh, G. V. Rao, K. C. Mittal, K. V. Nagesh, and D. P. Chakravarthy, "Intense gigawatt relativistic electron beam generation in the presence of prepulse," *J. Appl. Phys.* Vol. 101, pp. 034905, 2007.
- [18] C. W. Mendel, *Bull. Am. Phys. Soc.* Vol. 20, pp. 1322, 1975.

- [19] L. P. Mix, J. G. Kelly, G. W. Kuswa, B. W. Swain, and J. N. Olsen, "Holographic Measurements of the Plasmas in a High-Current Field Emission Diode," *J. Vac. Sci. Technol.* Vol. 10, pp. 951-953, 1973.
- [20] L. P. Bradley and G. W. Kuswa, "Neutron Production and Collective Ion Acceleration in a High-Current Diode," *Phys. Rev. Lett.* Vol. 29, pp. 1441-1445, 1972.
- [21] P. A. Miller, J. W. Poukey, and T. P. Wright, "Electron Beam Generation in Plasma-Filled Diodes," *Phys. Rev. Lett.* Vol. 35, pp. 940-943, 1975.
- [22] G. Venugopala Rao, A. S. Paithankar, and S. K. Iyyenger, "Relativistic electron-beam generation in a plasma-filled diode and its interaction with plasma," *J. Appl. Phys.* Vol. 69, pp. 3417-3420, 1991.
- [23] K. C. Mittal and V. K. Rothagi, "Control of gigawatt REB pulse duration using gas injection," *IEEE Trans. Plasma Sci.* Vol. 16, pp. 601-605, 1988.
- [24] Robert J. Kares, "One-dimensional particle-in-cell simulations of sheath erosion in a plasma-filled diode," *J. Appl. Phys.* Vol. 71, pp. 2155-2167, 1992.
- [25] B. V. Weber, D. D. Hinshelwood, D. P. Murphy, S. J. Stephanakis, and V. Harper-Slaboszewicz, "Plasma-Filled Diode for High Dose-Rate Bremsstrahlung," *IEEE Trans. Plasma Sci.* Vol. 32, pp. 1998-2003, 2004.
- [25a] Bystritsky V.M., Mesyats G.A., Kim A.A., Kovalchuk B.M., Krasik Ya.E. "Microsecond Plasma Opening Switches," *Physics of Elementary Particles and Atomic Nuclei*, Vol. 23, pp. 19, 1992.
- [26] C. W. Mendel, Jr., S. A. Goldstein, "A fast-opening switch for use in REB diode experiments," *J. Appl. Phys.* Vol. 48, pp. 1004-1006, 1977.

- [27] E. Thornton and R. R. Harris, "Development of an Intense Pulsed Relativistic Electron beam of Large Diameter and Uniform Flux," *J. Phys. E: Sci. Instruments*, Vol. 6, pp. 1223-1232, 1973.
- [28] Stephen B. Swanekamp, Gerald Cooperstein, Joseph W. Schumer, David Mosher, F. C. Young, Paul F. Ottinger and Robert J. Commisso, "Evaluation of Self-Magnetically Pinched Diodes up to 10 MV as High-Resolution Flash X-Ray Sources," *IEEE Trans. Plasma Sci.* Vol. 32, pp. 2004-2016, 2004.
- [29] Donald A. Shiffler, M. Ruebush, D. Zagar, M. LaCour, K. Golby, M. Collins Clark, Michael D. Haworth, and R. Umstattd, "Emission uniformity and emittance of explosive field-emission cathodes," *IEEE Trans. Plasma Sci.* Vol. 30, pp.1592-1596, 2002.
- [30] D. Shiffler, K. L. Cartwright, Kim Lawrence, M. Ruebush, M. LaCour, K. Golby and D. Zagar, "Experimental and computational estimate of bipolar flow parameters in an explosive field emission cathode," *Appl. Phys. Lett.*, Vol. 83, pp. 428-430, 2003.
- [31] Donald A. Shiffler, J. Luginsland, M. Ruebush, M. LaCour, K. Golby, K. Cartwright, M. Haworth, and T. Spencer, "Emission Uniformity and Shot-to-Shot Variation in Cold Field Emission Cathodes," *IEEE Trans. Plasma Sci.* Vol. 32, pp. 1262-1266, 2004.
- [32] John J. Watrous, John W. Luginsland, and Michael H. Frese, "Current and current density of a finite-width, space-charge-limited electron beam in two-dimensional, parallel-plate geometry," *Phys. Plasmas* Vol. 8, pp. 4202-4210, 2001.
- [33] R. J. Umstattd and J.W. Luginsland, "Two-Dimensional Space-Charge-Limited Emission: Beam-Edge Characteristics and Applications," *Phys. Rev. Lett.* Vol. 87, pp. 145002, 2001.

- [33a] G. Rosenman, D. Shur, Ya. E. Krasik, and A. Dunaevsky, "Electron emission from ferroelectrics," *J. Appl. Phys.* Vol. 88, pp - 6109-6161, 2000.
- [34] D. Shiffler, M. Ruebush, M. LaCour, K. Golby, R. Umstattd, M. C. Clark, J. Luginsland, D. Zagar, and M. Sena, "Emission uniformity and emission area of field emission cathodes," *Appl. Phys. Lett.* Vol. 79, pp. 2871-2873, 2001.
- [35] Y. E. Krasik, A. Dunaevsky, A. Krokhmal, and J. Felsteiner, "Emission properties of different cathodes at $E \leq 10^5$ V/cm," *J. Appl. Phys.* Vol. 89, pp. 2379-2399, 2001.
- [36] Yuri M. Saveliev and Wilson Sibbett, David M. Parkes, "Perveance of a planar diode with explosive emission finite-diameter Cathodes," *Appl. Phys. Lett.* Vol. 81, pp. 2343-2345, 2002.
- [37] Wook Jeon, Jeong Eun Lim, Min Wug Moon, Kyu Bong Jung, Won Bae Park, Hee Myung Shin, Yoonho Seo, and Eun Ha Choi, "Output Characteristics of the High-Power Microwave Generated From a Coaxial Vircator With a Bar Reflector in a Drift Region," *IEEE Trans. Plasma Sci.* Vol. 34, pp. 937-944, 2006.
- [38] "Study of plasma expansion in a vacuum diode by spectroscopic method," P. S. P. Wei, J. L. Adamski, and J. R. Beymer, *J. Appl. Phys.* Vol. 50, pp. 690-695, 1979.
- [39] Limin Li, Lie Liu, Jianchun Wen, Tao Men and Yonggui Liu "An intense-current electron beam source with low-level plasma formation," *J. Phys. D: Appl. Phys.* Vol. 41 pp. 125201 (7pp), 2008.
- [40] R. K. Parker, Richard E. Anderson, and Charles V. Duncan, "Plasma-Induced Field Emission and the Characteristics of High Current Relativistic Electron Flow," *J. Appl. Phys.* Vol. 45, pp. 2463-2479, 1974.
- [41] G. A. Mesyats and D. I. Proskurovsky, *Pulsed Electrical Discharge in Vacuum*. Berlin, Germany: Springer-Verlag, 1989.

- [42] G. A. Mesyats, "Explosive processes on the cathode in a vacuum discharge," *IEEE Trans. Elect. Insul.* Vol. EI-18, pp. 218–225, 1983.
- [43] J. G. Kelly, and L. P. Mix, "Measurement of high-current relativistic electron diode plasma properties with holographic interferometry," *J. Appl. Phys.* Vol. 46, pp. 1084-1090, 1975.
- [44] J. W. Maenchen, F. C. Young, R. Stringfield, S. J. Stephanakis, D. Mosher, Shyke A. Goldstein, R. D. Genuario, and G. Cooperstein, "Production of intense light ion beams on a multiterawatt generator," *J. Appl. Phys.* Vol. 54, pp.89-100, 1983.
- [45] D. J. Johnson, G. W. Kuswa, A. V. Farnsworth, Jr., J. P. Quintenz, R. J. Leeper, E. J. T. Burns, and S. Humphries, Jr., "Production of 0.5-TW Proton Pulses with a Spherical Focusing, Magnetically Insulated Diode," *Phys. Rev. Lett.* Vol. 42, pp. 610-613, 1979.
- [46] Y. Maron, E. Sarid, O. Zahavi, L. Perelmutter, and M. Sarfaty, "Particle-velocity distribution and expansion of a surface-flashover plasma in the presence of magnetic fields," *Phys. Rev. A* Vol. 39, pp. 5842-5855, 1989.
- [47] C. D. Child, "Discharge From Hot CaO," *Phys. Rev.* Vol. 32, pp. 492-511, 1911.
- [48] I. Langmuir, "The Effect of Space Charge and Residual Gases on Thermionic Currents in High Vacuum," *Phys. Rev.* Vol. 2, pp. 450-486, 1913.
- [49] J. W. Luginsland, Y. Y. Lau, R. J. Umstadtd, and J. J. Watrous, "Beyond the Child-Langmuir law: A review of recent results on multidimensional space-charge-limited flow," *Phys. Plasmas*, Vol. 9, pp.2371-2376, 2002.
- [50] J. W. Luginsland, Y. Y. Lau, and R. M. Gilgenbach, "Two-Dimensional Child-Langmuir Law," *Phys. Rev. Lett.* Vol. 77, pp. 4668-4670, 1996.

- [51] Y.Y. Lau, "Simple Theory for the Two-Dimensional Child-Langmuir Law," *Phys. Rev. Lett.* Vol. 87, pp. 278301, 2001.
- [52] I. Alexeff and W. D. Jones, "Transient Plasma Sheath-Discovered by Ion-Acoustic Waves," *Phys. Fluids*, Vol. 12, pp. 345-346, 1969.
- [53] T. H. Martin, "Design and Performance of the Sandia Laboratories Hermes II Flash X-Ray Generator," *IEEE Transactions on Nuclear Science* Vol. 16, pp. 59-63, 1969.
- [54] S. G. Clough, M. C. Williamson, and T. J. Williams, "PIM: Pre-Pulse Minimisation and Considerations," Pulsed Power Symposium, 2006. The Institution of Engineering and Technology (2006) Page(s): 52 – 54.
- [55] D. A. Phelps, D. Markins, V. Fargo and A. C. Kold, "Impedance Control in Relativistic Electron Diodes with Externally Applied Prepulse," *IEEE Trans. Plasma Sci.* Vol. 4, pp. 190-193, 1976.
- [56] R. J. Allen, J. R. Boller, R. J. Comisso, F. C. Young, F. Bayol, P. Charre, A. Garrigues, "Adaptation of ASTERIX to Positive Polarity for 2 to 4-MV Rod-Pinch Diode Experiments and Diode Electrical Analysis," *IEEE Proceedings*, pp. 446-449, 2002.
- [57] J. D. Lawson, *The Physics of Charged Particle Beams*. Oxford, U.K.: Clarendon, 1988, pp. 156–194.
- [58] D. Shiffler, M. Ruebush, M. Haworth, R. Umstattd, M. LaCour, K. Golby, D. Zagar, T. Knowles, "Carbon velvet field-emission cathode," *Rev. Sci. Instrum.* Vol. 73, pp. 4358-4362, 2002.
- [59] Don Shiffler, Michael Haworth, Keith Cartwright, Ryan Umstattd, Mitch Ruebush, Susan Heidger, Matthew LaCour, Ken Golby, Don Sullivan, Peter Duselis, and John Luginsland,

- “Review of Cold Cathode Research at the Air Force Research Laboratory,” *IEEE Trans. Plasma Sci.* Vol. 36, pp.718-728, 2008.
- [59a] V. Vekselman, J. Gleizer, D. Yarmolich, J. Felsteiner, Ya. Krasik, L. Liu, and V. Bernshtam, “Plasma characterization in a diode with a carbon-fiber cathode,” *Appl. Phys. Lett.* Vol. 93, pp. 081503, 2008.
- [59b] Ya. E. Krasik, J. Z. Gleizer, D. Yarmolich, A. Krokmal, V. Ts. Gurovich, S. Efimov, J. Felsteiner, V. Bernshtam, and Yu. M. Saveliev, “Characterization of the plasma on dielectric fiber (velvet) cathodes,” *J. Appl. Phys.* Vol. 98, pp. 093308, 2005.
- [59c] Ya.E. Krasik, A. Dunaevsky and J. Felsteiner, “Intense electron emission from carbon fiber cathodes,” *Eur. Phys. J.* Vol. D15, pp.345- 2001.
- [60] Don A. Shiffler, Matthew J. LaCour, Miguel D. Sena, Michael D. Mitchell, Michael D. Haworth, Kyle J. Hendricks, and Thomas A. Spencer, “Comparison of Carbon Fiber and Cesium Iodide-Coated Carbon Fiber Cathodes,” *IEEE Trans. Plasma Sci.* Vol. 28, pp. 517-522, 2000.
- [61] T. K. Statom, “Pulsed CsI-Coated Tufted Carbon Fiber Cathode Plasma,” *IEEE Trans. Electron Devices* Vol. 53, pp. 386-391, 2006.
- [62] D. Shiffler, M. LaCour, K. Golby, M. Sena, M. Mitchell, M. Haworth, K. Hendricks, and T. Spencer “Comparison of Velvet- and Cesium Iodide-Coated Carbon Fiber Cathodes,” *IEEE Trans. Plasma Sci.* Vol. 29, pp. 445-451, 2001.
- [63] D. Shiffler, M. Ruebush, D. Zagar, M. LaCour, M. Sena, K. Golby, M. Haworth and R. Umstattd, “Cathode and anode plasmas in short-pulse explosive field emission cathodes,” *J. Appl. Phys.* Vol. 91, pp. 5599-5603, 2002.

- [64] K. J. Hendricks, M. D. Haworth, T. Englert, Don Shiffler, G. Baca, P. D. Coleman, L. Bowers, R. W. Lemke, Thomas A. Spencer, and M. Joseph Arman, "Increasing the RF energy per pulse of an RKO," *IEEE Trans. Plasma Sci.* Vol. 26, pp. 320 – 325, 1998.
- [65] E. Garate, R. MacWilliams, D. Voss, A. Lovesee, K. Hendricks, T. Spencer, M. C. Clark, and A. Fisher, "Novel cathode for field-emission applications," *Rev. Sci. Instrum.* Vol. 66, pp. 2528-2532, 1995.
- [66] J. N. Benford, "Extension of HPM pulse duration by cesium iodide cathodes in crossed field devices," Air Force Research Lab. Tech. Rep., AFRL-DE-PS-TR-1998-1019, May 1998.
- [67] J. C. Gregory, "The specific light output of cesium iodide crystals," NASA Final Tech. Rep., NASA-CR-150267.
- [68] R. S. Snyder and W. N. Clotfelter, "Physical property measurements of doped cesium iodide crystals," NASA Tech. Mem., NASATMX-64898.
- [69] Vasilios Vlahos, John H. Booske and Dane Morgan, "Ab initio study of the effects of thin CsI coatings on the work function of graphite cathodes," *Appl. Phys. Lett.* Vol. 91, pp. 144102, 2007.
- [70] Don Shiffler, Susan Heidger, Keith Cartwright, Rich Vaia, David Liptak, Gary Price, Matthew LaCour and Ken Golby, "Materials characteristics and surface morphology of a cesium iodide coated carbon velvet cathode," *J. Appl. Phys.* Vol. 103, pp. 013302 2008.
- [71] D. Shiffler, J. Heggemeier, M. LaCour, K. Golby, and M. Ruebush "Low level plasma formation in a carbon velvet cesium iodide coated Cathode," *Phys. Plasmas* Vol. 11, pp. 1680-1681, 2004.

- [72] Y. M. Saveliev, Ya. E. Krasik, "Comment on 'Low level plasma formation in a carbon velvet cesium iodide coated cathode' [Phys. Plasmas 11, 1680 (2004)]," *Phys. Plasmas* Vol. 11, pp. 5730-5731, 2004.
- [73] D. Shiffler, J. Heggemeier, M. LaCour, K. Golby, and M. Ruebush "Response to 'Comment on 'Low level plasma formation in a carbon velvet cesium iodide coated cathode'," [Phys. Plasmas 11, 5730 (2004)], *Phys. Plasmas* Vol. 11, pp. 5732-5733, 2004.
- [74] H. Kosai, A. Fisher, "Long Pulse CsI Impregnated Field Emission Cathodes," *Rev. Sci. Instrum.* Vol. 61(7), pp. 1880-1882, 1990.
- [75] John Walter, John Mankowski, and James Dickens, "Imaging of the Explosive Emission Cathode Plasma in a Vircator High-Power Microwave Source," *IEEE Trans. Plasma Sci.* Vol. 36, pp.1388-1389, 2008.
- [76] A. E. Blaugrund, "Measurements of electron emission uniformity from cathodes in high-voltage electron beam diodes," *Appl. Phys. Lett.* Vol. 83, pp. 1264-1265, 2003.
- [77] B. V. Alyokhin, A. E. Dubinov, V. D. Selemir, O. A. Shamro, K. V. Shibalko, N. V. Stepanov, and V. E. Vatrugin, "Theoretical and Experimental Studies of Virtual Cathode Microwave Devices," *IEEE Trans. Plasma Sci.* Vol. 22, pp. 945, 959, 1994.
- [78] S. Humphries, J. J. Lee, and R. N. Sudan, "Generation of intense pulsed ion beams," *Appl. Phys. Lett.* Vol. 25, pp. 20-22, 1974.
- [79] C. A. Kapetanacos, P. A. Sprangle, R. A. Mahaffey, and J. Golden, "High-power microwaves from a non-isochronous reflecting electron system (NIRES)," US Patent 4150340, H 01 J 25/74, April 17, 1979.
- [80] D. J. Sullivan, "High power microwave generator using relativistic electron beams in waveguide drift tube," US Patent 4345220, H 03 B 9/01, August 17, 1982.

- [81] Eun Ha Choi, Myung Chull Choi, Sung Hyuk Choi, Kie Back Song, Yoon Jung, Yoon Ho Seo, Hee Myung Shin, Han Sup Uhm, Dong Woo Lim, Chun Ho Kim, Jae Min Lee, and Jae Woon Ahn, "Characteristics of Diode Perveance and Vircator Output Under Various Anode–Cathode Gap Distances," *IEEE Trans. Plasma Sci.* Vol. 30, pp. 1728-1732, 2002.
- [81a] T. Queller, A. Shlapakovski, and Ya. E. Krasik, "Plasma formation in a double-gap vircator," *J. Appl. Phys.* Vol. 108, pp.103302, 2010.
- [82] V. L. Granatstein and I. Alexeff, *High-Power Microwave Sources*. Boston, MA: Artech House, 1987, ch. 13–14.
- [83] Weihua Jiang, Magne Kristiansen, "Theory of the virtual cathode oscillator," *Phys. Plasmas* Vol. 8, pp. 3781-3787, 2001.
- [84] Eun-Ha Choi, Myoung-Chul Choi, Yoon Jung, Min-Woo Chong, Jae-Jun Ko, Yoonho Seo, Guangsup Cho, Han S. Uhm, and Hyyong Suk, "High-Power Microwave Generation from an Axially Extracted Virtual Cathode Oscillator," *IEEE Trans. Plasma Sci.* Vol. 28, pp. 2128- 2134, 2000.
- [85] Limin Li, Tao Men, Lie Liu, and Jianchun Wen, "Dynamics of virtual cathode oscillation analyzed by impedance changes in high-power diodes," *J. Appl. Phys.* Vol. 102, pp. 123309, 2007.
- [86] Y. Chen, J. Mankowski, J. Walter, M. Kristiansen, R. Gale, "Cathode and Anode Optimization in a Virtual Cathode Oscillator," *IEEE Transactions on Dielectrics and Electrical Insulation* Vol. 14, pp. 1037-1044, 2007.
- [87] Weihua Jiang, Kevin Woolverton, James Dickens and Magne Kristiansen, "High Power Microwave Generation by a Coaxial Virtual Cathode Oscillator," *IEEE Trans. Plasma Sci.* Vol. 27, pp. 1538-1542, 1999.

- [88] Kew Yong Sung, Wook Jeon, Yoon Jung, Jeong Eun Lim, Han S. Uhm, and Eun Ha Choi, "Influence of Anode–Cathode Gap Distance on Output Characteristics of High-Power Microwave From Coaxial Virtual Cathode Oscillator," *IEEE Trans. Plasma Sci.* Vol. 33, pp.1353-1357, 2005.
- [89] W. Jiang, K. Masugata, and K. Yatsui, "Mechanism of microwave generation by virtual cathode oscillation," *Phys. Plasmas* Vol. 2, pp. 982–986, 1995.
- [90] Xiaodong Chen, Wee Kian Toh and Peter A. Lindsay, "Physics of the Interaction Process in a Typical Coaxial Virtual Cathode Oscillator Based on Computer Modeling Using MAGIC," *IEEE Trans. Plasma Sci.* Vol. 32, pp.1191-1199, 2004.
- [91] Qingzi Xing, Dong Wang, Feng Huang, and Jingkang Deng, "Two-Dimensional Theoretical Analysis of the Dominant Frequency in the Inward-Emitting Coaxial Vircator," *IEEE Trans. Plasma Sci.* Vol. 34, pp. 584-589, 2006.
- [92] Hao Shao, Guozhi Liu, Zhanfeng Yang, Changhua Chen, Zhimin Song, and Wenhua Huang "Characterization of Modes in Coaxial Vircator," *IEEE Trans. Plasma Sci.* Vol. 34, pp.7-13, 2006.
- [93] Xupeng Chen, James Dickens, John Mankowski, Lynn L. Hatfield, Eun Ha Choi and Magne Kristiansen, "Microwave Frequency Determination Mechanisms in a Coaxial Vircator," *IEEE Trans. Plasma Sci.* Vol. 32, pp. 1799-1804, 2004.
- [94] I. Langmuir and K. Blodgett, "Currents limited by space charge between coaxial cylinders," *Phys. Rev.* Vol. 22, pp. 347-356, 1923.
- [95] K. G. Kostov and J. J. Barroso, "Space-charge-limited current in cylindrical diodes with finite-length emitter," *Phys. Plasmas*, Vol. 9, pp. 1039-1042, 2002.

- [96] Xupeng Chen, James Dickens, L.L Hatfield, Eun-Ho Choi and M. Kristiansen, "Approximate analytical solutions for the space-charge-limited current in one-dimensional and two-dimensional cylindrical diodes," *Phys. Plasmas* Vol. 11, pp. 3278-3283, 2004.
- [97] L. Oksuz, "Analytical solution of space charge limited current for spherical and cylindrical objects," *Appl. Phys. Lett.* Vol. 88, pp.181502, 2006.
- [98] S. B. Swanekamp, R. J. Commisso, G. Cooperstein, P. F. Ottinger, "Particle-in-cell simulations of high-power cylindrical electron beam diodes," *Phys. Plasmas* Vol. 7, pp.5214-5222, 2000.
- [99] Robert J. Commisso, Gerald Cooperstein, David D. Hinshelwood, David Mosher, Paul F. Ottinger, Stavros J. Stephanakis, Stephen B. Swanekamp, Bruce V. Weber, and F. C. Young, "Experimental Evaluation of a Megavolt Rod-Pinch Diode as a Radiography Source," *IEEE Trans. Plasma Sci.* Vol. 30, pp. 338-350, 2002.
- [100] A. Sharma, K. V. Nagesh, R. Agarwal, S. R. Raul, K. C. Mittal, G. V. Rao, J. Mondal, and R. C. Sethi, Proceedings of the IAEA Symposium on Utilization of Accelerators, 2005, (unpublished), Paper No. IAEA-CN-115-28.
- [101] P. H. Ron, "Configurations of Intense Pulse Power Systems for generation of Intense Electromagnetic Pulses" INCEMIC-99, New Delhi, India (1999).
- [102] W. Rogowski and W. Steinhaus, *Arch. Elektrotech.* (Berlin) Vol. 1, pp. 141, 1912.
- [103] J. D. Ramboz, "Machinable Rogowski coil, design, and calibration," *IEEE Trans. Instrum. Meas.* Vol. 45, pp. 511-515, 1996.
- [104] D. G. Pellinen, M. S. Di Capua, S. E. Sampayan, H. Gerbracht, and M. Wang, "Rogowski coils for measuring fast, high-level pulsed currents," *Rev. Sci. Instrum.* Vol. 51, pp. 1535-1540, 1980.

- [105] V. Godyak and R. Piejak, *J. Phys. IV Pr* 7, p. 243 (1998).
- [106] D. G. Pellinen and S. Heurlin, "A Nanosecond Risetime Megavolt Voltage Divider," *Rev. Sci. Instrum.* Vol. 42, pp. 824-827, 1971.
- [107] W. He, H. Yin, A. D. R. Phelps, A. W. Cross, and S. N. Spark, "Study of a fast, high-impedance, high-voltage pulse divider," *Rev. Sci. Instrum.* Vol. 71, pp. 4266-4269, 2001.
- [108] L. M. Earley, W. P. Ballard, L. D. Roose, and C. B. Wharton, "Comprehensive approach for diagnosing intense single-pulse microwave sources," *Rev. Sci. Instrum.* Vol. 57(9), pp.2283-2293, 1986.
- [109] Y. J. Chen, A. A. Neuber, J. Mankowski, J. C. Dickens, M. Kristiansen, and R. Gale, "Design and optimization of a compact, repetitive, high-power microwave system," *Rev. Sci. Instrum.* Vol. 76, pp. 104703, 2005.
- [110] M. Mazarakis *et al.*, in *Proceedings of the 11th IEEE Pulse Power Conference, Baltimore, MD, 1997* (IEEE, Piscataway, NJ, 1997), p. 642.
- [111] R. A. Anderson and W. K. Tucker, "Vacuum surface flashover from bipolar stress," *J. Appl. Phys.* Vol. 58, pp. 3346-3349, 1985.
- [112] Qingliang Liao, Yue Zhang, Yunhua Huang, Junjie Qi, and Zhanjun Gao, "Explosive field emission and plasma expansion of carbon nanotube cathodes," *Appl. Phys. Lett.* Vol. 91, pp. 151504, 2007.